October 2021

MECHANISMS OF MITOTIC CHECKPOINT SILENCING BY THE DISORDERED KINETOCHORE PROTEIN SPC105

Margaux Audett
University of Massachusetts Amherst

MECHANISMS OF MITOTIC CHECKPOINT SILENCING BY THE DISORDERED KINETOCHORE PROTEIN SPC105

Margaux Audett

MECHANISMS OF MITOTIC CHECKPOINT SILENCING BY THE DISORDERED KINETOCHORE PROTEIN SPC105

A Dissertation Presented

by

MARGAUX R. AUDETT

Submitted to the Graduate School of the
University of Massachusetts Amherst in partial fulfillment
of the requirements for the degree of

DOCTOR OF PHILOSOPHY

September 2021

Molecular and Cellular Biology

MECHANISMS OF MITOTIC CHECKPOINT SILENCING BY THE DISORDERED KINETOCHORE PROTEIN SPC105

A Dissertation Presented

by

MARGAUX R. AUDETT

Approved as to style and content by:

Dr. Thomas Maresca, Chair

Dr. Lilian Fritz-Laylin, Member

Dr. Margaret Stratton, Member

Dr. Patricia Wadsworth, Member

Dr.Thomas Maresca, Department Chair
Molecular and Cellular Biology

DEDICATION

To my friends and family.

ACKNOWLEDGMENTS

First and foremost I am extremely grateful to my supervisor, Dr. Thomas Maresca for your advice, continuous support, and patience during my PhD study. Thank you to my committee members, the Maresca Lab, Wadsworth Lab and Stratton Lab for all your help and advice. I would like to thank all of members of the Maresca Lab, and the MCB program at University of Massachusetts Amherst. It is their friendship and support that have made my time in the graduate school enjoyable, even when my experiments were not working. Especially thank you to my family and friends, for all your support through the years.

ABSTRACT

MECHANISMS OF MITOTIC CHECKPOINT SILENCING BY THE DISORDERED KINETOCHORE PROTEIN SPC105

SEPTEMBER 2021

MARGAUX R. AUDETT

B.Sc., GETTYSBURG COLLEGE

M.Sc., QUINNIPIAC UNIVERSITY

Ph.D., UNIVERSITY OF MASSACHUSETTS AMHERST

Directed by: Professor Dr. Thomas Maresca

The kinetochore protein Spc105R (*Dm*Spc105R) is a large intrinsically disordered protein (IDP) that recruits spindle assembly checkpoint (SAC) proteins and is required for SAC signaling in a conserved manner [18, 17, 64, 63]. Chromosome biorientation satisfies the SAC and while it has been proposed that SAC satisfaction may require the establishment of stable kinetochore-MT (KT-MT) attachments and tension generation, the question of whether tension directly regulates SAC signaling is unresolved and controversial. Here we present data in support of Spc105R as a tension-sensing IDP that directly regulates checkpoint protein localization and signaling independent of the establishment of stable KT-MT attachments. The N-terminus of *Dm*Spc105R binds directly to MTs via electrostatic interaction. The affinity of this interaction was measured *in vitro* (429 nM ± 190.9 nM) and required at least two distinct binding motifs. Pull-down experiments with purified components

demonstrated that the checkpoint protein Bub3 directly binds to the central disordered region of *Dm*Spc105 in the absence of phospho-regulation due to the presence of divergent, "phospho-mimetic" Bub3-interacting motifs in *Dm*Spc105R. Deletion of the N-terminal MT-binding region of Spc105R (Spc105RΔN) resulted in a 104 ± 15-minute delay in metaphase compared to an 8.7 ± 0.8-minute metaphase duration in control cells. Spc105RΔN-expressing cells retained ∼2-fold higher levels of Bub3 at bioriented KTs that were hyper-stretched relative to controls. Importantly Spc105RΔN-expressing cells established KT-MT attachments that were equally or more stable, as measured by PA-GFP-α-tubulin turnover, than KT-MT attachments in control cells. The metaphase delay was partially rescued upon introduction of either the MT-binding protein Tau or a protein phosphatase 1 (PP1) binding motif to the N-terminus of Spc105RΔN. The delay was fully rescued when the N-terminus of Spc105R was replaced with both the PP1 binding motif and Tau. Single molecule experiments are ongoing to directly test if physiological force application to *Dm*Spc105R reduces its affinity for checkpoint proteins. We propose that Spc105R acts as a tension sensor to directly regulate SAC signaling independent of KT-MT attachment stability. More specifically, we posit that the central IDP domain of *Dm*Spc105R binds SAC proteins under low tension, and when its N-terminus associates with dynamic MTs, tension-generation reduces its affinity for checkpoint proteins. We see no reason why this mechanical mechanism would not be conserved beyond *Drosophila* in systems where the focus has been exclusively on the phospho-regulation of Spc105R.

TABLE OF CONTENTS

LIST OF TABLES

Table **Page**

LIST OF FIGURES

Figure **Page**

CHAPTER 1

INTRODUCTION

1.1 Cell Division

Cell division occurs many times a second, millions of times a day in a single organism. Each division cycle requires correct segregation of the genome, after the DNA has been replicated and condensed into chromosomes. In order to achieve this, the process of cell division requires strict adherence to synchronous steps that must occur perfectly each time in order to have the same outcome. The goal of successful cell division is to result in two genetically identical daughter cells. When the cellular DNA is not divided up equally between the two daughters the result is aneuploidy which causes cancer and other genetic diseases. The cell has a surveillance system built into its cycle called the Spindle Assembly Checkpoint (SAC) that ensures equal distribution of the chromosomes. However, the molecular details of the SAC and its regulation are intensely debated in the field of mitosis.

Intrinsically disordered proteins are proteins that lack a well-defined and stable folded structure. Many essential proteins involved in cell division are disordered, and are therefore, potential drug targets for cancer treatments. However, we do not understand how they function in mitosis due to their paradoxical unstructured nature even though they play a relatively large role in an undeniably crucial cellular process. Much of the work on disordered proteins has been in isolation, and specifically in the field of phase transition. We have worked to better understand how an unstructured protein interacts with its structured binding partners in a novel way in order to contribute to a complex signaling pathway. This thesis is dedicated to discussing how

the flexible nature of a specific disordered protein is an important contributor to its function in cell division.

1.1.1 The Stages of Mitosis

During the mitotic (M) phase of cell division, the cell has already copied its DNA, and now must successfully divide up the chromosomes equally among the two daughter cells (Figure 1.1). The chromosomes and the mitotic spindle are both key players in proper chromosome segregation. Their roles are relatively straight forward; the chromosomes pack the DNA tightly and the mitotic spindle helps position sister chromatids along with the help of motor proteins. Kinetochores are the signaling hub of cell division, in that they initiate and regulate the movements of chromosomes during mitosis.

Entry into mitosis starts with the activation of Cdk1 by Cyclin B, which then proceeds to phosphorylate many substrates along with other mitotic kinases. This sparks the initial formation of the mitotic spindle which is made up of dimerizing tubulin subunits that grow at the plus end and shrink at the minus end. The second major step in mitosis is to then connect the DNA to the growing spindle, which is achieved by assembly of the kinetochore.

1.2 The Kinetochore

The kinetochore is a fascinating structure, due to its layers of multifunctional proteins, as well as its ability to execute such a diverse array of features. Kinetochore functions include forming attachments between chromosomes and microtubules, regulating and ensuring those attachments are correct, activating the spindle assembly checkpoint, and generating/harnessing forces to drive the movement of chromosomes during cell division.

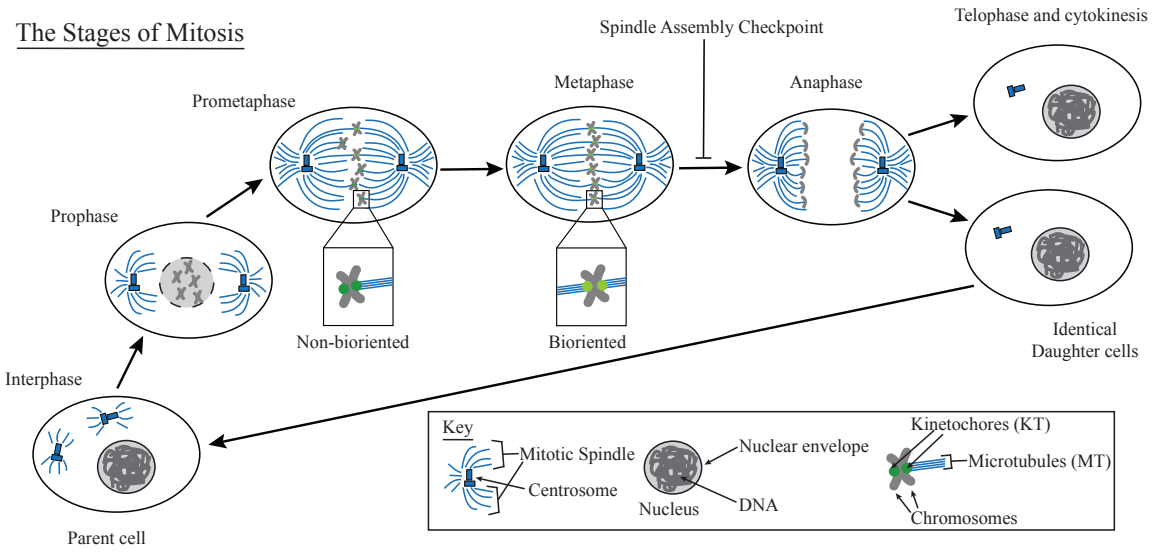

Figure 1.1. The stages of mitosis: First the cell duplicates its DNA and centrosomes in prophase. The mitotic spindle begins to form, and the centrosomes move away from each other, while DNA condenses into chromosomes. The chromosomes attach to the mitotic spindle via the kinetochores. Once every chromosome is bioriented or attached to microtubules from opposite spindle poles, then the spindle assembly checkpoint is turned off and the cell enters anaphase. The nuclei of the daughter cells reforms, and the cell undergoes cytokinesis resulting in two genetically identical daughter cells.

1.2.1 Kinetochore Architecture

Kinetochores (KTs) are essential to the spindle assembly checkpoint (SAC), which is a wait signal that is generated to prevent the transition from metaphase to anaphase until all chromosomes are correctly attached to the mitotic spindle [107]. The function of the SAC is to prevent premature chromosome segregation, and the negative downstream effects of an aneuploidy cell [88, 77]. Each sister chromatid has its own KT; therefore, each chromosome pair has two so-called sister KTs. The general architecture of KTs can be divided into layers; the inner and outer kinetochore and the fibrous corona [17, 79]. These layers were first observed by transmission electron microscopy and have since been verified by more modern methods [82] that better preserve physiological structures. The inner KT is comprised of proteins that bind to DNA and nucleosomes at the centromere. The outer KT regulates the SAC and mediates binding to microtubules (MTs). The fibrous corona, is located at the out-

ermost part of the KT and is readily observed only in the absence of MTs [36]. The corona is enriched for SAC proteins and MT-based motors and is involved in SAC signaling, MT capture, and chromosome movements [66].

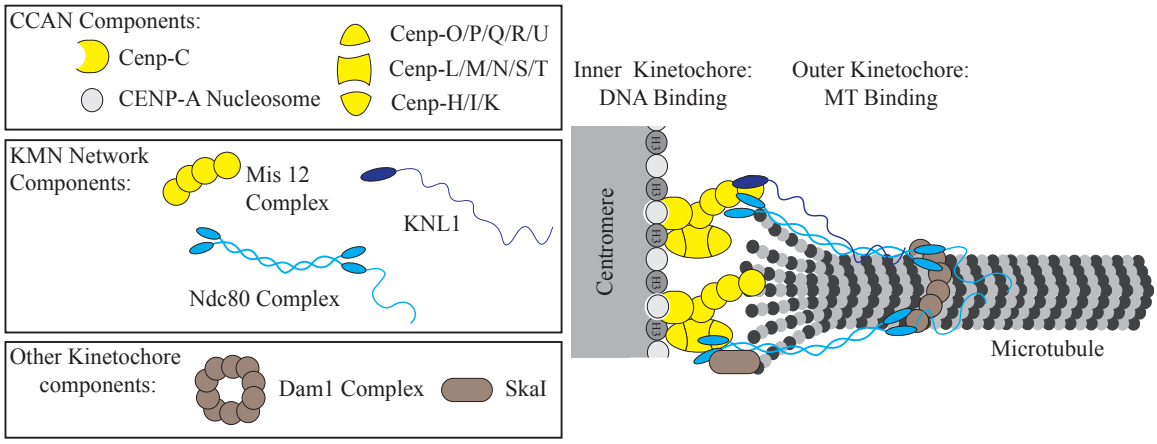

Figure 1.2. The Architecture of the Kinetochore This schematic demonstrates the main components disucessed further in this introductory chapter. The inner KT is responsible for binding to the DNA by binding to CENP-A nucleosome. The CCAN binds to the outer KT via the KMN network component the Mis12 complex. The outer KT which contains the KMN network, links the inner KT to the microtubules. The other two KMN network components bind to the Mis12 complex to link the inner KT to the microtubules. The load-bearing attachment between the KT and the MT is through interactions with the Ndc80 complex, but KNL1 also binds MT, although the function of this interaction is not fully understood.

Like many cellular processes, cell division is highly regulated by phosphorylation and the KT is a prime target. Phospho-regulation impacts many aspects of KT biology including: assembly and disassembly, KT-MT attachment stability and a related process called error correction and SAC signaling. Since MTs are highly dynamic polymers, the outer KT has the weighty task of making productive interactions with a binding partner that is not static. Even when established, proper KT-MT attachments have to be stable enough to maintain the interaction between chromosomes and MTs, but dynamic enough to harness MT dynamics to move chromosomes [44]. Phospho-regulation of MT-binding proteins at the KT is central to the goldilocks (not too stable, but not too weak) nature of KT-MT attachments. Additionally,

the KT must monitor whether every chromosome is bioriented - attached to MTs that are oriented toward opposite spindle poles [84]. This is monitored by the SAC, which is a biochemical signal that pauses cell division until all chromosomes are correctly attached to the mitotic spindle thereby preventing the premature entry into anaphase [86]. In doing so, the SAC helps to maintain the correct chromosome number (ploidy) through cell division thereby avoiding the negative downstream effects of producing aneuploid daughter cells with the incorrect number of chromosomes [45]. If one chromosome is not bioriented, then the cell will delay anaphase onset. In fact, the wait-anaphase signal produced by a single unattached KT (10s-100s of nanometers in size) is robust enough to signal the inhibition of anaphase onset to the entire cell (10s-100s of microns in size) [106, 21].

Vertebrate KTs are made up of over a hundred proteins and that can be divided into two major subcomplexes: the Constitutive centromere-associated network (CCAN) and the KMN network (KNL1 complex, Mis12 complex, and Ndc80 complex) (Figure 1.2) [16]. While it is likely there are more KT proteins that have yet to be discovered, relatively few of the known KT proteins have their functions and localization patterns characterized. Additionally, studies on KT proteins become complex very quickly because many of them have overlapping functions, which makes knockout experiments more difficult to interpret. Understanding what is currently known about KT architecture is the foundation for building new models to explain the mechanisms behind this complex molecular structure.

1.2.1.1 The Constitutive Centromere-Associated Network (CCAN)

The KT assembles at a specialized site, often cytologically identified as the primary constriction on a mitotic chromosome, called the centromere [47]. The centromere is epigenetically marked and is therefore sequence independent in most model organisms studied to date with the exception of the budding yeast *S. cerevisiae* [76, 105].

Centromere-specific histone H3 variant centromere protein A (CENP-A) forms a centromere-specific nucleosome with histone H4 and H2A/B dimers [96]. The centromere is epigenetically marked and, therefore, is sequence independent in most model organisms studied to date with the exception of the budding yeast S. cerevisiae. A histone H3 variant called centromere protein A (CENP-A) assembles into a centromere-specific nucleosome with histone H4 and H2A/B dimers [40]. CENP-A-containing nucleosomes are interspersed with H3-containing nucleosomes at centromeric chromatin throughout the cell cycle with deposition of new CENP-A nucleosomes occurring outside of S-phase, which depending on the organism occurs between M-phase to G1 phase. CENP-A nucleosomes serve as the epigenetic marker for the centromere and direct recruitment of a network of other inner KT-localized proteins known as the constitutive centromere associated network (CCAN) – referring to the fact that a majority of these components localize to the centromere throughout the cell cycle [17].

The CCAN is made up of 16 proteins that are generally distributed into multi-protein sub-complexes: CENP-C, CENP-L/CENP-N (CENP-LN), CENP-H/CENP-I/CENP-K/CENP-M (CENP-HIKM), CENP-O/CENP-P/CENP-Q/CENP-U/CENP-R (CENP-OPQUR), CENP-T/CENP-W (CENP-TW) and its binding partner CENP-S/CENP-X (CENP-SX) [99, 65, 54, 4](Pesenti, Weir and Musacchio, 2016). Broadly speaking the CCAN fulfills two fundamental roles: 1) to recruit the outer kinetochore proteins during mitosis; thereby translating the epigenetic mark of CENP-A into the specific locale at which a functional mitotic KT will assemble, and 2) to maintain the epigenetic mark by contributing to the deposition of new CENP-A nucleosomes at the centromere. Recent cryo-electron microscopy structures of the budding yeast CCAN have revealed that it assembles into a Y-shaped structure that nestles a CENP-A containing nucleosome and is spatially organized to support assembly of outer KT

components [51, 134]. Some CCAN components function as molecular bridges between centromeric DNA/CENP-A containing nucleosomes and the outer KT [54].

In many model organisms, there are two independent pathways by which the CCAN recruits the outer kinetochore [41]. One is through the CCAN component CENP-C, a large, disordered protein that binds to DNA and CENP-A via its C-terminal and central regions and to a tetrameric complex called the Mis12 complex through its N-terminus. Interestingly, human CENP-C also contains distributed binding sites for other CCAN components (CENP-HIKM and CNP-LN) along its length, leading to the proposal that CENP-C serves as a structural blueprint for the spatial organization of CCAN components within the KT [65]. The Mis12 complex acts as an outer KT hub [98] for recruiting the large disordered protein KNL1, which coordinates SAC signaling, and the tetrameric Ndc80 complex, which is the key KT-MT attachment factor. An alternative pathway by which the outer KT is recruited to centromeres is via another large and disordered linker called CENP-T. The C-terminus of CENP-T dimerizes with CENP-W and together they bind a dimer of CENP-SX. Since all four proteins possess histone fold domains, the C-terminus of CENP-T may assemble into a specialized centromeric nucleosome structure to bind DNA (Nishino et al., 2012). Once the N-terminus of CENP-T has been phosphorylated by the mitotic CDK1 kinase, it binds to the outer KT via direct physical interactions with the Spc24 and Spc25 subunits of the Ndc80 complex [41, 2, 93]. While the molecular identity of the linkages is different, CENP-C and CENP-T are similar in that they are both large intrinsically disordered proteins that bridge the inner and outer KT by binding the centromeric chromatin via their C-termini and outer KT proteins through their N-termini.

Kinetochores from different species and tissues bind different numbers of MTs - ranging from a single MT in budding yeast to (typically) tens of MTs in metazoans. The number of bound MTs scales with the physical size of the KT that is assembled.

It is therefore, not surprising that the budding yeast KT, which is built on a 125 base pair (bp) point centromere that is so small that it recruits a single (possibly up to 2-5) CENP-A nucleosome(s), binds to a single MT while KTs built on kb-Mb-sized regional centromeres can bind as many as ∼100 MTs. The notion of a simple versus complex KT has often been defined by the number of MTs it binds meaning that the budding yeast KT has traditionally been viewed as simpler than a human KT. This is a naïve view from a molecular perspective. In terms of molecular composition, the budding yeast KT is as complex as a human KT while fly and worm KTs, which like human KTs can bind tens of MTs, are far simpler in their composition. The CCAN is the most notable difference between simple versus complex KTs (Figure 1.3). CENP-C is the only CCAN component present in the simple KTs found in flies and worms (Figure 1.3 A) while KTs in most other model ophistokonts (fungi/metazoans) including budding and fission yeasts, frogs, mice, and humans possess a full complement of CCAN components (Figure 1.3 B). Many CCAN components have not been identified in plants although the complete picture of the complexity of plant KTs is unclear at this time. The fact that simple KTs in worms and flies still mediate high-fidelity chromosome segregation raises interesting questions around the utility of having the more complex CCAN, which presumably conveys additional functionality that is advantageous to these organisms. Needless to say, the difference in KT composition across species is fertile ground for evolutionary analyses. Ultimately, the association between the chromosome and a KT-MT is mediated by a linkage of proteins arranged in series with one end of the linkage associating with centromeric chromatin and the other binding directly to MTs (Figure 1.3). Productive binding of a KT to a MT requires numerous linkages arranged in parallel around the MT lattice. Thus, multiple copies of each component are present at KTs to support the formation of a functional MT binding module. Interestingly, the copy number of KT proteins per MT binding module is well-conserved. For example, KTs in budding yeast, fission yeast, chicken

DT40 cells, and human cells all possess ∼15-25 Ndc80 complexes per MT [72, 119]. Since budding yeast only binds a single MT this translates into ∼20 Ndc80 complexes per KT while a typical human KT, which binds ∼20 MTs, possesses hundreds of copies of the Ndc80 complex. It is becoming increasingly evident that binding of multiple MTs by a KT is mediated by repeated MT-binding modules, comprised of either simple or complex linkages depending on the organism, arranged around each KT-MT. This type of association of a binding module with a MT is referred to as an end-on KT-MT interaction and is mediated by components of the KMN network.

1.2.1.2 The KMN Network

The two essential functions of the KT are: 1) to bind MTs and 2) to regulate the SAC. Both of these functions are mediated by the KMN network of proteins at the outer KT. The KMN network consists of: 1) KNL1, 2) the heterotetrameric Mis12 complex, and 3) the heterotetrameric Ndc80 complex (Figure 1.4)). The KMN network is essential for accurate chromosome segregation and SAC function, and is functionally well-conserved among species, although the particular constituent components may vary slightly (e.g. Dsn1 (see below) is absent from the Mis12 complex in Drosophila). The Mis12 complex is a stiff rod-like complex (∼20 nm in length) composed of the proteins Mis12, PMF1, Nsl1 and Dsn1. The Ndc80 complex is an elongated complex (∼60 nm in length) consisting of a shorter heterodimer (via alpha-helical coiled coil) of Spc24 and Spc25 bound to a longer heterodimer (also via alpha-helical coiled coil) of Ndc80 and Nuf2. Interestingly, the Ndc80 complex is flexible due to the presence of a disordered region in the middle of the Ndc80 alpha-helix that loops out of the coiled-coil interface of the Ndc80/Nuf2 dimer. KNL1 is a relatively large protein (orthologues are typically ∼2000 aa) that has tandem RWD domains at its C-terminus while the remainder of the protein is predicted to be disor-

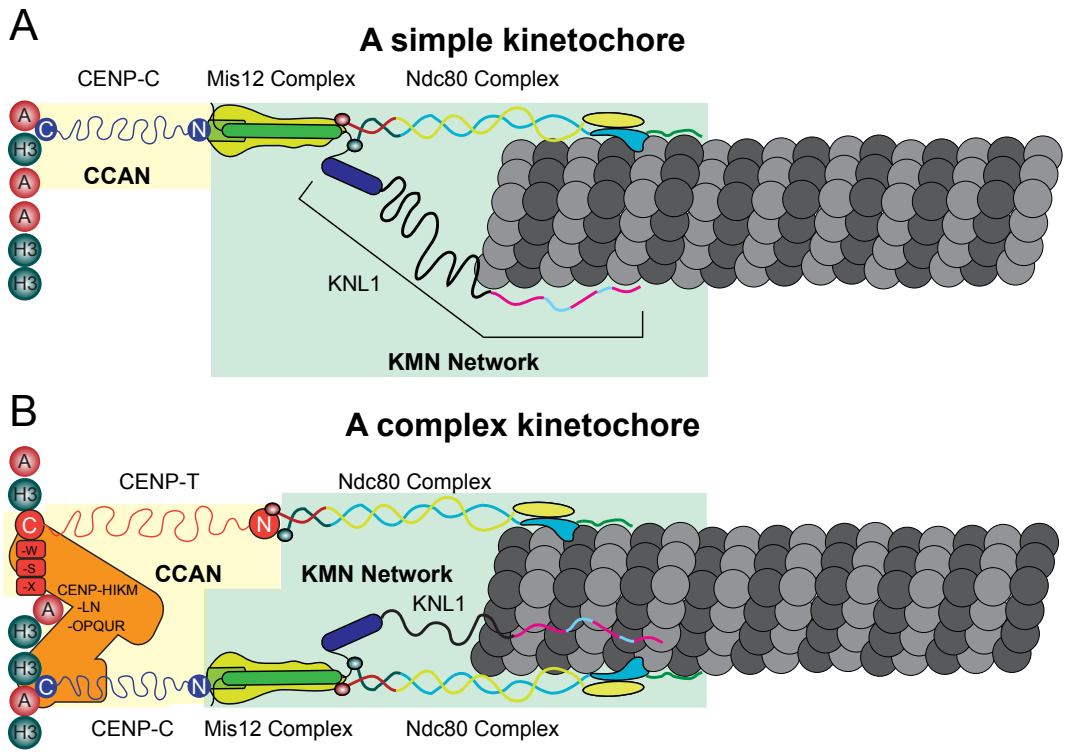

Figure 1.3. Simple vs complex KTs (A) The molecular composition of a simple KT (flies and worms) consists of only one CCAN component CENP-C, which links the centromeric DNA to the outer KT. The KMN network consists of KNL1, the Mis12 complex, and the Ndc80 complex. It is the core interface with the MT and coordinates SAC signaling. (B) The complex kinetochore also contains the KMN network, but has a much more complex CCAN consisting of CENP-C and 15 additional components that are absent from the simple kinetochore. CENP-T is similar to CENP-C in that it is a long, disordered linker between the centromeric chromatin and the outer KT. However, the N-terminus of CENP-T binds directly to the Ndc80 complex while the N-terminus of CENP-C binds to the Mis12 complex. A specialized nucleosome containing the H3 variant CENP-A is interspersed with H3-containing nucleosomes at centromeric chromatin in both simple and complex KTs.

dered. In many model systems KNL1 forms a complex with a protein called Zwint-1 although there is no Zwint-1 orthologue in flies.

As discussed earlier, one end of the Mis12 complex binds to the N-terminus of CENP-C while the other end associates with both the Ndc80 complex and KNL1. Specifically, Spc24 and Spc25, each of which possess RWD domains, interact with

motifs located at the C-termini of Dsn1 and Nsl1, and the C-terminal RWD domains of KNL1 bind to another C-terminal motif in Nsl1. KNL1 serves as a hub for SAC regulation through recruitment of checkpoint proteins via an array of repeated motifs (discussed further below). KNL1 also contains MT- and protein phosphatase 1 (PP1)-binding motifs in its N-terminal region that regulate SAC signaling although the molecular bases by which they do so are not fully understood. The Ndc80 complex is the key mediator of KT-MT attachments through direct interactions with spindle MTs via a calponin homology (CH) domain assembled from the Ndc80/Nuf2 heterodimer. Although the Ndc80 complex is the key load-bearing attachment factor at the kinetochore, it also recruits other proteins to the KT including MT binding accessory factors through its loop region and the checkpoint kinase Mps1 via its CH domain [94, 5].

1.3 SAC Signaling

The KT is the physical locale at which a biochemical signal is produced that delays cells in mitosis when chromosomes are not properly bioriented. The molecular mediator of the wait-anaphase signal is a heterotetramer called the mitotic checkpoint complex (MCC) comprised of the checkpoint proteins Bub3, BubR1, Mad2 and the APC/C co-activator Cdc20. All four proteins are abundant at unattached KTs, but associate in a highly dynamic manner (half of the molecules turnover in tens of seconds) [53, 55]. The MCC components are depleted from KTs as they attach to MTs and biorient. Thus, the unattached KT serves as a platform that brings checkpoint proteins together in order to promote their assembly into the MCC. Since the MCC components turnover so rapidly at unattached KTs, a signaling KT continually pumps out the diffusible wait-anaphase signal (Fig.1.5A).

The means by which the MCC delays anaphase onset is through direct binding to and inhibition of the anaphase promoting complex/cyclosome (APC/C). MCC

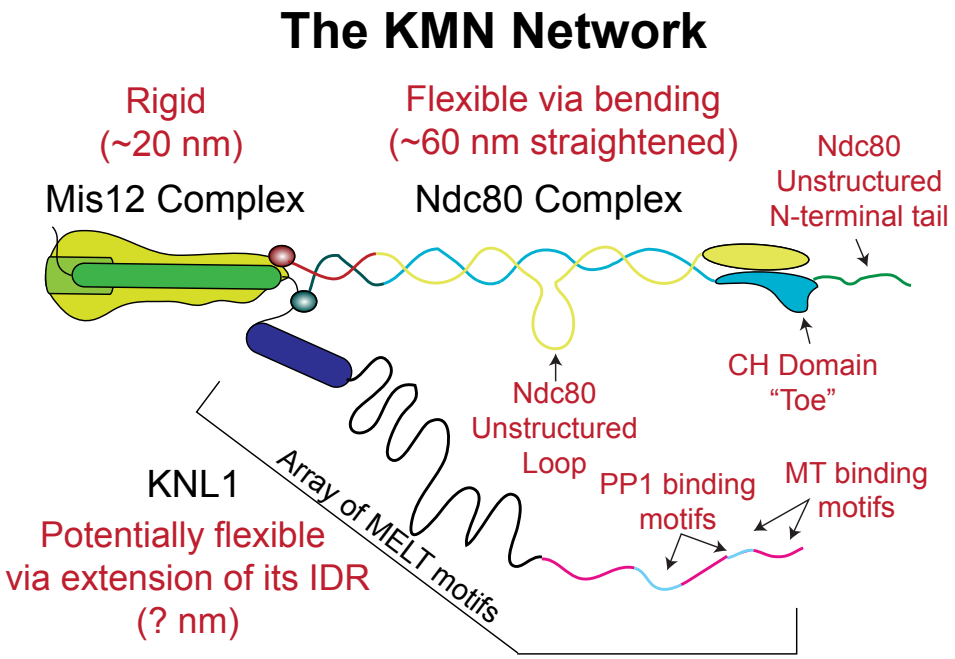

Figure 1.4. The KMN Network The Mis12 complex is a rigid 20 nm long complex that binds both the Ndc80 complex and KNL1 at a common junction point. The Ndc80 complex consists of a heterodimer of Spc24 and Spc25 that binds to the Mis12 complex associated with a heterodimer of Ndc80 and Nuf2. The Ndc80 complex can be considered flexible since it can bend due to the presence of an unstructured loop in Ndc80. Thus, the distance between the two ends of the Ndc80 complex can be shorter when bent and longer (up to 60 nm) when straightened; for example, when bound to the MT lattice. Ndc80 and Nuf2 assemble into a CH domain containing a "toe" that binds between tubulin monomers and acts as MT conformation sensor by binding preferentially to straight protofilaments over curled protofilaments. The N-terminus of Ndc80 is unstructured and associates with MTs via electrostatic interactions due to its highly basic nature. KNL1 is a large protein that binds to the Mis12 complex via tandem RWD domains at its C-terminus. The remainder of the protein is predicted to be highly disordered. The middle of KNL1 possesses an array of MELT motifs that bind to checkpoint proteins when phosphorylated. The N-terminus of KNL1 contains two PP1-binding motifs and makes multiple interfaces with MTs. In theory, KNL1 is flexible since the intrinsically disordered region (IDR) could be extended; for example, upon the N-terminus binding to a MT.

binding to the APC/C 1) prevents recognition of substrates by Cdc20 and 2) inhibits the ubiquitination activity of the APC/C thereby preventing degradation of its key mitotic substrates: cyclin B and securin [118, 2, 133]. It is unknown if the MCC is created entirely at KTs, or also in the cytosol, however, during active SAC signaling the MCC is constantly produced and disassembled. The disassembly of the MCC is mediated by an AAA-ATPase called Trip13 that is targeted to the MCC by the Mad2-binding partner p31comet [1]. The balance between production and disassembly of the MCC results in the SAC acting as a "rheostat rather than a switch" meaning that the strength of the wait-anaphase signal, as measured by the duration of the mitotic delay it induces, is proportional to the number of KTs actively producing MCC [22, 32, 49].

The concentration of Bub3 and BubR1 are reduced 3-5 times at attached relative to unattached KTs, but the concentration of another MCC subunit, Mad2 is 100 times higher at unattached KTs than at attached KTs [53]. This is likely due to the much higher levels of coronal Mad2, which is stripped by dynein. Mad2 binds to a KT receptor called Mad1 and also to Cdc20. Mad2 has two distinct protein conformations, called open (O-Mad2) and closed (C-Mad2). C-Mad2 is adopted when in complex with Cdc20 or Mad1 while the O-Mad2 conformation is adopted when it is not bound to these partners. The template model [25] proposes that a dimer of Mad1 bound to C-Mad2 at the KT can recruit an O-Mad2 molecule and then hand it off to Cdc20 to produce a C-Mad2-Cdc20 dimer, which can assemble into the MCC with Bub3 and BubR1. The conformational differences in Mad2 occur due to changes in a mobile element called the 'safety belt' at the C-terminus [115]. The safety belt is a 50 residue stretch of amino acids that positions itself around a binding partner (Mad1 or Cdc20) and promotes tighter interactions. As discussed previously, Mad1 and Mad2 are highly enriched at the corona of unattached KTs, but there is also a population of Mad1/2 recruited to KNL1 through interaction with a Bub3 binding partner called

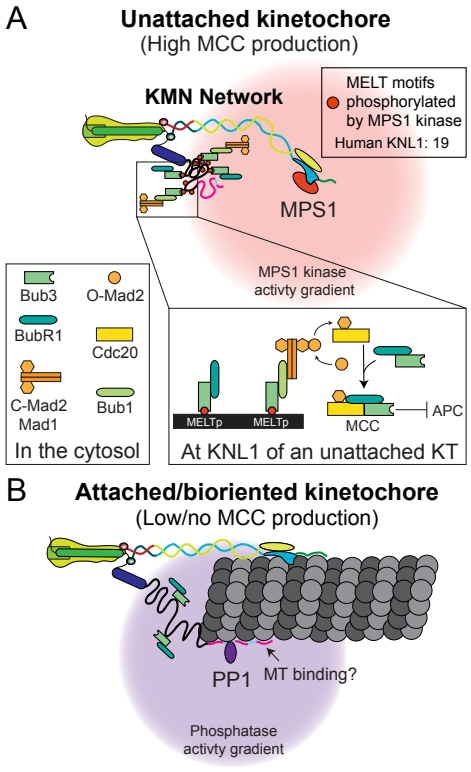

Figure 1.5. Phosphoregulation of the SACA) MPS1 kinase binds to the CH domain of the Ndc80 complex at unattached KTs presumably generating a local activity gradient that phosphorylates the MELT motifs in KNL1 (19 MELTs in human KNL1). Phosphorylated MELT motifs create a binding platform to recruit SAC proteins specifically through binding to Bub3. Bub3, in turn, brings its binding partners BubR1 and Bub1 to the unattached KT. Bub1 can also bind a tetramer of Mad1/closed (C)-Mad2, which converts open (O)-Mad2 to C-Mad2 bound to the APC/C coactivator Cdc20. A dimer of Bub3/BubR1 associates with the C-Mad2/Cdc20 dimer to form the mitotic checkpoint complex (MCC), which binds to and inhibits APC/C activity to prevent anaphase onset and mitotic exit. The association of checkpoint proteins with unattached KTs is highly dynamic meaning that individual components or subcomplexes likely bind to unattached KTs where their assembly into the MCC is promoted through localized enrichment and post-translation modifications. The assembled MCC then dissociates to act as a soluble inhibitory signal. (B) MPS1 is displaced from the CH domain upon MT binding by the Ndc80 complex. Furthermore, PP1 is recruited to bioriented KTs by binding to the N-terminal motifs in KNL1. It is unclear if and how MT binding by KNL1 plays a role in this process. The loss of KT-associated MPS1 kinase combined with the local recruitment of PP1 results in dephosphorylation of the MELT motifs in KNL1, which reduces their affinity for Bub3 and extinguishes production of the MCC. This schematic reflects the model for SAC signaling in human KTs, some organisms utilize a different kinase than MPS1 but the molecular mechanism of MCC production is likely similar.

Bub1 [139]. Thus, KNL1 plays a central role in SAC signaling by bringing the core constituents of the MCC into close proximity (Figure 3A).

The SAC is highly phospho-regulated (Fig.1.5). The association of a key population of MCC components to the KT occurs through Bub3, which binds directly to KNL1 via phosphorylated motifs called "MELTs" at non-bioriented KTs (Fig.1.5A). MELT motifs are phosphorylated by different kinases depending on the species, for example in human cells and yeasts, the motifs are phosphorylated by MPS1 kinase [95, 67, 68, 132, 113, 100, 126, 140]. Upon biorientation, dephosphorylation of the MELT motifs is promoted by phosphatases, including a population of protein phosphatase 1 (PP1) that is recruited to the N-terminus of KNL1 and a population of protein phosphatase 2A (PP2A) that binds to BubR1 [24]. Dephosphorylation of the MELT motifs reduces the affinity of Bub3 for KNL1, thereby lowering the rate (or ceasing production) of MCC assembly by the KT (Fig.1.5B). The remaining MCC is presumably disassembled by p31comet and TRIP-13 and anaphase ensues. Interestingly, MPS1 kinase binds to the CH domain of the Ndc80 complex in a manner that is mutually exclusive with MT-binding by the Ndc80 complex [33, 52, 58]. Thus, unattached KTs recruit high levels of MPS1 that can phosphorylate the MELT motifs in KNL1 while the establishment of KT-MT attachments contributes to SAC silencing by displacing MPS1 from the Ndc80 complex.

1.3.1 Phosphoregulation of the SAC

One of the most well characterized mitotic kinases is the serine/threonine kinase Aurora B, a subunit of the activating complex called the Chromosome Passenger Complex (CPC) [13]. The most well characterized pool of Aurora B localizes to the inner centromere at the region between kinetochores where it phosphorylates a myriad of its substrates in the inner and outer kinetochore [12]. More recently a pool of Aurora B that localizes to the kinetochore was identified, although the function of this

population is not understood [11, 10]. Aurora B is involved in both the regulation of the checkpoint and promoting correct kinetochore-microtubule attachments. Aurora B activity is dependent on whether the kinetochore is attached to a microtubule and declines once the kinetochore has bioriented [75, 131, 27, 111]. One model suggests that the regulation of Aurora B activity is based on the ability of Aurora B to reach its substrates. Once bioriented, kinetochores undergo a stretch that moves the substrates of Aurora B out of its reach, presumably to tip the balance and allow opposing phosphatases to dephosphorylate those substrates [121, 81, 71]. While this model elegantly explains observations of Aurora B activity during cell division, more work needs to be done before it can be accepted in the field.

One way Aurora B contributes to SAC signaling by recruiting checkpoint proteins through phosphorylating its substrates. One of the most crucial proteins recruited by Aurora B is Mps1 kinase, which binds to Ndc80 in a phoshpo-dependent manner. In some organisms, Mps1 phosphorylates KNL1 which creates docking sites for the recruitment of MCC subunits, including Bub3 and Mad1/2. In humans, the Ska complex interacts with Ndc80 once it's been phosphorylated by Aurora B and Cdk1. The Ska complex is essential to the metaphase-anaphase transition in that it recruits PP1 to kinetochores that have attached to spindle microtubules. PP1 counteracts the phosphorylation by Aurora B, thereby increasing the affinity of microtubules and kinetochores [13]. These phosphorylation events are counteracted by several mitotic phosphatases, most notably PP1 and PP2A. PP1 binds to KMN network subunit protein KNL1, where it dephosphorylates proteins that have been phosphorylated by Aurora B. In contrast, PP2A promotes rapid dephosphorylation of Cdk1 substrates after Cdk1/Cyclin B has been inactivated. These phosphatases are involved in disassembly of the kinetochore when the bi-polar attachment of microtubules to kinetochores has been established [47]. A challenging aspect of understanding the

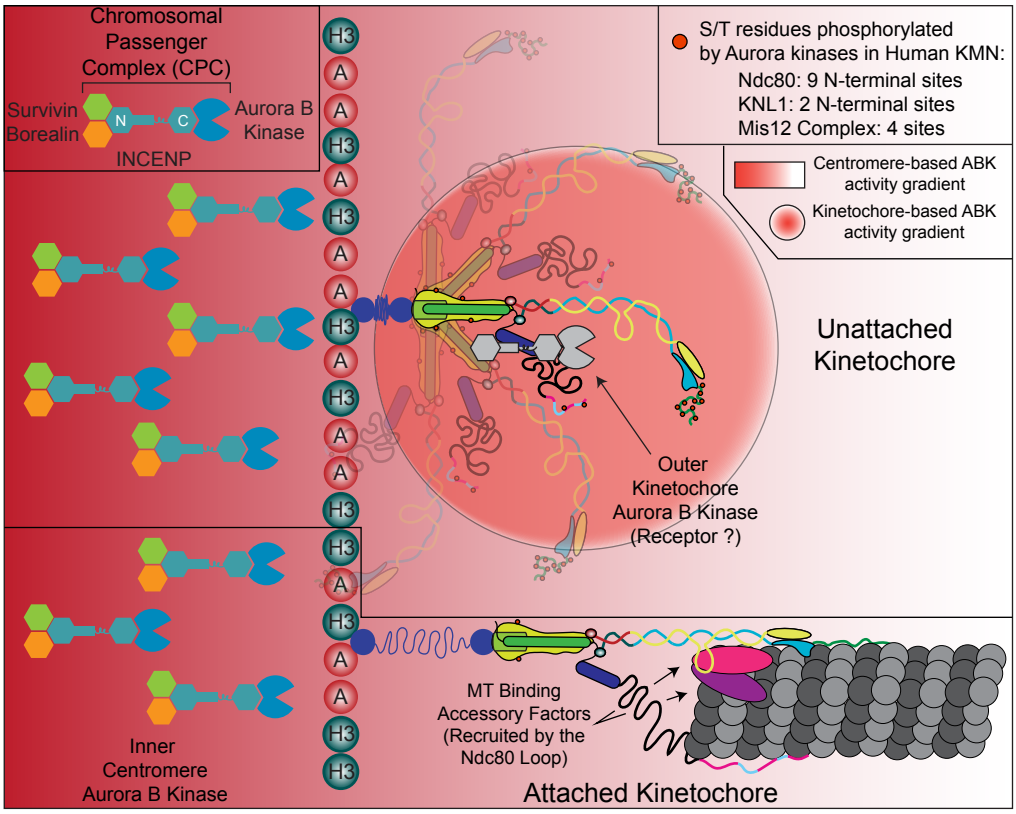

Figure 1.6. Phosphoregulation of KT-MT attachment and the spatial positioning model The KMN network is hyperphosphorylated by Aurora B kinase at unattached KTs and less phosphorylated at attached KTs. There are multiple relevant pools of Aurora B kinase. The major pool is enriched at the inner centromere between sister KTs through its association with the chromosomal passenger complex (CPC) that consists of: Survivin, Borealin, INCENP, and Aurora B. The extent to which the outer KT is phosphorylated correlates with the amount of inner centromeric CPC, which is more abundant at unattached KTs than at attached KTs. An outer KT pool of Aurora B was recently characterized at unattached KTs that phosphorylates KMN substrates. Displacement of this population of Aurora B upon MT attachment, the mechanism of which is unknown, would reduce phosphorylation of substrates. Spatial positioning of KMN substrates relative to Aurora B populations may also impact the extent to which they are phosphorylated. At an unattached KT, the KMN is positioned closer to the inner centromeric population of Aurora B. Therefore, upon MT association, Aurora B substrates in the KMN would be positioned further from the inner centromere through extension of the CENP-C or CENP-T linker, orientation of the rigid Mis12 complex along the long axis of the MT, and straightening of the Ndc80 complex when it is bound to the MT lattice. It is unclear if a spatial positioning mechanism could also function relative to an outer KT pool of Aurora B kinase. The affinity of the KT for MTs is increased when the KMN network is dephosphorylated. Aurora B kinase also reduces the MT binding affinities of a number of accessory factors that are recruited by the Ndc80 complex upon attaching to MTs.

function of mitotic kinases and phosphatases is that each has many substrates, and some of these substrates overlap with complementary proteins.

Aurora B contributes to SAC signaling by recruiting checkpoint protein through phosphorylating its substrates. One of the most crucial proteins recruited by Aurora B is Mps1 kinase, which binds to Ndc80 in a phoshpo-dependent manner. In some organisms, Mps1 phosphorylates KNL1 which creates docking sites for the recruitment of MCC subunits, including Bub3 and Mad1/2. In humans, the Ska complex interacts with Ndc80 once it's been phosphorylated by Aurora B and Cdk1. The Ska complex is essential to the metaphase-anaphase transition in that it recruits PP1 to kinetochores that have attached to spindle microtubules. PP1 counteracts the phosphorylation by Aurora B, thereby increasing the affinity of microtubules and kinetochores.

These phosphorylation events are counteracted by several mitotic phosphatases, most notably PP1 and PP2A. PP1 binds to KMN network subunit protein KNL1, where it dephosphorylates proteins that have been phosphorylated by Aurora B. In contrast, PP2A promotes rapid dephosphorylation of Cdk1 substrates after Cdk1-Cyclin B has been inactivated. These phosphatases are involved in disassembly of the kinetochore when the bi-polar attachment of microtubules to kinetochores has been established. A challenging aspect of understanding the function of mitotic kinases and phosphatases is that each has many substrates, and some of these substrates overlap with complementary proteins.

1.3.2 Kinetochore-Microtubule Interactions

A MT is a tubular filament (25 nm in diameter) that possesses polarity - meaning its two ends are different – due to the fact that its subunits are α- and β-tubulin heterodimers that by their very nature have intrinsic polarity. Heterodimers are arranged end-to-end into a protofilament – 13 of which assemble into the tube-shaped filament that is a MT. The plus-end (β-tubulin exposed) and minus-end (α-tubulin exposed)

of a MT are defined as the fast and slow growing ends of a free MT respectively. In a metaphase spindle, in which all the chromosomes are aligned, the bioriented KTs are bound to MT plus-ends while the minus-ends are oriented toward the spindle poles.

The most important KT component for establishing and maintaining stable end-on KT-MT attachments is the Ndc80 complex, which possesses a CH domain that binds directly to MTs [3]. The toe print overlaps with a structural feature of the α/β tubulin heterodimer called the hinge point such that curled protofilaments, which are abundant at the plus-ends of shortening MTs, sterically hinder Ndc80 complex binding. Thus, the Ndc80 complex has a higher affinity for straight protofilaments than for curled protofilaments. This behavior allows the Ndc80 toe to act as a MT conformation sensor that preferentially binds to straightened portions of the MT lattice rather than to bending protofilaments at the plus-ends. The disordered N-terminal tail of Ndc80 (Fig.1.4) is highly basic in many organisms and, therefore, also directly contacts the MT via electrostatic interactions with the acidic C-terminal tails of α/β tubulin. The N-terminal tail of Ndc80 allows ensembles (multiple Ndc80 complexes bound to a single MT) to remain associated with shortening MT plus-ends [127]. Thus, fully functional KT-MT interactions require the structured CH domain of Ndc80 to bind the MT lattice and the unstructured tails of multiple Ndc80 complexes to remain attached to shortening MTs and to efficiently harness MT depolymerization forces. The Ndc80 complex also recruits a number of accessory factors that contribute to KT-MT attachment stability and plus-end-tracking on shortening MTs. In budding yeast, the Ndc80 complex recruits and promotes assembly of the ring-shaped Dam1 complex that encircles the KT-MT - an ideal force coupling arrangement for moving chromosomes. In vertebrates, the Ndc80 complex recruits the MT-binding Astrin-SKAP complex to further stabilize properly bioriented attachments. Interestingly, the loop domain of Ndc80 in many metazoans also recruits MT-binding accessory factors including Cdt1 and the Ska complex (Fig.1.6). While the N-terminus of KNL1

possesses MT binding activity, it is unclear whether it contributes significantly to KT-MT attachment stability. Thus, of the two MT-binders in the KMN network, it is the Ndc80 complex that, via direct MT binding and recruitment of other MT binding factors, is the key mediator of end-on KT-MT attachments.

Once the initial microtubule has interacted with a kinetochore, the associated chromosome migrates toward the minus end of microtubule, located near the spindle pole where there is a high density of microtubules. The cytoplasmic motor protein dynein is most likely involved in this activity, which is enriched at kinetochores that are not bound to microtubules. However, the binding of the first microtubule is followed by the kinetochore acquiring more microtubules, which then releases dynein and thereby slows its movement toward the pole. The movement of sister chromatids to towards the equator is call chromosome congression, and is driven by the plus-end microtubule motor CENP-E. Both dynein and CENP-E also mediate converting laterally associated microtubules to stable end-on attachments with kinetochores. Additionally, the opposing activities of Aurora B and PP2A also regulate this conversion, as well as another kinetochore complex made up of proteins Astrin and SKAP.

1.4 Kinetochore-associated motor proteins

Motor proteins harness the energy from ATP hydrolysis to move directionally on MT filaments meaning that some motors walk toward the plus-end and others walk toward the minus-end. A large number of plus- and minus-end directed mitotic motor proteins organize MTs into a spindle and are essential for successful cell division. Two motor proteins localize to the KT where they make important contributions to its functions: the plus-end directed CENP-E and the minus-end directed cytoplasmic dynein. While the two motors move in opposite directions, there are some commonalities in their KT localization pattern and functions. Both motors localize to the fibrous corona and are abundant at unattached KTs early in mitosis. As mitosis

proceeds, both motors are depleted from KTs when they attach to MTs and biorient although a significant portion of CENP-E remains at bioriented KTs while dynein is either absent or at levels too low to easily observe. Both motor proteins mediate lateral KT-MT interactions, meaning they associate the KT with the side-walls of the MT lattice along its length, and move chromosomes directionally on the MT. Of course, a key difference is that the two motors move chromosomes in opposite directions on spindle MTs.

Prometaphase is the period in mitosis when the dissolution of the nuclear envelope first exposes unattached KTs to cytoplasmic MTs, which at this point are predominantly assembled and emanating from two nucleation centers called centrosomes. Under ideal circumstances, the centrosomes were previously positioned on opposite sides of the nucleus during prophase (the time in mitosis prior to nuclear envelope breakdown). The proper positioning of centrosomes in prophase facilitates assembly of an American football-shaped bipolar spindle in which one centrosome resides at each spindle pole. Centrosome-derived MTs are typically embedded in pericentriolar material that is enriched with a MT nucleator called the gamma-tubulin ring complex, which caps the minus-end of the MT. The free plus-ends of these astral MTs undergo dynamic instability in which they stochastically transition between states of growth and shrinkage resulting in highly dynamic and short-lived MTs (half-life of $\sim$30s). KT-associated dynein dominates in early prometaphase when fully unattached KTs enriched with dynein laterally bind astral MTs and zip chromosomes toward the centrosome at $\sim$25 μm/min. Dynein's velocity and the absence of much opposing force at this point in time means that KT-associated dynein can position a number of unattached chromosomes near centrosomes in early prometaphase despite the astral MT tracks being so short-lived.

While the polar localization of chromosomes contributes to an important process called error correction (discussed below), successful segregation of the genome cannot

occur if chromosomes permanently reside near the spindle poles and centrosomes. Thus, circumstances change vis-a-vie dynein dominance in chromosome movements as cells advance through prometaphase and the spindle matures. The plus-end directed motility of KT-associated CENP-E is an important contributor to the shift in chromosome movement away from spindle poles and toward the mid-spindle and the metaphase plate. A new population of spindle MTs comes into existence as a subset of chromosomes become bioriented in prometaphase. As opposed to astral MTs that live for tens of seconds, end-on attached KT-MTs are much more stable and persist for tens of minutes with their plus-ends embedded in the KT and their minus-ends oriented toward the spindle poles. The biochemical properties of KT-MTs are also distinct from astral MTs because their increased stability provides time for enzymes to make a number of post-translation modifications (PTM) to them. Since the acidic and unstructured C-termini of α- and β-tubulin are exposed on the surface of the MT lattice, the so-called C-terminal tails: 1) mediate interactions between MTs and many binding partners, and 2) are hotspots for PTMs that modulate these protein-protein interactions. An important PTM of MTs in the context of KT motor dominance is detyrosination – removal of a terminal tyrosine residue from the C-terminal tail of α-tubulin. While dynein motility is activated by tyrosinated MTs, CENP-E preferentially walks on detyrosinated MTs. Thus, dynein more effectively walks KTs toward the minus-ends of the highly dynamic astral MTs while KT-associated CENP-E moves chromosomes toward the metaphase plate by walking on the more stable, detyrosinated KT-MTs of previously bioriented chromosomes [8, 80]. Another important PTM that regulates the directionality of chromosome movements in prometaphase is the phosphorylation and activation of CENP-E by the centrosome and spindle pole-enriched Aurora A kinase.

In addition to moving chromosomes in prometaphase, CENP-E and dynein also contribute to the KTs two main functions: 1) attaching chromosomes to spindle MTs,

and 2) regulating the SAC. CENP-E contributes to the establishment of end-on KT-MT attachments at a subset of KTs in early prometaphase by capturing short (non-centrosomal) MTs that are nucleated in the vicinity of KTs and sliding them (relative to the KT) to convert them from lateral to end-on interactions [114]. Furthermore, contrary to dynein, a significant portion of (non-coronal) CENP-E remains at bioriented KTs where the motor helps maintain end-on interactions with the dynamic plus-ends of KT-MTs. This function is likely mediated by the ability of CENP-E to track (remain associated) with the plus-ends of growing and shortening MTs [46]. At first glance it is counterintuitive that CENP-E, rather than dynein, is a key contributor to anaphase chromosomes movements, but the ability of KTs (and KT-associated CENP-E) to maintain end-on interactions with shortening KT-MT plus-ends allows the KT to harness MT depolymerization forces to move chromosomes poleward during anaphase. While KT-associated dynein likely plays a minor direct role compared to CENP-E in contributing to KT-MT attachment stability and anaphase chromosome movements, there is no doubt that KT-bound dynein is a critical and direct regulator of SAC signaling.

As discussed earlier, the fibrous corona is highly enriched with both dynein and SAC proteins – most notably Mad1 and its binding partner Mad2. The coronal checkpoint proteins at unattached KTs contribute to the production of a robust wait-anaphase signal (discussed in further detail in previous sections). Assembly of the fibrous corona depends on a trimeric complex of Rod, Zwilch, and Zw10 (RZZ) that oligomerizes into the fibrous meshwork of the corona and recruits Mad1/2 via direct association with a complex of Cyclin B1-Mad1 [66]. Importantly, RZZ is also linked to dynein through an adaptor protein called Spindly. In the absence of opposing forces, coronal dynein moves the chromosome poleward, however, once an opposing force is established, dynein physically strips the corona from the KT. Consequently, dynein depletes RZZ, Spindly, and most-importantly, with regards to SAC signaling,

a majority of KT-associated Mad1/2 – all of which can be seen streaming poleward as large "chunks" of corona are pulled from KTs and rapidly transported toward the minus-ends of spindle MTs. Depletion of checkpoint proteins from KTs is critical to silencing production of the wait anaphase signal by KTs and dynein contributes to this phenomenon in dramatic fashion.

1.5 Conclusions and Further Reading

The KT is an incredible molecular super-structure that possesses "brains" and "brawn". In the brains department, it orchestrates a biochemical SAC signal that helps ensure anaphase only occurs once every chromosome is best-positioned for equal segregation of the genome. In the brawn department, the KT grabs onto MTs in a manner that is robust enough to maintain association with KT-MTs throughout cell division while still allowing MT polymerization and depolymerization forces to be harnessed for chromosome movements. Much has been learned about the molecular composition, structural organization, and major functions of the KT in the past few decades, but the coming years hold significant promise as vigorous investigations continue - especially at the interface of mechanobiology and biochemical pathways. It is an exciting time to study kinetochore biology and we hope that this chapter will provide an accessible entry-point to the field.

Further Reading:

Audett, M.R. and Maresca, T.J., 2020. The whole is greater than the sum of its parts: at the intersection of order, disorder, and kinetochore function. Essays in Biochemistry, 64(2), pp.349-358.

Carmena, M., Wheelock, M., Funabiki, H. and Earnshaw, W.C., 2012. The chromosomal passenger complex (CPC): from easy rider to the godfather of mitosis. Nature reviews Molecular cell biology, 13(12), pp.789-803.

Hara, M. and Fukagawa, T., 2020. Dynamics of kinetochore structure and its regulations during mitotic progression. Cellular and Molecular Life Sciences, pp.1-15.

Kops, G.J. and Gassmann, R., 2020. Crowning the kinetochore: the fibrous corona in chromosome segregation. Trends in cell biology.

Maresca, T.J. and Salmon, E.D., 2010. Welcome to a new kind of tension: translating kinetochore mechanics into a wait-anaphase signal. Journal of cell science, 123(6), pp.825-835.

Monda, J.K. and Cheeseman, I.M., 2018. The kinetochore–microtubule interface at a glance. Journal of cell science, 131(16).

Musacchio, A. and Desai, A., 2017. A molecular view of kinetochore assembly and function. Biology, 6(1), p.5.

1.6 Intrinsically Disordered Proteins (IDPs)

Intrinsically disordered proteins (IDP) are a relatively newly discovered subset of proteins that lack a stable tertiary structure. They often have a higher proportion of charged amino acids that repel or attract each other, and also prevent them from having a hydrophobic core and hydrophilic outer layer that is characteristic of folded globular proteins. Due to their lack of a structure, they can be difficult to work with in typical experimental settings and therefore are not able to be characterized using the same methods as folded proteins. It is difficult to use the amino acid sequence to characterize IDPs because they often lack conserved domains among homologs from different species. While the accepted paradigm is that structure dictates function, like that of an ion channel or a chaperone protein, IDPs unstructured nature defines them and gives them their function. Interestingly, some IDPs can adopt a folded structure in certain environmental conditions. Studies have shown that pH, temperature, salt concentrations and PTMs can all change the ability of IDPs to fold ([35]). There are

short sequences called Molecular Recognition Features (MoRFs) that are domains that, upon interacting with binding partners, induce a conformational change where the IDPs then undergo a disorder-to-order transition. Additionally, they have unique and significant differences in their amino acid composition. They lack the bulky hydrophobic residues that often stabilize a globular structured protein, as well as possessing a lower abundance of Cys and Asn resdues. However, IDPs tend to be rich in polar and "structure breaking residues like Gly and Pro ([124]).

Another interesting property of IDPs, which is also a topic of peaked interest recently, is the ability of these proteins to phase-transition. There many names used to describe this phenomenon in the literature, essential it is the ability of the protein to interact with itself and form a large conglomerate that acts like a liquid-like substance. Often these large complexes are called membrane-less organelles due to their ability to include or exclude certain proteins without having a physical barrier separating them. The phase-transitioned state can be experimentally distinguished from a protein aggregate in that it has different properties and is thought to serve a cellular function ([56]). For example, some phase-transitioned proteins can form a liquid or a gel by a mechanism that has been called "liquid-liquid demixing." These proteins have liquid-like properties that can be visualized via microscopy. They can be observed forming large droplet shaped masses that have similar dynamics to a liquid drop and have been observed to fuse with other droplets when they make contact *in vitro* ([59]). Other phase-transitioned IDPs form a gel, which does not fuse with other gels, and has a more viscous consistency. Gels are often formed in conjunction with other molecules such as RNA or organelle membranes, and serve to concentrate that molecule in an area without a physical barrier so that other molecules can diffuse into the gel. Membrane-less organelles are often made by this gel formation, give an example here.

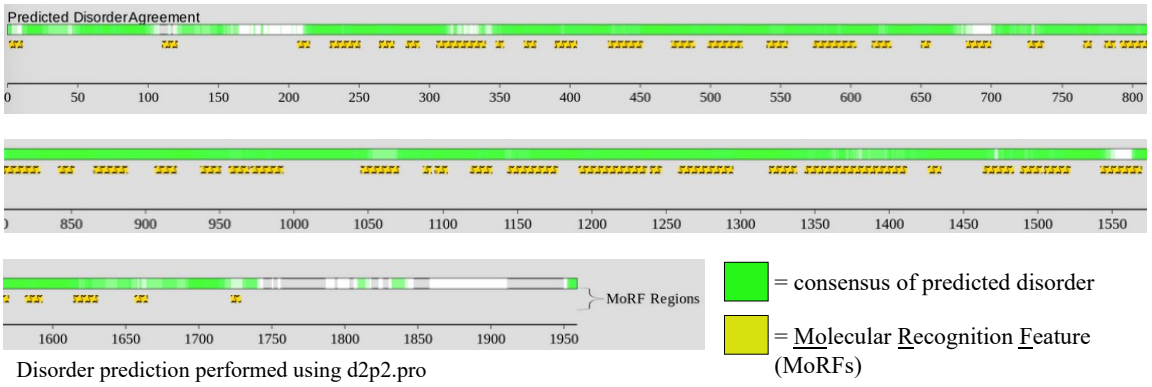

Figure 1.7. The predicted disorder profile of *Drosophila* Spc105B By computational prediction, the amino acid sequence of KNL1 is predicted to be intrinsically disordered throughout most of its length, excluding the C terminus which contains TPR repeats that bind to Mis12. The intrinsic disorder profile shown here was generated by the D2P2 disorder prediction program. The region of predicted disorder lies between the N-terminal (MT and PP1 binding) and the C-terminal (KT Mis12 complex binding) regions. Additionally, this schematic demonstrates that KNL1 is predicted to contain many Molecular Recognition Features (MoRFs) in the disordered middle region. This is consistent with the known function of KNL1 as a binding scaffold for many mitotic proteins.

KNL1 is predicted to be almost entirely disordered except for its C terminus which has RWD repeats that interact with the Mis12 complex at the outer KT. Additionally, much of the amino acid sequence of KNL1 is predicted to contain MoRFs (Figure 1.7). Since the main function of KNL1 is a binding platform, the idea that it contains many MoRFs is interesting, however we do not yet know if any binding interaction changes the disordered nature of KNL1. Additionally, recent work from the Cheeseman lab demonstrated that the N terminus of KNL1 *C. elegans* KNL1 has been shown to form a gel in purified conditions [61]. Therefore, it would be interesting to determine if the ability for KNL1 to form a gel and thereby concentrate certain proteins, and/or phase transition upon binding or PTMs, would be a very interesting characteristic which should be explored in the future.

APC/C	Anaphase Promoting Complex/Cyclosome
CCAN	Constitutive Centromere-Associated Network
CENP-	Centromere Protein-
CH	Calponin Homology
C-Mad2	Closed Mad2
CPC	Chromosomal Passenger Complex
IDR	Intrinsically Disordered Region
KT	Kinetochore
KT-MT	Kinetochore-Microtubule
KMN	KNL1, Mis12 Complex, Ndc80 complex
KNL1	Kinetochore Null 1
MCC	Mitotic Checkpoint Complex
MT	Microtubule
O-Mad2	Open Mad2
PP1	Protein Phosphatase 1
PP2A	Protein Phosphatase 2A
PTM	Post-translational Modification
RZZ	Rod-Zwilch-Zw10
SAC	Spindle Assembly Checkpoint

Table 1.1. Abbreviations

CHAPTER 2

THE MICROTUBULE- AND PP1-BINDING ACTIVITIES OF *DROSOPHILA* SPC105 CONTROL THE KINETICS OF SAC SATISFACTION INDEPENDENT OF REGULATING ATTACHMENT STABILITY

2.1 Introduction

Accurate chromosome segregation is necessary to maintaining genomic integrity through cell division. The spindle assembly checkpoint (SAC) is a chemical signal that delays anaphase onset until every pair of chromosomes is properly attached and aligned within the spindle [86]. Once all chromosomes are bioriented, or properly attached to microtubules (MTs) emanating from opposite spindle poles, the SAC signal is extinguished, and sister chromatids can physically separate. MT attachment and SAC regulation are mediated by a multi-protein complex called the kinetochore (KT) that assembles at centromeres during cell division [14, 87]. Structural KT proteins, which are stably maintained at centromeres throughout cell division, are essential to both the attachment and SAC regulatory functions since they possess MT- and checkpoint protein-binding activities. Unlike the stable KT constituents, checkpoint proteins, which associate with KTs in a highly dynamic manner, are abundant at unattached KTs and become diminished as KTs establish end-on attachments to MTs and biorient [53, 55, 69]. The KT is the physical locale where checkpoint proteins become enriched and post-translationally modified to promote assembly of a diffusible mitotic checkpoint complex (MCC) that acts as a wait-anaphase signal through inhibition of the anaphase promoting complex/cyclosome (APC/C) [118, 2, 133]. When checkpoint proteins are depleted from bioriented KTs they cease to produce the wait-

anaphase signal, but it remains unclear precisely how the KT-MT attachment state is translated into reduced checkpoint protein binding affinities and, consequently, SAC satisfaction.

No protein better exemplifies how the KT lies at the nexus of MT attachment and SAC regulation than KNL1 (D40/AF15q14/Blinkin/KNL1/Spc105/CASC5) [130, 48, 31, 91, 64, 42], which was deemed dmSpc105R (referred to hereafter as Spc105) in *Drosophila* [101]. KNL1 is the largest component of the KMN network; an outer kinetochore complex made up of KNL1, the Mis12 complex, and the Ndc80 complex [16]. KNL1 is predicted to be highly disordered except for conserved tandem RWD domains in its C-terminus that anchor it to the outer KT by binding to the Mis12 complex via physical interactions with Nsl1 [98, 97]. Its large size and disordered nature make KNL1 energetically expensive relative to a small, well-folded protein that could, in theory, mediate the same functions. While KNL1 orthologues are highly divergent at the amino acid level; the large size and unstructured nature are well-conserved indicating that these features are essential for its function.

Work in multiple model systems has shown that KNL1 orthologues bind MTs [16, 131, 37, 110], although the precise purpose of the interaction is not well understood. There is a conserved MT binding patch located at the extreme N-terminus that has been characterized in yeast, *C. elegans*, and humans [16, 62, 95, 37]. In addition, the N-terminus has protein phosphatase 1 (PP1) binding "SILK" and "RRVSF" motifs that are well-conserved [50, 75, 83, 109, 37, 78, 113, 7]. The middle region of KNL1 orthologues contains a large array of so-called MELT motifs that recruit multiple checkpoint proteins (BubR1, Bub1, Bub3, Mad1, and Mad2) through direct binding to the checkpoint protein Bub3. The interaction between MELT motifs and Bub3 is highly phospho-regulated by a balance of localized kinase and phosphatase activities. In many organisms the checkpoint kinase monopolar spindle 1 (Mps1) generates MELTp, which promotes a higher affinity association with Bub3 and its

recruitment to KTs in cells [95, 67, 113, 78, 100, 126, 140]. However, this function of Mps1 is not universally conserved as MELT motifs in *C. elegans* are phosphorylated by Polo-like kinase 1 (PLK1) [38], which has also been implicated in phosphorylating MELT motifs in human cells [57, 24]. Furthermore, Mps1 is dispensable for Bub3 localization to unattached KTs in *Drosophila* S2 cells [23]. Thus, if Bub3 binds to Spc105 then it occurs independent of phospho-regulation or is promoted by a different kinase.

Recruitment of PP1 to the N-terminus of KNL1 promotes de-phosphorylation of the MELT motifs, although the precise mechanism is unclear as recent work has shown that PP1 does not directly dephosphorylate MELT motifs [24]. Nonetheless, the KNL1-bound population of PP1 is a key contributor to SAC satisfaction [83, 109, 37, 92, 110] most likely through reducing the affinity of Bub3 for KNL1. Interestingly, the recruitment of PP1 to KNL1 is itself phospho-regulated by Aurora B kinase, which negatively regulates PP1 binding to the N-terminus of KNL1 [75, 7, 90]. During the process of biorientation, enzyme dominance shifts from Aurora B kinase to PP1 but it is unclear how this is accomplished. It is also unclear how MT binding - the other major N-terminal activity in KNL1 - impacts PP1 recruitment *in vivo* and contributes to SAC silencing.

2.2 Results

2.2.1 The Spc105-Bub3 interaction is phospho-regulated by Aurora B kinase in *Drosophila*

Spc105 contains divergent "MELT-like" Bub3-binding motifs with the consensus sequence EP[M/I]EE[E/D] [122] - referred to hereafter as "MEED" motifs. MEED motifs have a phospho-mimetic quality since the conserved serine/threonine residues in conventional MELT motifs are replaced by acidic residues. Since Mps1 is dispensable for Bub3 localization to unattached KTs in *Drosophila* cells [23] and the MEED

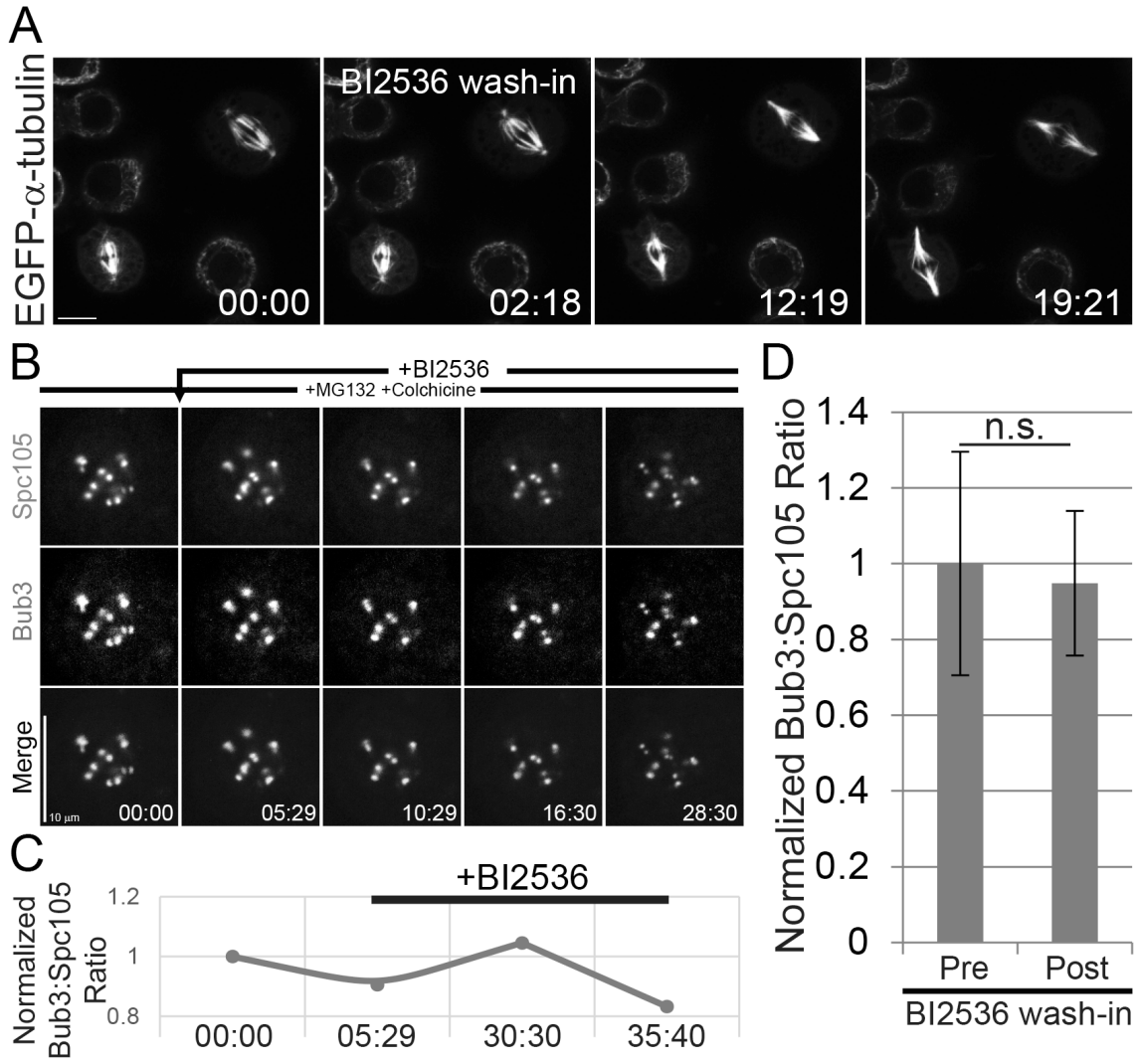

Figure 2.1. Aurora B, but not POLO, kinase activity is required for Bub3 localization to unattached KTs in *Drosophila* cells and promotes binding of Bub3 to Spc105 *in vitro* (A) Still frames from spinning disk confocal time-lapse imaging of EGFP-α-tubulin expressing cells pre- and post-BI2536 (1 μM) treatment. (B) Still frames from spinning disk confocal time-lapse imaging of a cell co-expressing Spc105-EGFP and Bub3-TagRFP-T treated with MG132 (10 μM) and colchicine (25 μM) and imaged as BI2536 (1 μM) was added to the imaging chamber. (C) Quantification of the ratio of normalized Bub3:Spc105 intensity over time in the BI2536-treated cell shown in "B". (D) Quantification of Bub3 levels at KTs in pre- and post- BI2536 wash-in experiments ($n = 5$ cells for the pre-wash-in condition and 4 cells for the post-wash-in condition).

motif regions have acidic and hydrophobic properties reminiscent of the PLK1 consensus motif [89], we tested if PLK1 (POLO in *Drosophila*) activity was required for Bub3 recruitment to unattached KTs in S2 cells. Cells co-expressing Spc105-EGFP

and Bub3-TagRFP-T were treated with colchicine to generate unattached KTs and MG132 to maintain a mitotic state. Cells with Bub3 at unattached KTs were visualized via 2-color, time-lapse confocal microscopy while introducing the PLK1 inhibitor BI2536 [117], which inhibits POLO activity in S2 cells as evidenced by rapid changes in metaphase spindle morphology (Figure 2.1 A). Inhibition of POLO did not result in a statistically significant reduction in Bub3 levels at KTs (Figure 2.2 A-D) revealing that POLO kinase activity is not a major contributor to Bub3 recruitment to unattached KTs in *Drosophila* cells.

Since a putative Aurora kinase motif [15] lies upstream of nearly every MEED motif in Spc105 [112, 126, 122], we next investigated the contribution of Aurora B kinase activity to Bub3 localization at unattached KTs. Addition of the *Drosophila* Aurora B kinase-specific inhibitor Binucleine 2 [34, 116] resulted in a rapid and significant (>80%) reduction of Bub3 from unattached KTs (Figs. 1A, B, S1E, and Videos 3, 4). These results revealed that Aurora B kinase activity is required for a significant majority of Bub3 binding to unattached KTs in *Drosophila* cells.

In order to directly test if Spc105 is a bona-fide substrate of Aurora kinase, *in vitro* kinase assays were conducted with budding yeast Ipl1 (Aurora kinase orthologue) and a purified portion of the central intrinsically disordered region (IDR) of Spc105 containing ten MEED motifs (10xMEED) each of which was preceded by a putative Aurora kinase consensus motif (Figure 2.2 C). Incubation of the 10XMEED with ATP and purified Ipl1, which was hyper-activated through fusion with the Sli15 (budding yeast INCENP) INBOX (gift of the Biggins Lab), yielded an evident shift on an SDS-PAGE gel compared to unphosphorylated control samples (Figure 2.2 D). Importantly, the slower mobility of Spc105 was abrogated in the presence of alkaline phosphatase, demonstrating that the observed shift was due to Aurora kinase-mediated phosphorylation.

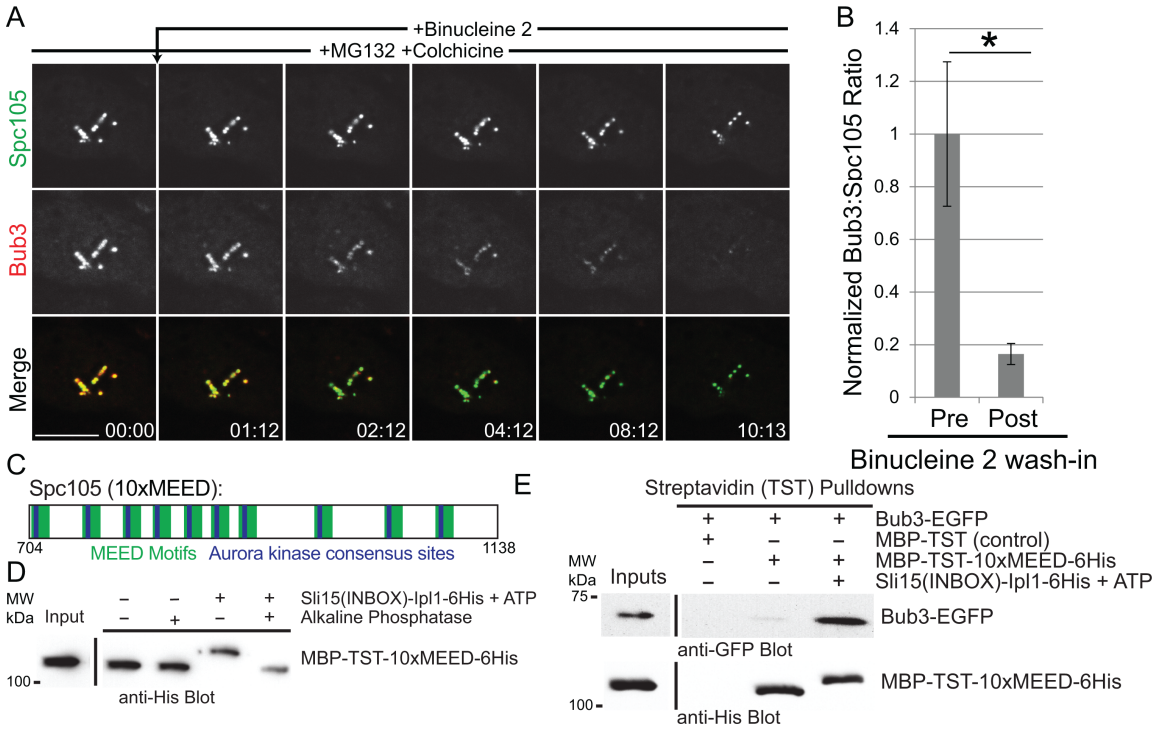

Figure 2.2. Aurora kinase phospho-regulates the Bub3-Spc105 interaction. (A) Still frames from spinning disk confocal time-lapse imaging of a cell co-expressing Spc105-EGFP and Bub3-TagRFP-T treated with MG132 (10 μM) and colchicine (25 μM). The Aurora B kinase inhibitor binucleine 2 (40 μM) was added to the imaging chamber $\sim$1 minute into the time-lapse. (B) Quantification of Bub3 signal ratioed to Spc105 signal intensity pre- and post- binucleine 2 treatment in wash-in experiments ($n = 8$ cells for pre-wash-in; $n = 12$ cells for post-wash-in). (C) Schematic of Spc105 (10xMEED). (D) Western blot of *in vitro* kinase assay reactions showing a pronounced shift in the migration of 10xMEED in the presence of activated Sli15(INBOX)-Ipl1. (E) Western blots for GFP (upper panel) and the His-tag (lower panel) of pulldowns showing that Bub3 interacts with 10xMEED and, to a much greater extent, with phospho-10xMEED, but not with MBP-TST. Scale bar is 10 μm. Error bars are SEM. Two-tailed p-value of Student's t-test is reported: * p-value<0.05.

With confirmation that 1) Aurora B kinase activity was required for Bub3 localization to unattached KTs in cells, and 2) Aurora kinase phosphorylates Spc105 *in vitro*, pulldown assays using purified Bub3-EGFP and either MBP-TST-tagged 10xMEED or MBP-TST control protein were conducted to determine if Spc105 and Bub3 directly interact and if phosphorylation increases their binding affinity. In the absence of phosphorylation, $\sim$2-fold more Bub3 bound to the 10xMEED than to the MBP-TST control ($n = 3$ independent experiments) (Figure 2.2 E). The binding

affinity was significantly boosted upon phosphorylation of Spc105 as the addition of ATP and activated Sli15-Ipl1 resulted in a ∼30-fold increase in Bub3 binding to the 10XMEED compared to the unphosphorylated MBP-TST ($n = 3$ independent experiments) (Figure 2.2 E).

2.2.2 Characterization of the MT binding activity of the N-terminal region of Spc105

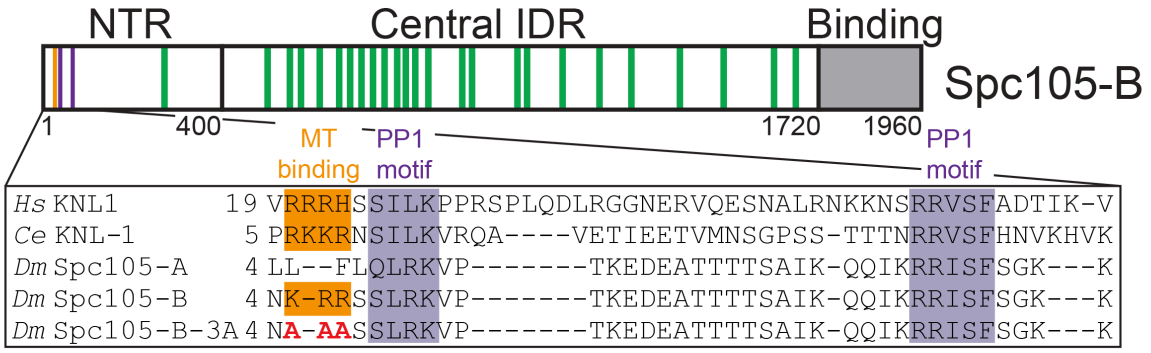

Figure 2.3. The NTR of Spc105 Schematic of *Drosophila* Spc105 highlighting the N-terminal region (NTR) and its alignment with conserved MT binding and PP1 binding motifs (Hs: *Homo sapiens*; Ce: *C. elegans*; Dm: *D. melanogaster*

Since Spc105 binding to MTs has not been demonstrated before, we next investigated if the N-terminal region (NTR) of Spc105 binds directly to MTs *in vitro*. There are two isoforms of Spc105 in *Drosophila*: Spc105-A and Spc105-B that differ only in the first nine amino acids such that Spc105-B possesses the conserved N-terminal MT binding patch while Spc105-A does not (Figure 2.3). MT binding activities of the Spc105 orthologues in yeast and worm were previously investigated using a microscopy-based assay where Spc105 or KNL-1 were coupled to polystyrene beads and incubated with taxol-stabilized MTs [37, 110]. In order to better control the binding conditions, we aimed to conduct TIRF-based imaging assays with purified Spc105-EGFP in the absence of polystyrene beads. However, the N-terminus of Spc105 was insoluble by conventional purification methods. The addition of N-terminal solubility tags such as sfGFP and MBP conferred solubility, but the protein

was insoluble after cleavage of the tags (unpublished data). Since intrinsically disordered proteins (IDPs), which are highly susceptible to proteolysis and aggregation, have been purified previously using buffers supplemented with arginine [9], we applied this method to the purification of the Spc105 NTR. Indeed, soluble Spc105 variants were purified in the presence of 500 mM arginine and subsequently diluted in buffer with a final concentration of 100 mM arginine, which did not compromise Spc105 solubility, for use in TIRF-based MT binding assays (include gels?).

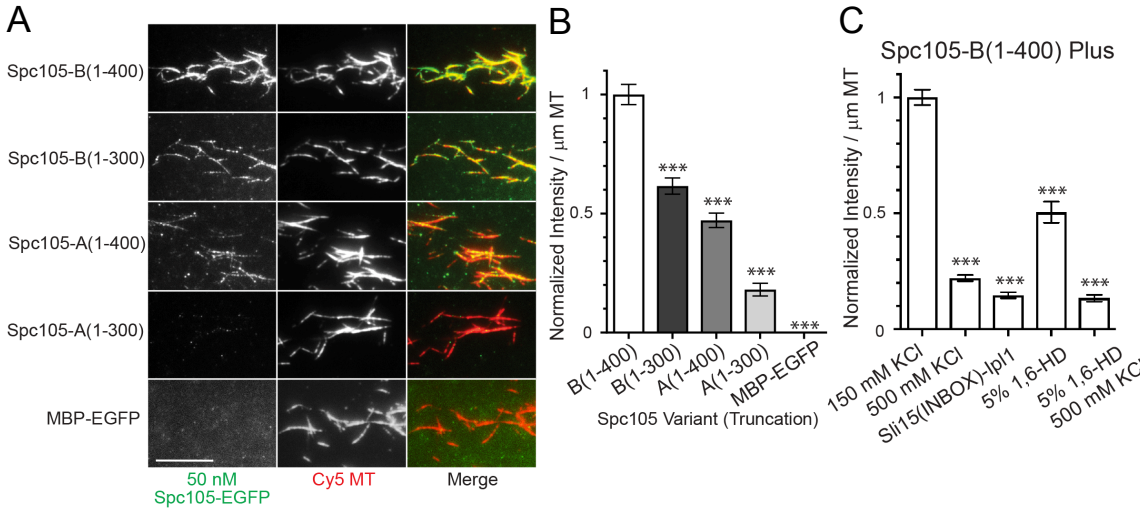

Figure 2.4. Characterization of MT binding by the NTR of Spc105 (A) Representative images of *in vitro* TIRF assays with taxol-stabilized Cy5-labeled MTs (red) plus 50 nM of the indicated Spc105-EGFP (green) truncations/variants. (B) Quantification of the background corrected intensity of each Spc105 protein (at 50 nM concentration) per micron of MT normalized to Spc105-B(1-400) (n = 150 MTs per Spc105 fragment from three independent experiments). (C) Quantification of intensity of 50 nM Spc105-B(1-400) per micron of MT in varying binding conditions normalized to Spc105-B(1-400) in 150 mM KCl (n = 150 MTs for 150 mM KCl, +Sli15(INBOX)-Ipl1, and 500 mM KCl conditions from three independent experiments; n = 75 MTs for 5% 1,6-HD and 5% 1,6-HD + 500 mM KCl from three independent experiments). Scale bar is 10 μm. Error bars are SEM. Two-tailed p-values of Student's t-tests are reported: *** p-value ¡ 0.0005 for pair-wise comparisons to the B(1-400) in "C" and the 150mM KCl in "D".

Spc105-B(1-400)-EGFP bound robustly to taxol-stabilized MTs *in vitro* at 50 nM concentration and could be readily detected on MTs at concentrations as low as 10 nM (Figure 2.4 A,B,C and unpublished data). To assess the binding efficiencies of

Spc105 variants (A vs. B) and truncations, a final concentration of 50 nM of each EGFP-tagged Spc105 protein was incubated with Cy5-labeled taxol-stabilized MTs in imaging chambers and visualized by TIRF microscopy. Binding was quantified by measuring the background-corrected fluorescence intensity of the EGFP signal per micron of MT for each Spc105 fragment and, for comparison, the data was normalized against Spc105-B(1-400). The order of binding efficiency from best to worst was: Spc105-B(1-400) set to 100%, Spc105-B(1-300) at 61.%, Spc105-A(1-400) at 47.5%, and Spc105-A(1-300) at 18% (Figure2 B,C, E). Taken together the data indicate that 1) the basic binding patch at the immediate N-terminus of Spc105-B, which is lacking in Spc105-A, makes an important contribution to MT binding, 2) the region between amino acids (aa) 300-400 of Spc105 contributes to MT binding efficiency, and 3) additional MT binding sites must be located at the N-terminus since Spc105-A(1-400) binds to MTs nearly as well as Spc105-B(1-300).

Binding relative to Spc105-B(1-400) 150 mM KCl

150 mM KCl	B(1-400)	B(1-300)	A(1-400)	A(1-300)
	100%	61.5%	47.5%	18.0%
B(1-400) Plus	14.6%	63.4%	12.5%	22.1%
	500 mM KCl	5% 1,6-HD	5% 1,6-HD 500 mM KCl	Sli15(INBOX) -Ipl1

Figure 2.5. Summary of the results from Figure 2.3 B,C.

We next focused on altering the experimental conditions of the binding assay using Spc105-B(1-400) to further dissect the nature of how Spc105 interacts with MTs (Figure 2.4 B, C). We first examined the contribution of electrostatic interactions by repeating the MT binding experiment in the presence of high salt (500mM KCl), which reduced binding of Spc105-B(1-400) by ∼85% - a level comparable to Spc105-A(1-300) binding at 150 mM KCl. It is well-established that electrostatic

interactions between basic MT binding patches and negatively charged MTs can be disrupted by phosphorylation. Indeed, Spc105-B(1-400) contains multiple Aurora B consensus sites that are well-conserved and overlap with the basic patch and the PP1 binding motifs. Phospho-mimetic mutants of the Aurora sites in human and worm KNL1 abolished MT binding of the N-terminus in co-sedimentation assays [131]. In agreement with this finding, we found that phosphorylation with Sli15-Ipl1, which resulted in an observable shift in Spc105-B(1-400) on an SDS-PAGE gel (Figure 2.7), reduced MT binding of Spc105-B(1-400) (22.1%) to nearly the same extent as the high salt condition (14.6%). The importance of electrostatic interactions was further evidenced by the fact that the affinity of Spc105-B(1-400) for soluble tubulin was significantly reduced in a triple alanine mutant (3A) of the N-terminal basic patch (Figure 2.6 F).

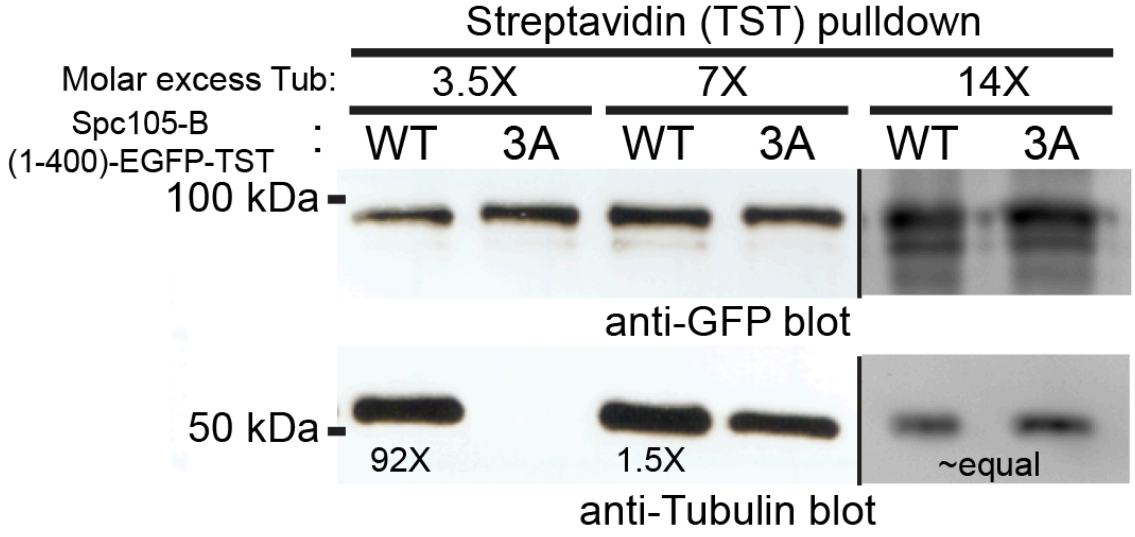

Figure 2.6. Characterization of MT binding by the NTR of Spc105. Western blot of GFP (upper panel) and tubulin (lower panel) for pulldown assays. Tubulin intensity was quantified in ImageJ and the relative signal intensities of tubulin binding to the WT versus 3A mutant is indicated for each concentration of tubulin in the anti-tubulin blot panel.

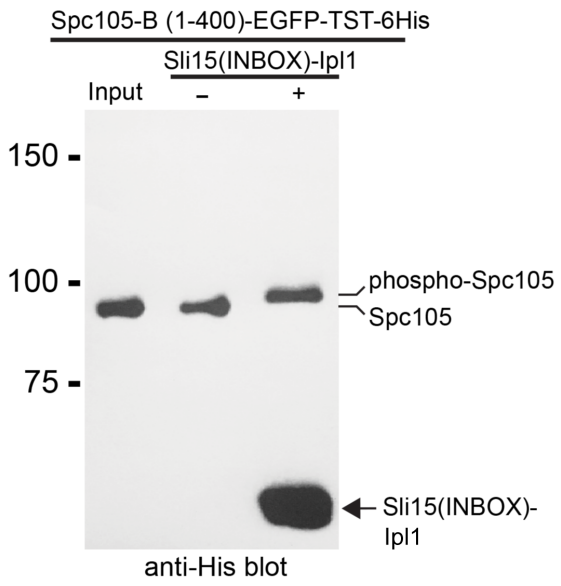

Figure 2.7. *In vitro* phosphorylation of the NTR of Spc105 by Aurora Kinase. Western blot for the His-tag of Spc105-B(1-400) showing a gel shift when incubated with ATP + Sli15(INBOX)-Ipl1, indicating that Ipl1 phosphorylates the NTR of Spc105-B. This phosphorylated Spc105-B(1-400) was used in the *in vitro* TIRF-based MT binding assays reported in Figures 2.3 D, E.

2.2.3 Deletion of the Spc105 NTR results in a metaphase delay with hyper-stretched KTs that retain elevated levels of Bub3

We next characterized how the NTR of Spc105 contributes to cell division by transfecting S2 cells with a truncated version of Spc105 lacking the first 400 amino acids (Spc105ΔN). While stable cells that expressed full length Spc105 were readily made, we were unable to make stable cell lines expressing Spc105ΔN due to the mutant exhibiting a dominant negative effect. Thus, all experiments with Spc105ΔN were done via transient transfections in which dividing cells expressing the mutant were found in the population, albeit with decreasing frequency, over the course of ∼7-10 days. When Spc105ΔN-EGFP was transfected into cells stably expressing TagRFP-T-α-tubulin we found that it localized normally, which was expected since the C-terminus of Spc105 targets it to the KT [125]. Interestingly, cells expressing the truncation were often delayed in metaphase when compared to cells that were not

expressing Spc105ΔN in the same imaging chamber (Figure 2.8 A). Furthermore, cells expressing Spc105ΔN exhibited KT hyper-stretch as the distance between bioriented kinetochores (K-K) increased to 1.33 ± 0.02 μm (mean ± SEM) compared to 1.19 ± 0.02 μm in non-expressing cells (Figure 2.8 B). Although the NTR of Spc105 binds directly to MTs *in vitro*, in cells the NTR was required for timely SAC satisfaction but was dispensable for the establishment of stable KT-MT attachments and chromosome biorientation.

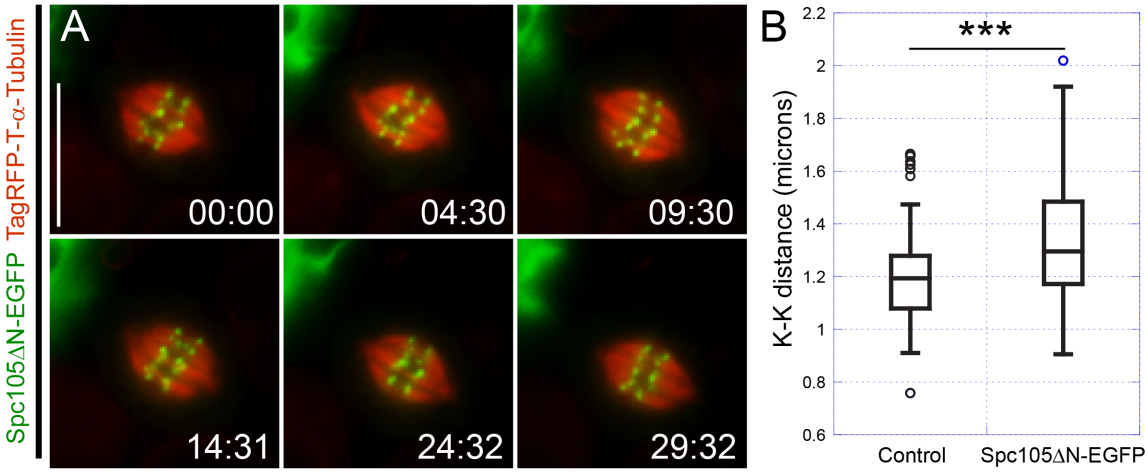

Figure 2.8. Deletion of the NTR of Spc105 results in a metaphase delay (A) Still frames from widefield time-lapse imaging of a cell expressing Tag-RFP-T-α-tubulin (red) and Spc105ΔN-EGFP (green) delayed in metaphase. (B) Quantification of the distance between bioriented KTs in metaphase (K-K distance) shown in box-and-whisker plots (control, $n = 144$ KT pairs from 17 cells; Spc105ΔN, $n = 171$ KT pairs from 15 cells). Scale bar is 10 μm. Error bars are SEM. Two-tailed p-values of Student's t-tests are reported: *** p-value < 0.0005.

The observed metaphase delay in Spc105ΔN-expressing cells led us to next examine the behavior of the checkpoint protein Bub3, which was already shown to bind directly to the central IDR of Spc105 *in vitro* (Figure 2.2 E). Time-lapse imaging of Bub3-TagRFP-T-expressing cells revealed that Bub3 levels were highest at misaligned KTs and became depleted from KTs during chromosome congression until reaching its nadir (pre-anaphase onset) at bioriented KTs, which retained ∼20% of the Bub3 that was originally at misaligned KTs (Figure 2.9 A,C). Interestingly, bioriented KTs

in Spc105ΔN-expressing cells retained 2-fold higher levels of Bub3 (∼46% relative to misaligned KTs) than was measured at bioriented KTs in control cells (Figure 2.9 B,C). Thus, deletion of the NTR of Spc105 resulted in a metaphase delay with hyper-stretched KTs that retained elevated levels of the checkpoint protein Bub3.

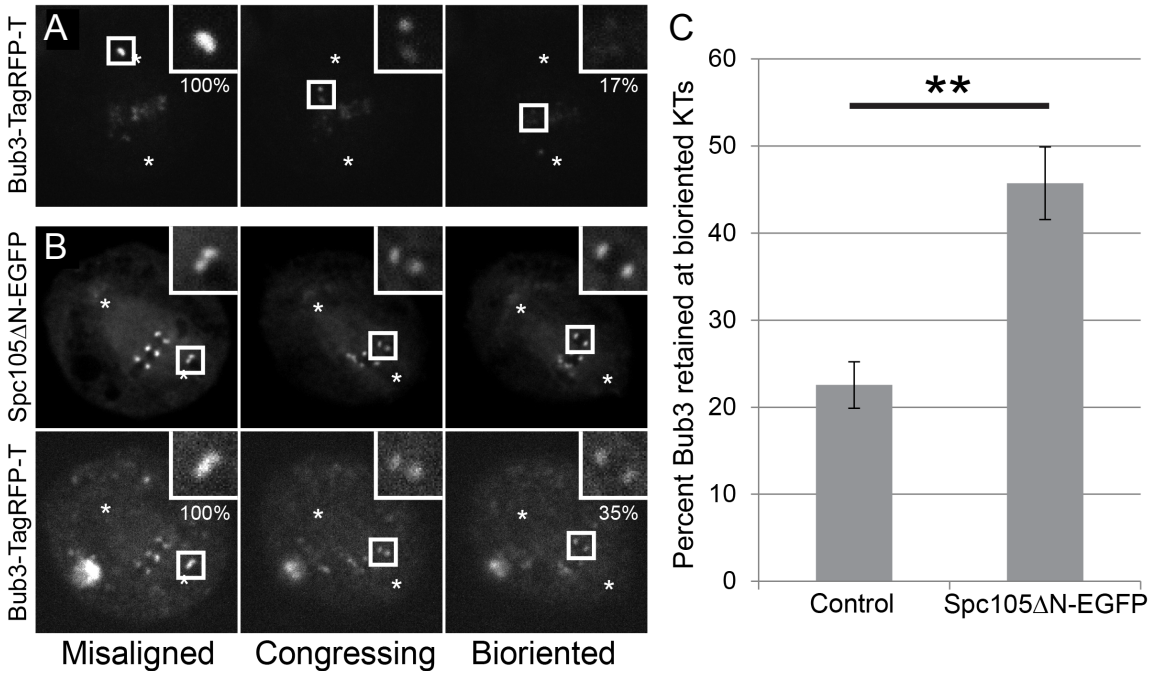

Figure 2.9. Deletion of the NTR of Spc105 results in elevated levels of Bub3 retained at bioriented KTs (A) Representative images of still frames from spinning-disk confocal time-lapse imaging of a control cell expressing only Bub3-TagRFP-T with insets highlighting Bub3 levels that decline as a misaligned KT pair becomes bioriented. (B) Representative images of still frames from spinning-disk confocal time-lapse imaging of a cell co-expressing Spc105ΔN-EGFP and Bub3-TagRFP-T with insets highlighting the congressing KTs. (C) Quantification of average Bub3 retention at bioriented KTs relative to misaligned KTs in control cells compared to Spc105ΔN-expressing cells (Control, $n = 9$ cells; Spc105ΔN, $n = 20$ cells). In "A" and "B", the asterisks denote locations of the spindle poles and the percent below the insets indicate the relative levels of Bub3 at the pair of misaligned and bioriented sister KTs. Scale bar is 10 μm. Error bars are SEM. Two-tailed p-values of Student's t-tests are reported: ***p-value < 0.0005.

2.2.4 Deletion of the Spc105 NTR results in the establishment of hyper-stable kinetochore-microtubule attachments independent of Aurora B kinase mis-localization

While the KT hyper-stretch phenotype observed in Spc105ΔN-expressing cells was indicative of stable (or potentially hyper-stable) KT-MT attachments, we next sought to more quantitatively assess the nature of attachments by measuring photo-activatable (PA)-GFP-α-tubulin turnover in metaphase spindles. Cells co-transfected with PA-GFP-α-tubulin and either Spc105ΔN (experimental) or full length Spc105-B (control) were subjected to spinning-disk confocal time-lapse imaging during which 405 nm laser light was focused on a rectangular region adjacent to the metaphase plate to locally photo-activate PA-GFP-α-tubulin molecules in the spindle (Figure 2.10 A). Broadly speaking, mitotic spindles are comprised of KT-MTs, which are more stable, and non-KT-MTs that are more dynamic. The relative abundance and stability (T1/2) of each MT population can be measured in a spindle by quantification of its background- and bleach-corrected PA-GFP signal as it dissipates over time and applying a double-exponential fit to the data [20] (Figure 2.10 B). The flux rate (poleward movement of MT polymer within the spindle) was quantified by measuring the movement of the photo-activated region over time.

PA-GFP-α-tubulin turnover measurements revealed that 75% of the spindle MTs in Spc105ΔN-expressing metaphase cells were KT-MTs compared to only 20% of the spindle MTs in control cells expressing Spc105-B (Figure 2.10 C). Interestingly, consistent with the prior K-K measurements, KT-MTs were more stable in Spc105ΔN-expressing cells as the KT-MT T1/2, which is the time for half of the MT polymer to turnover, was 6.6 minutes compared to 5.1 minutes in Spc105-B-expressing control cells. The stability of non-KT-MTs was comparable between experimental and control cells as the non-KT-MT T1/2 was measured to be 32.4 seconds and 37.6 seconds for metaphase spindles in Spc105-B- and Spc105ΔN-expressing cells respec-

tively. Finally, the flux rate was reduced significantly to 0.4 μm/minute in cells expressing Spc105ΔN compared to 1.0 μm/minute in control cells. Thus, expression of Spc105ΔN results in a metaphase delay with elevated Bub3 levels at bioriented KTs that are hyper-stretched, due to the establishment of more stable KT-MT attachments, within metaphase spindles that exhibit suppressed poleward flux.

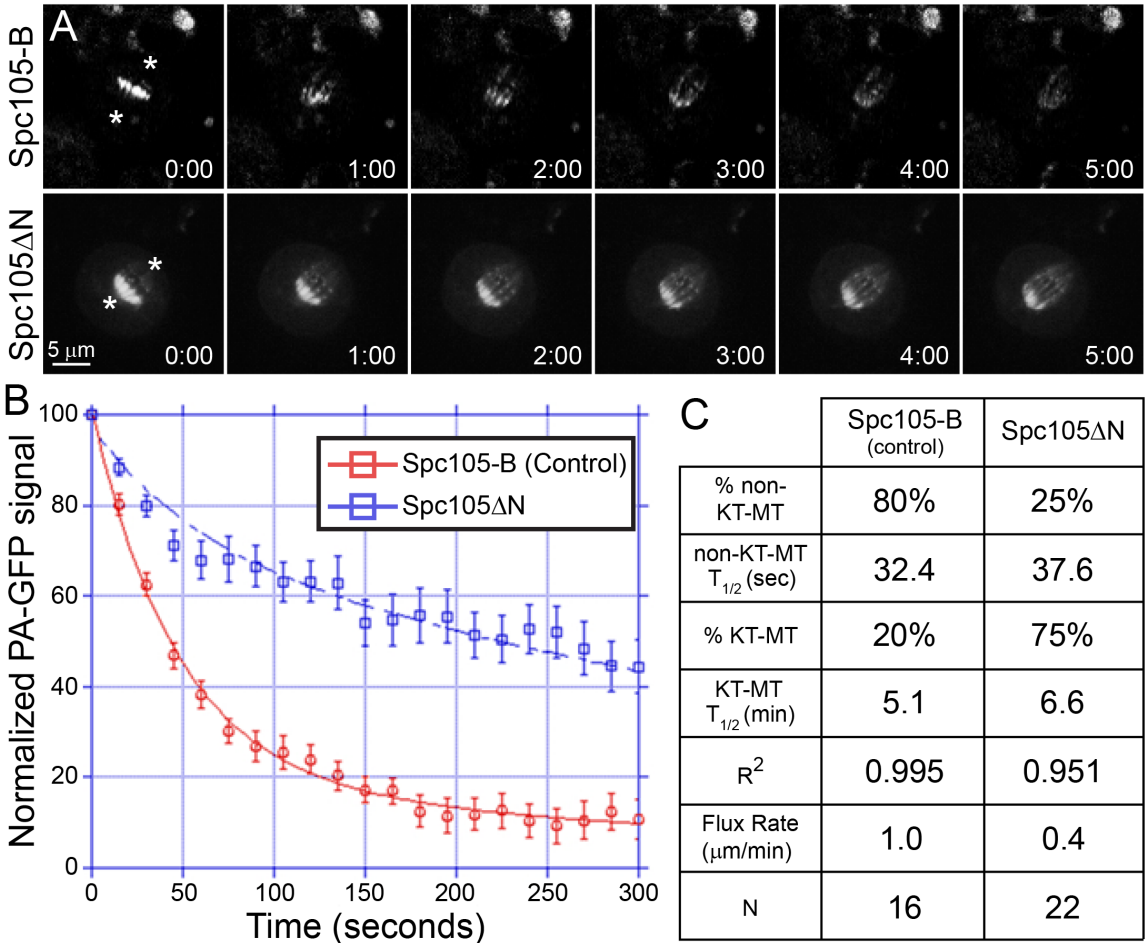

C

	Spc105-B (control)	Spc105ΔN
% non-KT-MT	80%	25%
non-KT-MT $T_{1/2}$ (sec)	32.4	37.6
% KT-MT	20%	75%
KT-MT $T_{1/2}$ (min)	5.1	6.6
R^2	0.995	0.951
Flux Rate (µm/min)	1.0	0.4
N	16	22

Figure 2.10. Spc105ΔN-expressing cells establish hyper-stable KT-MT attachments (A) Still frames from spinning-disk confocal time-lapse imaging of a metaphase cell co-expressing Spc105-B (top) or Spc105ΔN (bottom) and photo-activatable (PA)-GFP-α-tubulin. (B) Double exponential fit (generated in KaleidaGraph) of the decay in PA-GFP signal over time in Spc105-B- and Spc105ΔN-expressing cells (control, $n = 16$ cells; Spc105ΔN, $n = 22$ cells). (C) Summary of the measurements from the double exponential fit applied in "B".Scale bars, 5 μm (A, B).Error bars are SEM.

Prior work reported that the N-terminus of human KNL1 promoted Aurora B activity and its deletion reduced Aurora B-mediated phosphorylation of the outer KT, which resulted in premature stabilization of KT-MT attachments [11]. Thus, reduced Aurora B activity could explain the increased KT-MT attachment stability observed in Spc105ΔN expressing cells. Multiple populations of active Aurora B kinase have been identified across the centromere and kinetochore in mammalian cells [27]. We previously observed distinct populations of active, phosphorylated Aurora B kinase by immunostaining with two phospho-Aurora kinase antibodies [138]. Staining with one antibody (referred to as pABK-CEN) preferentially labeled a population of centromeric phospho-Aurora B kinase that persistently localized to the inner centromere at both unattached and bioriented KTs. The other antibody (referred to as pABK-KT) preferentially labeled a more punctate population of phospho-Aurora B kinase in close proximity to Ndc80 that was high at unattached KTs and depleted from bioriented KTs.

Immunofluorescence for pABK-CEN or pABK-KT was conducted on colchicine-treated cells transfected with Spc105ΔN to determine if either population of active Aurora B kinase was mis-localized in cells expressing the mutant. The levels of both populations of phospho-Aurora B kinase were not significantly different between Spc105ΔN-expressing cells and control cells on the same coverslip that were not expressing Spc105ΔN (Figure 2.11 A-C). We also found that pABK-CEN localized normally in metaphase cells expressing Spc105ΔN when compared to control cells that were not (Figure 2.11 D). The KT population of phospho-Aurora B kinase was not evaluated in metaphase cells since it is depleted from bioriented KTs. Thus, distinct from the consequence of deleting the N-terminal region of human KNL1, deletion of the NTR of Spc105 did not evidently impact Aurora B kinase activity at centromeres or kinetochores. Aurora B kinase may be differentially regulated visa vie Spc105 in *Drosophila*, alternatively the observed differences could be attributed to the fact

that a smaller portion of the N-terminus (relative to the human N-terminal truncations), containing only 1/∼25 MEED motifs, was deleted in Spc105ΔN. Regardless, the K-K hyper-stretch and KT-MT hyper-stability phenotypes in cells expressing Spc105ΔN were unlikely due to significant downregulation of Aurora B kinase activity – a conclusion that is internally consistent with the observed elevation in Bub3 levels at bioriented KTs in Spc105ΔN-expressing cells since Bub3 localization to KTs predominantly relies on Aurora B kinase activity in *Drosophila* cells (Figure 2.2 A-C).

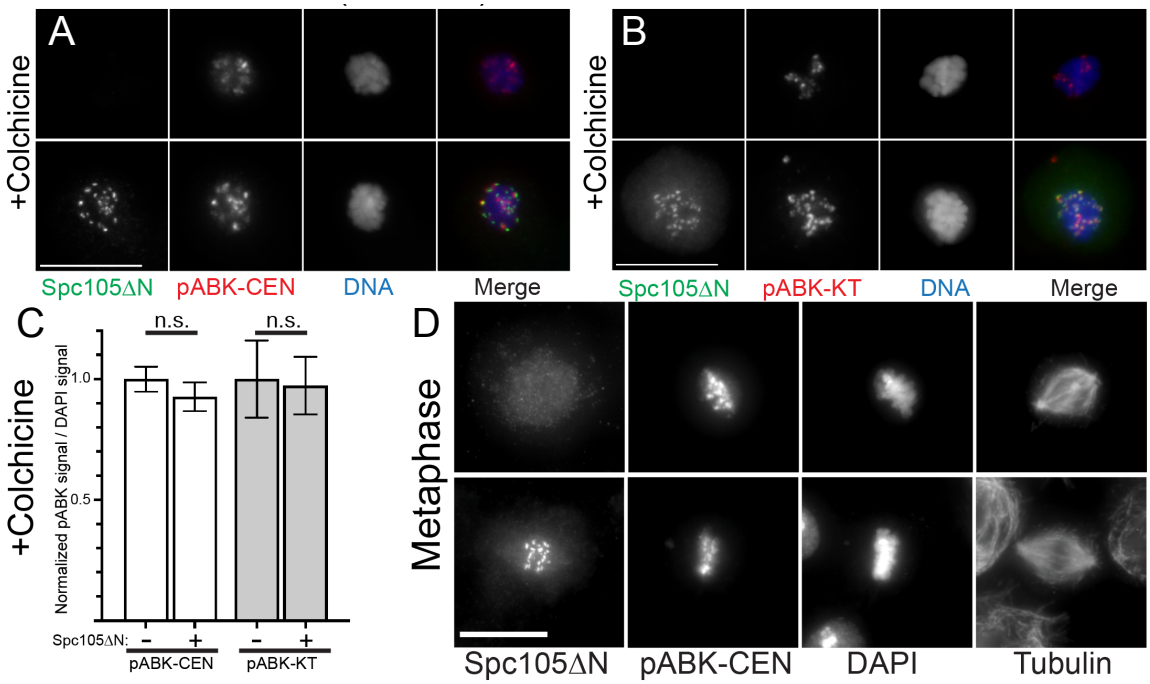

Figure 2.11. Spc105ΔN-expressing cells establish hyper-stable KT-MT attachments independent of Aurora localization (A) Maximum projections of widefield fluorescence Z-sections of Spc105ΔN-transfected cells treated with colchicine (25 μM) overnight and stained with anti-pABK-CEN (red), anti-GFP (green), and DAPI (blue). (B) Maximum projections of widefield fluorescence Z-sections of Spc105N-transfected cells treated with colchicine (25 μM) and stained with anti-pABK-KT (red), anti-GFP (green), and DAPI (blue). (C) Quantification of normalized pABK:DAPI signal (n = 30 cells from three independent experiments for each condition). (D) Representative maximum projections of widefield fluorescence Z-sections of Spc105ΔN-transfected cells in metaphase stained with anti-GFP (Spc105ΔN), anti-pABK-CEN, DAPI, and anti-Tubulin. Non-expressing and expressing cells from the same coverslips are shown in "A", "B", and "C". Scale bars 10 μm (A, B, D). Error bars are SEM. Two-tailed p-values of Student's t-tests are reported: n.s. (not significant) = p-value>0.05.

2.2.5 The Spc105 NTR is the primary receptor for PP1-87B at bioriented KTs in *Drosophila* cells

In addition to MT binding activities, the NTR of Spc105 has two well-conserved PP1 binding motifs [75, 109, 37, 78, 7] (Figure 2.3 A). Depletion of the PP1 orthologue (PP1-87B) from S2 cells yielded the same phenotype observed in Spc105ΔN-expressing cells - namely a metaphase delay with stable KT-MT attachments [85]. Thus, we characterized PP1-87B in living cells and investigated whether deletion of the Spc105 NTR impacted PP1-87B localization to KTs. Stable S2 cells co-expressing RFP-PP1-87B and EGFP-α-tubulin were generated to visualize the localization of PP1 throughout mitosis in living cells, which has been quite limited to date [75]. PP1-87B enveloped the body of the mitotic spindle throughout mitosis in a manner reminiscent of spindle matrix components [128, 103, 102, 104, 73] without apparent enrichment on spindle MTs, but with discrete puncta evident at the end of k-fiber bundles in metaphase (Figure 2.12 A). Indeed, EGFP-PP1-87B co-localized with Spc105-TagRFP-T from metaphase through anaphase (Figure 2.12 B). We next co-transfected PP1-87B and either full length Spc105-B or Spc105ΔN to characterize how PP1 localization was affected by deletion of the NTR (Figure 2.13 B). A linescan-based method was used to quantify PP1-87B localization to KTs in the context of the high local spindle matrix-like signal. In brief, linescans were drawn through bioriented KT pairs and if a PP1-87B peak 1) co-localized with a Spc105 peak, and 2) was at least 10% higher than the local spindle PP1-87B signal then the KT was scored as PP1-87B positive (Figure 2.13 B). Using this method, 69.4 ± 4.1% (mean ± SEM) of KTs in Spc105-B-expressing cells scored as PP1-positve versus only 0.4 ± 0.4% in Spc105ΔN-expressing cells revealing that the NTR of Spc105 is the primary binding site to localize PP1-87B to bioriented KTs in *Drosophila* (Figure 2.13 C).

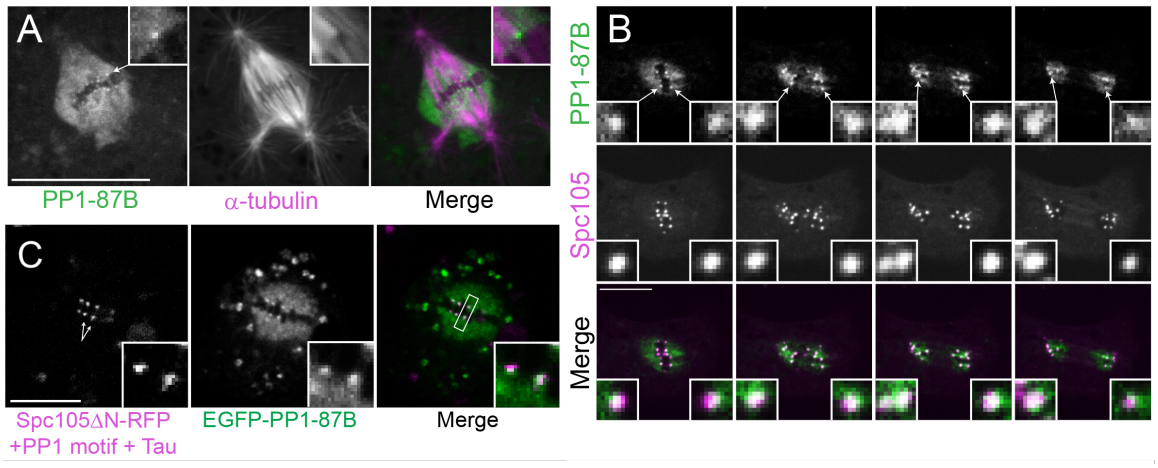

Figure 2.12. Dissecting the relative contributions of PP1-87B recruitment and MT binding by Spc105 to SAC satisfaction (A) Maximum projection of spinning disk confocal Z-sections of a metaphase cell co-expressing RFP-PP1-87B (green) and EGFP-α-tubulin (magenta). Arrow points to the puncta of PP1-87B shown in the zoomed inset. (B) Still-frames from a spinning disk confocal time-lapse of a cell co-expressing RFP-PP1-87B (green) and Spc105-EGFP (magenta) progressing from metaphase through anaphase. Arrows point to the KTs shown in the zoomed insets. (C) Spc105ΔN-TagRFP-T + PP1 motif + Tau (magenta) co-localizes with EGFP-PP1-87B (green) in a representative spinning disk confocal plane. Arrows point to the KTs shown in the zoomed insets. Boxed region highlights the KT pair subjected to linescan analysis shown in Figure 2.12 B.

2.2.6 The N-terminal activities of Spc105 contribute to SAC satisfaction

We next sought to understand the molecular mechanisms by which the NTR of Spc105 contributed to timely SAC satisfaction. The Spc105ΔN truncation removed both PP1-87B and MT binding activities. In order to dissect the relative contributions of each of these activities to Spc105's function in SAC satisfaction, Spc105 chimeras were created that restored each activity individually and in combination (Figure 2.13 A). We conducted live-cell imaging of cells expressing Spc105-B, Spc105ΔN, or one of the chimeras to measure metaphase duration. We also imaged cells that co-expressed fluorescent protein tagged PP1-87B and Spc105-B, Spc105ΔN, or one of the chimeras to measure the efficiency of PP1-87B recruitment to bioriented KTs (Figure 2.13 C,D). Metaphase duration, which was defined as the time between biorientation of the last pair of sister KTs and anaphase onset, was 8.7 $\pm$ 0.8 minutes (mean $\pm$ SEM)

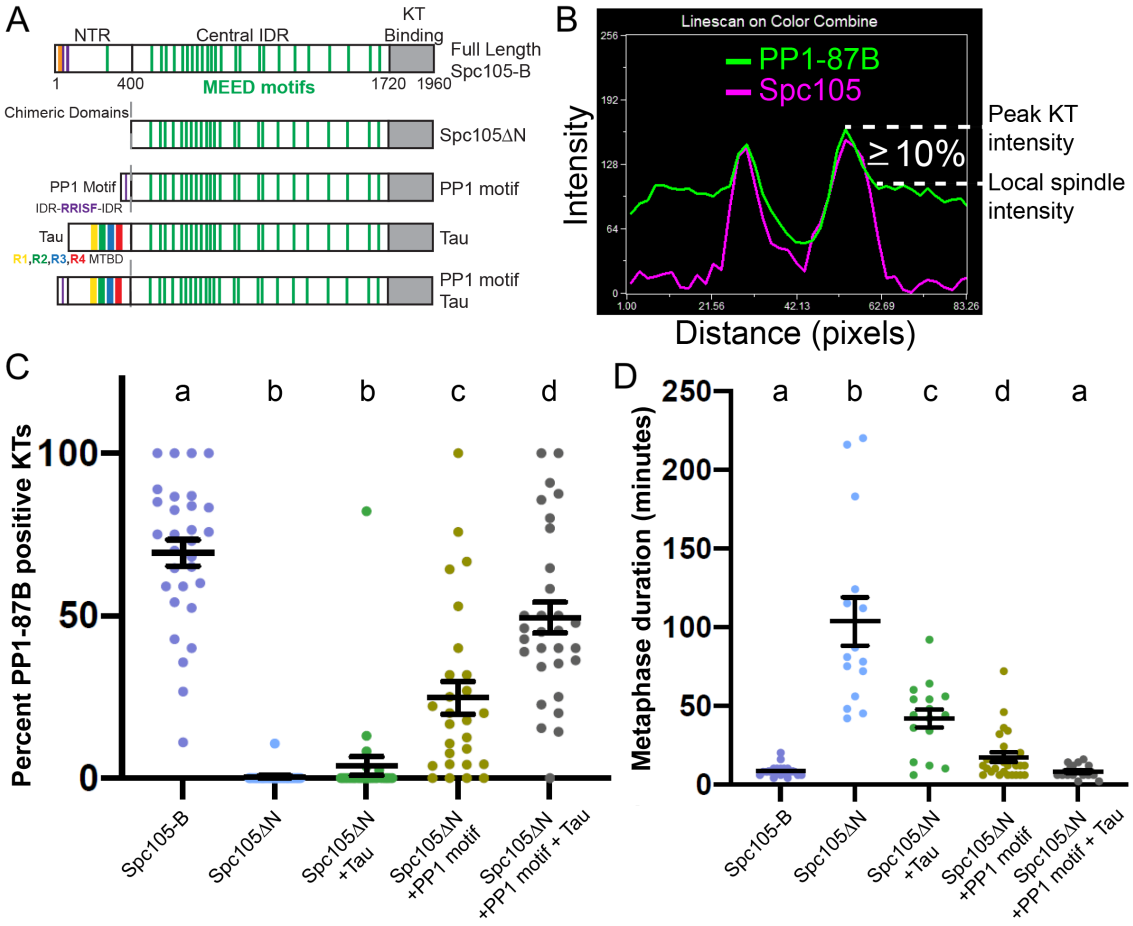

Figure 2.13. Dissecting the relative contributions of PP1-87B recruitment and MT binding by Spc105 to SAC satisfaction (A) Schematics of full-length Spc105-B, Spc105ΔN, and the Spc105ΔN chimeras. (B) Representative linescan on the merged image shown in "D" highlighting how PP1-87B positive KTs were identified. (C) Percent of PP1-87B positive KTs in cells co-expressing fluorescently tagged PP1-87B and Spc105-B, Spc105ΔN, or the indicated Spc105ΔN chimera (Spc105-B, $n = 30$ cells; Spc105ΔN, $n = 28$ cells; Spc105ΔN + Tau, $n = 29$ cells; Spc105ΔN + PP1 motif, $n = 27$ cells; Spc105ΔN + PP1 motif + Tau, $n = 30$ cells). (D) Metaphase durations (defined as the time between biorientation of the last pair of sister KTs and anaphase onset) in cells expressing Spc105-B, Spc105ΔN, or the indicated Spc105ΔN chimera (Spc105-B, $n = 20$ cells; Spc105ΔN, $n = 15$ cells; Spc105ΔN + Tau, $n = 16$ cells; Spc105ΔN + PP1 motif, $n = 26$ cells; Spc105ΔN + PP1 motif + Tau, $n= 20$ cells). Scale bars, 10 m. Error bars are SEM. Each dot in the scatter plots represents an individual cell. An average of 24 KTs per cell were analyzed for the data presented. In "C" Different letters above each scatter plot column indicate significant differences ($p<0.05$) as determined by two-tailed Student's t-tests for all pairwise combinations.Same letters indicate that the difference is not significant ($p<0.05$).

in control cells expressing full length Spc105-B. By contrast, Spc105ΔN-expressing cells delayed in metaphase for 104 ± 15 minutes. Replacing the NTR of Spc105 with the intrinsically disordered microtubule-associated protein dTau (*Drosophila* Tau homologue) resulted in a reduction in the metaphase delay to 42 ± 6 minutes; yet the percent of PP1-87B positive KTs (3.8 ± 2.8%) was not statistically significantly different than that measured in Spc105ΔN-expressing cells (0.4 ± 0.4%) (Figure 2.13 C,D). Thus, MT binding by the Tau-Spc105ΔN chimera contributed to the timing of SAC satisfaction independent of recruiting detectable levels of PP1-87B above the levels observed for Spc105ΔN.

To test the contribution of PP1-87B recruitment to SAC satisfaction, a second chimera was generated in which the PP1-binding motif (RRISF) flanked by IDRs was introduced at the N-terminus of Spc105ΔN (Figure 2.13 A). Addition of the PP1 motif resulted in a statistically significant increase in the percentage of PP1-87B positive KTs (24.8 ± 5.1%) relative to cells expressing either the Spc105ΔN or the Tau-Spc105ΔN chimera (Figure 2.13 C). Metaphase duration in cells expressing the PP1 chimera was 17.2 ± 3.0 minutes; a rescue that was considerably stronger than Tau-Spc105ΔN, but not a complete rescue as metaphase was still statistically significantly longer (∼2X) than in control cells (Figure 2.13 D). A third chimera introducing both the PP1- and MT-binding activities into Spc105ΔN was generated that included the RRISF site followed by dTau (Figure 2.13 A). Interestingly, the combination of the PP1 motif and Tau resulted in higher levels of PP1 recruitment to KTs (49.5 ± 4.8%) than the PP1 motif alone, but statistically significantly lower than the 69.4 ± 4.1% measured in Spc105-B-expressing control cells (Figure 2.13 C). Nonetheless, expression of the PP1 motif+Tau-Spc105ΔN chimera produced a complete rescue of the metaphase delay phenotype with a metaphase duration of 8.2 ± 0.8 minutes – statistically indistinguishable from the 8.7 ± 0.8 minutes measured in control cells (Figure 2.13 D). Taken together, the data from the chimeras demonstrated that,

consistent with prior work on *C. elegans* KNL-1 [37], PP1 recruitment and, to a lesser extent, MT-binding activity in the NTR of Spc105 make separable contributions to SAC satisfaction in *Drosophila* cells.

2.3 Discussion

2.3.1 The phospho-regulatory circuit in *Drosophila*

Phosphorylation of repeated motifs in KNL1 orthologues is the key mediator of checkpoint protein recruitment to KTs in every model system that has been examined with the exception of flies. This work clarifies the picture in *Drosophila* by demonstrating that a phospho-regulatory circuit exists that relies on Aurora B kinase activity, rather than Mps1 or PLK1, promoting the interaction between Spc105 and Bub3. We do not exclude the possibility that Aurora A kinase, which targets KT substrates [28] especially near spindle poles [19, 138], may also contribute to this mechanism. The fact that Bub3 binds to unphosphorylated 10xMEED *in vitro* suggests that lower affinity interactions between the two proteins exist in the absence of phosphorylation, potentially due to electrostatic interactions between the phosphomimetic MEED motifs in Spc105 and Bub3. Aurora A kinase activity and/or direct electrostatic interactions independent of phosphorylation may account for the residual levels of Bub3 observed at unattached KTs in cells following Aurora B kinase inhibition (Figure 2.2 B). Further investigation of this phenomenon and the nature of the Bub3-Spc105 interface and how it is regulated is warranted. Although Mps1 is not directly involved in the regulation of Bub3 binding to kinetochores in *Drosophila* [23], our findings demonstrate that the utilization of a phospho-regulatory circuit (here controlled by Aurora B) is evolutionarily conserved in flies.

Current models hold that recruitment of PP1 to the NTR of KNL1 homologues contributes to SAC satisfaction by promoting dephosphorylation of the MELT motifs and, consequently, reduction of their affinity for Bubs. Similar phospho-regulatory

mechanisms are likely to promote SAC satisfaction in *Drosophila* since it is well-established that PP1 opposes Aurora B kinase activity. Interestingly, a prior study in *Drosophila* reported that BubR1 recruitment to KTs and checkpoint function were unaffected in embryos expressing Spc105 lacking a portion of the central IDR, leading the authors to conclude that the middle region of Spc105 is dispensable for its function in flies [112]. Yet our findings support the conclusion that the Spc105 IDR is a critical platform for SAC signaling in *Drosophila*. One possible explanation for this discrepancy is that the mutant used in the prior study possessed more than the single MEED motif presumed at that time since subsequent analyses identified at least 6 more repeats in *Drosophila* Spc105 including some outside of the deleted region [126, 122]. Importantly, the presence of just one additional motif may support SAC signaling in *Drosophila* given that as few as 2-3 MELT motifs are sufficient for KNL1 function in human cells [140].

2.3.2 Implications for MT binding by Spc105 orthologues

In this study we demonstrated that *Drosophila* Spc105 binds microtubules. Our results support the interpretation that affinity for the MT is mediated by electrostatic interactions between basic patches in the first 300 aa of Spc105 and that higher avidity is accomplished through oligomerization via hydrophobic interactions between aa 300 - 400. While the data suggests that the basic patch at the immediate N-terminus (present only in the Spc105-B variant) is the highest affinity interaction site, additional lower affinity basic patches must exist in the N-terminal region since Spc105-A(1-400) binds to MTs nearly as well as Spc105-B(1-300), which our model would attribute to Spc105-A(1-400) having decreased affinity, but increased avidity compared to Spc105-B(1-300). Indeed, recent work has identified other basic regions beyond the immediate N-terminus that contribute to MT binding in human KNL1 and budding yeast Spc105 [7, 110]. Furthermore, a hydrophobic region in the first

~240 aa of *C. elegans* KNL-1 has been shown to mediate oligomerization *in vitro*. Interestingly, deletion of this region phenocopied a basic patch MT binding mutant in *C. elegans* as both mutants exhibited a reproducible delay in anaphase onset [37, 61]. As in other aspects of kinetochore biology, this mechanism suggests multiple and parallel low-affinity interactions additively contribute to functionality *in vivo*.

2.3.3 The MT binding and PP1-recruiting activities in the Spc105 NTR regulate SAC signaling but do not contribute to KT-MT attachment stability

Despite the fact that the NTR of Spc105 binds directly to MTs, this activity is not required for establishing stable end-on KT-MT attachments in cells and its deletion results in a metaphase delay that is not a consequence of defective KT-MT attachment stability. What, therefore, is the biological role of the KT-MT interaction mediated by Spc105? Our data are consistent with the interpretation that MT binding by the NTR of KNL1 acts as a SAC sensor [37] rather than in establishing stable, load-bearing KT-MT attachments capable of supporting congression and segregation [11, 140]. It is also noteworthy that phenotypes associated with Spc105ΔN expression (hyper-stretched and hyper stable KT-MT attachments with reduced spindle flux) are identical to those observed in mammalian PtK1 cells following micro-injection of an antibody that binds to the N-terminal region of the Ndc80 complex component HEC1 [26]. Thus, it would be interesting to investigate the interplay between the NTR of Spc105 and the Ndc80 complex given the latter's role as the key KT-MT interface and mediator of stable end-on attachments.

The KNL1-bound pool of PP1 has also been implicated in promoting KT-MT attachment stability [75, 83]. The facts that 1) Spc105ΔN-expressing cells fail to satisfy the SAC with normal kinetics, yet 2) establish hyper-stable KT-MT attachments that 3) fail to recruit PP1-87B supports the conclusion that the Spc105-bound

pool of PP1-87B promotes SAC satisfaction but not KT-MT attachment stability in *Drosophila* cells, which fully agrees with key findings of a recent study of Spc105 in budding yeast [110].

2.3.4 PP1 recruitment by Spc105 and synergy between the MT- and PP1-binding activities

The Spc105 chimeras offer a physiological context for understanding the relevant aspects of PP1 recruitment and MT binding by KNL1 *in vivo*. Multiple studies have identified the second motif (RVXF) as the key binding site for PP1 [75, 109, 37, 7], but the SILK and RVXF motifs have also been shown to work co-operatively to mediate the highest affinity interaction between PP1 and KNL1 as well as other substrates [50, 83, 7]. The fact that the RRISF-Spc105ΔN chimera recruited less PP1-87B than full length Spc105-B supports the conclusion that both the SILK and RVXF motifs are required for maximal PP1 recruitment in vivo, consistent with *in vitro* data [83, 7]. Functionally, however, SAC satisfaction was significantly accelerated in the RRISF chimera and fully rescued in the RRISF + Tau chimera, each of which had less than maximal PP1 recruitment to the KTs. Thus, a critical threshold of Spc105-bound PP1 that is sufficient to satisfy the SAC can be recruited in the absence of the SILK motif and, therefore, we presume without the highest possible binding affinity between Spc105 and PP1-87B. It remains to be established in which situations *in vivo* the SILK motif becomes functionally important for PP1 binding to kinetochores.

It was particularly interesting that the RRISF+Tau chimera more effectively recruited PP1-87B than the RRISF chimera despite the fact that the Tau chimera did not effectively recruit PP1-87B (Figure 2.13 C,D). What could explain the synergy between MT binding and PP1 recruitment to Spc105? The spatial positioning model offers one possibility [74, 75, 81], namely that MT binding by Tau in the chimeric protein could position the RRISF motif, which cannot effectively bind PP1 when it is

phosphorylated [75, 7, 110], further away from a source of Aurora B kinase activity at the centromere or kinetochore to favor PP1 recruitment. In support of this hypothesis, recent work in human cell lines concluded that stretching the outer KT away from the inner KT promoted PP1 recruitment to bioriented KTs [123]. Admittedly, this model is complicated by the fact that both the MT- and PP1-binding activities in the NTR are negatively regulated by Aurora B kinase. Furthermore, the interaction of human KNL1 with PP1 and MTs was recently shown to be mutually exclusive *in vitro* [7]. Clearly, further investigation of the interplay between Aurora B kinase activity, MT binding, and PP1 recruitment by Spc105 in living cells is necessary.

2.3.5 MT binding by Spc105 as a direct and separable input to SAC satisfaction

Our data are consistent with MT binding contributing to SAC satisfaction through a synergistic mechanism via promotion of PP1 recruitment, but it also supports the non-mutually exclusive conclusion that MT binding by the Spc105 NTR makes a direct contribution to silencing the SAC. How could MT binding be translated into SAC satisfaction independent of PP1 recruitment? It is compelling to envision a mechanical mechanism in which MT binding introduces tension-dependent structural changes in the intrinsically disordered Spc105 that contribute to extinguishing the SAC [6, 10, 123]. Interestingly, a recent study in which in-depth, image-based analyses of protein ensembles were applied to the human KT led the authors to propose that KNL1 may act as a tension sensor by "unraveling" to relay tension [108]. The possibility that KNL1 regulates the SAC through tension sensing via conformational deformation of its IDRs necessitates additional examination.

2.4 Materials and Methods

2.4.1 Protein Purification

All protein expression constructs were transformed via heat shock into Rosetta (DE3) E. coli. After reaching an OD600 of ∼0.5, expression was induced by adding 0.25 mM IPTG and incubating for 12-16 hours at 16°C. Cultures were pelleted in a Sorvall RC-5 centrifuge in a GSA rotor at 5,000 x g for 30 minutes at 4°C, and pellets were resuspended in HEPES purification buffer unless otherwise indicated (50 mM HEPES pH 7.4, 100 mM KCl, 1 mM MgCl2, 1 mM DTT, 10% glycerin, and Roche protease inhibitor cocktail). Cells were lysed using an EmulsiFlex-B30 cell disruptor (Avestin), and spun at 15,000 x g for 30 minutes at 4°C in a Sorvall centrifuge in an SS-34 rotor. The lysate was incubated on either amylose or Nickel resin depending on the affinity tags for 1 hour at 4°C. The lysate-bead mixture was poured over a column, washed with HEPES purification buffer, then eluted with 400 mM Imidazole for Nickel purification or 250 mM D-Maltose for the amylose resin. The eluted protein was dialyzed into HEPES purification buffer overnight in a 10 kDa MWCO dialysis cassette and an additional two hours in fresh buffer the following morning. The protein was then removed from the dialysis cassette and spun down for 10 minutes at 15,000 RPM in an Eppendorf tabletop microcentrifuge (model 5424) at 4°C. The concentration was determined using a Bradford assay (BioRad), followed by aliquoting and flash freezing before being stored at -80°C. Spc105 MT binding truncations/variants were purified in a Tris purification buffer (10 mM Tris ph8, 150 mM KCl, 1 mM MgCl2, 1 mM DTT, and 0.1

2.4.2 *In vitro* kinase assays

The *in vitro* kinase assay was performed using Sli15(INBOX)-Ipl1-6His (construct courtesy of the Biggins' lab), which was purified using the methods outlined above with the HEPES purification buffer. The Sli15(INBOX)-Ipl1-6His was pre-activated

by incubating with 0.2 mM ATP-MgCl2 (pH 7.0) and 1X phosphatase inhibitor cocktail (PhoSTOP-Roche) for 20 minutes at 30°C. The activated Sli15(INBOX)-Ipl1-6His was then incubated with MBP-Spc105(10xMEED)-TST in HEPES kinase buffer (20 mM HEPES pH 7.4, 100 mM KCl, 10 mM MgCl2, 1 mM DTT) + 1X PhoSTOP Roche for 20 minutes at 30°C.

For phosphatase treatment, the Ipl1 + Spc105 kinase mixture was bound to washed magnetic Streptactin-XT beads (IBA Lifesciences) for 30 minutes at room temperature. The beads were next resuspended in 1X FastAP buffer (Thermo Fisher Scientific) with or without 10 U of FastAP enzyme (Thermo Fisher Scientific), and incubated for 1 hour at 37°C. After washing the beads three times with 1X FastAP buffer, the mixture was eluted in SDS and run on a 10% SDS/PAGE gel. The proteins were detected via western blotting and/or Coomassie staining.

2.4.3 Spc105 pulldowns with Bub3-EGFP

Sli15(INBOX)-Ipl1-6His was activated as previously described. Magnetic Streptactin-XT beads (IBA Lifesciences) were pre-blocked with 10 mg/ml BSA in HEPES kinase buffer for 1 hour. To cleave off the MBP tag, MBP-Bub3-EGFP was dialyzed in Slide-A-Lyzer MINI Dialysis 10 kDa MWCO device (ThermoFisher Scientific) 2X 15 minutes into Factor Xa Buffer (20 mM Tris-HCl pH 8, 100 mM NaCl and 2 mM CaCl2) and incubated with Factor Xa Protease (New England Biolabs) for 3 hours at room temperature. Factor Xa inhibitor (CALBiochem 251700) was then added at a final concentration of 2 μM and the cleaved Bub3-EGFP was then dialyzed 2X 15 minutes in 250 mls of fresh HEPES kinase buffer. Pulldown mixtures of 0.15 μM MBP-Spc105(10XMEED)-TST or MBP-TST and 1.5 μM Bub3-EGFP (10-fold molar excess) were incubated in HEPES kinase buffer with 1 mg/ml BSA and 1xPhoSTOP for 1 hour at 30°C in the presence or absence of activated Sli15(INBOX)-Ipl1-6His. After the incubation period, the BSA pre-block was removed from the Streptactin-

XT beads, and the beads were washed 3X 100 L on a MagRack 6 (General Electric) with HEPES kinase buffer. After removal of the final wash, the pulldown mixtures were added to the washed beads, vortexed, and incubated at room temperature for 30 minutes with flicking every 5 minutes to maintain the beads in suspension. The beads were then recovered on the magnet, washed 3X 100 μl in the HEPES kinase buffer, and eluted in 1X SDS sample buffer after removal of the final wash. The beads were then incubated in sample buffer for 5 minutes before retrieving them on the magnet and removing the elution sample, which was then boiled at 98°C for five minutes before running on a 10% SDS/PAGE gel and subjecting the samples to western blot analyses. Band intensities from 3 independent pulldown experiments were quantified using ImageJ.

2.4.4 *In vitro* microtubule TIRF assay

Taxol-stabilized MTs were made by supplementing 10 l of 100 μM unlabeled tubulin with 1% Dylite-649-labeled tubulin (Cytoskeleton) with an equal volume of microtubule polymerization buffer (1xBRB80, 5mM MgCl2, 2 mM GTP, 66.6% glycerol). MTs were polymerized at 37°C for 30 minutes. Taxol was added at 5 μM final concentration and the mixture was incubated for 5 minutes at 37°C. Taxol was then added up to a final concentration of 20 μM and incubated for an additional 5 minutes at 37°C. The polymerized taxol-stabilized MTs were spun down at room temperature in an Eppendorf benchtop microcentrifuge at 15,000 RPMs for 20 minutes to pellet MTs, which were then resuspended in 20 μl of 1xBRB80 + 20 μM taxol. Taxol-stabilized MTs were used for experiments within 1-3 days of being made.

Spc105 microtubule binding variants (Spc105-B(1-400), Spc105-B(1-300), Spc105-A(1-400), and Spc105-A(1-300)) were diluted into buffer containing 0.1 M L-arginine monohydrochloride and pre-cleared in a TLA-100 rotor in a Beckman Coulter Optima

Max-TL ultracentrifuge for 20 minutes at 80,000 RPM at 4°C before being used in any experiments.

Flow chambers were made by adhering an acid-washed and silanized glass coverslip to a glass slide using double sided tape, leaving a chamber volume of 10μL. Anti-tubulin antibody YL1/2 (Abcam) was diluted to 100 μg/ml in 1xBRB80 and incubated in the chamber for 5 minutes. 5% Cellomics Pluronic F127 blocking solution (Thermo Scientific) was diluted into 1xBRB80 then incubated in the chamber for 5 minutes by wicking the solution through the chamber using Whatman paper (Whatman Limited). Taxol-stabilized 647-labeled microtubules (1 μM) were then flowed into the chamber via wicking and incubated for 5 minutes before washing, via wicking, 2X 10 μls with 1xBRB80 + 20 μM Taxol. Pre-cleared ultra-centrifuged Spc105 microtubule binding variants were diluted to 50 nM in Tris purification buffer with 100 mM L-arginine monohydrochloride, 20 μM taxol and 1 mg/ml BSA. The high salt chambers had Tris purification buffer with 500 mM KCl and the 1,6-hexanediol chambers contained 5% 1,6-HD (Sigma Aldrich) in Tris buffer. Sli15(INBOX)-Ipl1-6His was pre-activated and incubated in the same conditions as previously described, with the exception of using Tris buffer instead of HEPES kinase buffer.

Chambers were imaged on a TIRF-Spinning Disk system assembled on an Eclipse Ti-E inverted microscope (Nikon) equipped with a Borealis (Andor) retrofitted CSU-10 (Yokogawa) spinning disk head and two ORCA-Flash4.0 LT Digital CMOS camera (Hamamatsu) using a 100x 1.49 numerical aperture (NA) Apo differential interference contrast TIRF objective (Nikon). Metamorph software (Molecular Devices) was used to control the imaging system. Imaging began approximately two minutes after adding the binding variants at 1x1 binning, 100 millisecond TIRF-488, and 50 millisecond TIRF-641. Each chamber was imaged for no more than twenty minutes after introducing the binding variant.

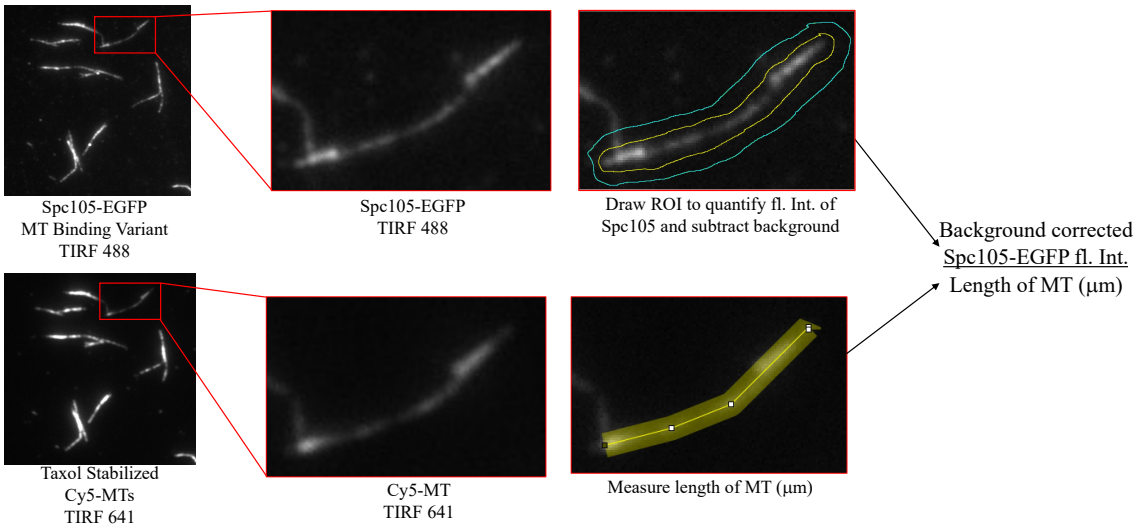

Figure 2.14. Measuring microtubule binding to Spc105 N terminus by TIRF microscopy An example of how microtubule binding of the N terminal mutatns of Spc105 were quantified using ImageJ (NIH). First ten MT per field of view were chosen to be quantified. The length of the MT was measured and the ROI was transferred to the 488 channel. The fluorescence intensity of the Spc105-EGFP N terminal variant was background corrected using the previously published region-in-region method. Then the background corrected fluorescence intensity of 488 was divided by the length of the MT to get the value for MT binding of the Spc105 N terminal variants.

Quantification of MT binding was done in ImageJ by first measuring the length of a MT then drawing a region of interest (ROI) around that MT. The ROI was transferred to the Spc105 channel where the total fluorescence intensity of the Spc105 binding variant bound to the MT was measured. Background was corrected by moving the same ROI to a nearby area of the image without MTs. The background signal was subtracted from the Spc105 signal on the MT and divided by the length of the MT to yield a fluorescence intensity per micron of MT (Figure 2.14).

2.4.5 Live-cell imaging of metaphase duration

Metaphase duration measurements were done on living cells, which were previously transfected with C-terminally fluorescent protein (FP)-tagged Spc105-B, Spc105ΔN, or one of the Spc105ΔN chimeras, seeded onto Concanavalin A coated coverslips. The cells were imaged on a TiE inverted microscope (Nikon) equipped with an iXON3

EMCCD camera (Andor Technology) using a 100 1.4 NA Plan Apo violet-corrected (VC) series differential interference contrast objective (Nikon). Metamorph software (Molecular Devices) was used to control the imaging system. Prometaphase cells with 1-2 misaligned polar chromosomes were identified by scanning the coverslips by eye on the appropriate channel corresponding to the transfected Spc105-FP. The prometaphase cell was then subjected to time-lapse imaging by acquiring images every 2 minutes to follow the cell from prometaphase until anaphase. Metaphase duration was defined as the time from the last chromosome to biorient, as determined by the position of the sister KTs onto the metaphase plate and an observed increase in centromere stretch, until the separation of sister KTs at anaphase onset. All cells were imaged with the ND4 filter inserted into the light path to limit photo-toxicity.

2.4.6 Photoactivation experiments and quantification

For the photoactivation experiments cells co-expressing PA-GFP-α-tubulin and either Spc105-B-TagRFP-T or Spc105ΔN-EGFP were seeded onto Concanavalin A treated coverslips and imaged with a 100X 1.4 NA Plan Apo VC oil objective on a Nikon TiE stand outfitted with a Yokogawa X1 spinning disk, a Nikon LUN4 laser launch for imaging, an iXON Ultra 897 EMCCD camera (Andor Technology), a Bruker Galvo Miniscanner, and a second Nikon LUN4 laser launch that is used for photoactivation. The system was controlled with NIS-Elements software. Methodology for these experiments and analyses was adapted from [20]. Cells in metaphase were found with fully aligned fluorescent kinetochores. A rectangular region of interest (ROI) was drawn along one side of the mitotic spindle parallel to the aligned kinetochores. Cells were first imaged with 488 nm laser for two frames and were then photoactivated within the ROI with the 405 nm laser for 2 milliseconds under stimulation settings. They were subsequently imaged with 488 nm laser acquisition every 15 seconds for 10 minutes. In Spc105-B-TagRFP-T-expressing cells kineto-

chores were found in the TRITC channel and imaged with 561 nm and 448 nm for two time-points prior to photoactivation. In the Spc105ΔN-EGFP expressing cells, kinetochores were found in the FITC channel and imaged with 488 nm as previously described. To measure PA-GFP-α-tubulin photobleaching in our imaging conditions, whole cells expressing only PA-GFP-α-tubulin were activated by drawing a circular ROI around the entire cell (n = 10 cells) and subjecting them to identical activation and imaging conditions as was applied to cells in which an ROI within the spindle was used.

PA-GFP turnover was analyzed in NIS Elements (Nikon). First, a rectangular ROI was drawn around the photoactivated region in the spindle and quantified for the Summed Intensity. The region was moved and centered around the photoactivated signal and the Summed Intensity was re-recorded with each time point to follow the fluxing microtubules. The background signal for each time-point was the Summed Intensity for an identical ROI placed equidistant from the metaphase plate on the other half of the spindle. The Summed Intensity of the background measurements were subtracted from the Summed Intensity of the photoactivation measurements and the values were normalized in each cell as a percent change in fluorescence over time with the first time-point post-photo-activation set to 100%. The normalized background-corrected fluorescence for each spindle was then corrected for photobleaching using the experimentally-defined bleach rate from the whole-cell photoactivation measurements. The mean values of the normalized, background/bleach corrected PA-GFP signal at each time-point from 0 – 300 seconds (n = 16 Spc105-B-expressing cells, n = 22 Spc105ΔN-expressing cells) were plotted and fit with a double exponential curve using the function $F = A1^{(-k1\times t)} + A2^{(-k2\times t)}$ to define the microtubule turnover rates for the kinetochore microtubules and the non-kinetochore microtubules. A1 is the percentage of non-kinetochore microtubules and A2 is the percentage of kinetochore microtubules. The turnover rate constants of dissipation for each of these

populations are k1 and k2 respectively and t is the time following photoactivation [20]. From these rate constants the half-lives of each microtubule population were derived by dividing ln(2) by the rate constant for each population. Curve fitting was performed using KaleidaGraph (Synergy Software). Flux rates were also measured during the analyses by measuring the distance between the center of the photoactivated ROI for control (Spc105-B) and experimental (Spc105ΔN) conditions from t = 0 to t = 300 seconds.

2.4.7 Cell culture

Drosophila S2 cells were grown in Schneider's medium (Life Technologies) supplemented with 10% heat inactivated fetal bovine serum (FBS) and 0.5x antibiotic/antimycotic cocktail (Sigma), and maintained at 25°C. All cell lines were generated by transfecting the plasmid with Effectene Transfection Reagent system (Qiagen), following the manufacturers protocol. Expression of the proteins was confirmed by fluorescence microscopy. Cells expressing the constructs were selected by splitting them in the presence of 25 μg/ml Blasticidin S HCl (Fisher) until cell death ceased at which point the cells were maintained in media without drugs.

2.4.8 DNA constructs

All DNA constructs were made using isothermal (Gibson) cloning [43]. Primers designed by the authors and purchased from Thermo Fisher. The pMal-Spc105(10xMEED)-TST-6His construct was generated in multiple steps: (1) The original insert was a longer portion of Spc105-IDP (amino acids 229-1720) which was originally amplified from the cDNA (Clone IP22012) purchased from DGRC, with 5'BamHI and 3'XbaI sites and inserted into pMal-c2X plasmid (New England Biolabs). A 6His tag was added to the C-terminus by incorporating the DNA sequence in the reverse primer; (2) the TST tag was inserted after the Spc105(IDP) sequence with flanking SpeI sites by ligating a Genestring (ThermoFisher) into the above plasmid; (3) The IDP re-

gion was replaced with the 10xMEED region of Spc105 (amino acids 704-1138) with flanking XbaI sites.

The pMal-MBP-Bub3-EGFP-6His construct was made by first amplifying the Bub3-EGFP (Bub3 cDNA; DGRC clone FI07632) sequence from a previously cloned construct using primers with XbaI site and inserted into the pMal-Spc105(10xMEED)-TST-6His plasmid described above after XbaI digestion.

The first microtubule binding variant, pET21a-Spc105-B(1-400)-EGFP-TST-6His was generated in multiple steps, (1) Spc105-B(1-400) was amplified from cDNA with 5' NdeI and 3'XhoI sites. An isothermal reaction was done with pET21a-Spc25-EGFP that was digested with NdeI, (2) The TST tag was amplified using the previously described pMal-Spc105(10xMEED)-TST-6His plasmid as a template and inserted into step 1 that was digested with XhoI. The pET21a-Spc105-B(1-300)-EGFP-TST-6His was made by amplifying the insert from pET21a-Spc105-B(1-400)-EGFP-TST-6His construct and inserting into pET21a-Spc105-B(1-400)-EGFP-TST-6His that was digested with NdeI. pET21a-Spc105-A(1-400)-EGFP-TST-6His and pET21a-Spc105-A(1-300)-EGFP-TST-6His were made in the same way using primers that contain the sequence for the first nine amino acids and inserting it into the digested pET21a-Spc105-B(1-400)-EGFP-TST-6His vector.

The *Drosophila melanogaster* gene Bub3 (DGRC clone FI07632) was PCR amplified from the cDNA with a 5' SpeI site and 3' XbaI site. Tag-RFP-T was PCR amplified with a 5' XbaI site and 3' SacII site. The resultant PCR products were inserted into a pMT/V5 His-B vector containing the CENP-C promoter inserted at the KpnI site.

The *Drosophila melanogaster* Spc105 gene corresponding to amino acids 401-1959 (Spc105ΔN) and containing a start codon, were PCR amplified from the Spc105 cDNA (DGRC) with a 5' BamHI site and 3' XbaI site. The Spc105 promoter (Spc105P) was PCR amplified from a previously generated construct containing the

genomic sequence template with a 5' KpnI site and 3' BamHI site. The resulting products were inserted into the multiple cloning site of a pMT/V5 His-B vector containing the RFP gene with three-piece Gibson assembly cloning. The Tau segment of pMT-Spc105P-Tau-Spc105ΔN was generated by PCR amplifying the Tau sequence from cDNA (DGRC clone IP17254) with flanking BamHI sites. The piece was inserted into the previously described pMT-Spc105-Spc105ΔN sequence that was digested with BamHI. The RRISF segment flanked by GGSGGGGSGG disordered sequences of the pMT-Spc105P-RRISF-Spc105ΔN was purchased as a Genestring from Thermofisher and inserted into pMT-Spc105P-Spc105ΔN digested with SpeI. The pMT-Spc105P-RRISF-Tau-Spc105ΔN was generated by digesting pMT-Spc105-Tau-Spc105ΔN with SpeI and inserting the RRISF PCR segment that was amplified from the Genestring described above with flanking SpeI sites.

The PP1 constructs were both made the same way, where the first step was to digest a pMT/V5-His-B vector containing the CENP-C promoter with KpnI and SacII. The sequence for EGFP-PP1 and RFP-PP1 was amplified from constructs from the Przewloka group using PCR with the appropriate overhangs and inserted into the digested pMT vector downstream of the promoter sequence.

2.4.9 Western Blotting

Samples were loaded onto a 10% SDS/PAGE gel, run out and transferred to a nitrocellulose membrane using Trans-Blot Turbo transfer system (Bio-Rad Laboratories) for 10 min. Blocking was done in 5% Non-fat milk in 1X TBS and 0.1% Tween for one hour. Membranes were incubated with primary antibodies diluted into TBS-Tween and 5% milk for at least 1 hour at room temperature or overnight at 4°C. The dilutions of primary antibodies were as follows: chicken anti-GFP (Abcam) at 1:5000, rabbit anti-His (Cell Signaling) at 1:5000, mouse anti-DM1α (Sigma Aldrich) at 1:5000, and sheep anti-Spc105 (gift of Marcin Przewloka) at 1:5000. Following

3X 5-minute washes in TBS-Tween, the membrane was incubated in the appropriate HRP secondary antibodies (Jackson ImmunoResearch) diluted at 1:2000 in 5% milk TBS-Tween. The membrane was washed 3X 5 minutes in TBS-Tween before developing using Immobilon Western Chemiluminescent HRP substrate solution (Millipore). Membranes were imaged using a GBox system controlled by GeneSnap software (Syngene).

2.4.10 Immunofluorescence and quantification of ABK

Drosophila S2 cells transfected with fluorescent Spc105R were treated with 25 μM colchicine overnight. They were then allowed to adhere to acid-washed Concanavalin A (Sigma-Aldrich)-coated coverslips for 1 hour before being quickly rinsed with 1X BRB80 buffer, and then fixed with 10% paraformaldehyde in 1X BRB80 for 10 minutes. Cells were then permeabilized with phosphate-buffered saline (PBS) containing 1% Triton X-100 for 8 minutes, rinsed three times with PBS plus 0.1% Triton X-100, and blocked with boiled donkey serum (BDS from Jackson ImmunoResearch) for one hour. After the block, the coverslips were incubated at room temperature for 1 hour in primary antibody diluted in BDS. The coverslips were then washed 3X 5 minutes in PBS plus 0.1% Triton X-100 before adding the appropriate secondary antibodies diluted at 1:200 in BDS containing 1 μg/μl concentration of 4',6'-diamidino-2-phenylindole (DAPI). After secondary treatment, coverslips were washed 3X 5 minutes in PBS plus 0.1% Triton X-100 and then mounted face down on a slide in 7 l of mounting media (20 mM Tris, pH 8.0, 0.5% N-propyl gallate, and 90% glycerol). The following antibodies and dilutions were used: rabbit anti-Phospho-aurora A/B/C and rabbit anti-Phospho-aurora A (Cell Signaling Technology) were diluted 1:1000, chicken anti-GFP 1:1000 (Abcam), and mouse anti-DM1α at 1:1000 (Sigma Aldrich).

Three-color widefield Z-series consisting of 41 planes acquired at 0.2-μm intervals were acquired for the green fluorescent protein (GFP), Cy3, Cy5 (where appropriate), and DAPI channels on the microscope system previously described. In Metamorph, the background-corrected fluorescence intensities were measured for the maximum-intensity projections of the Z-series of both the pABK-CEN or pABK-KT and DAPI channels using the region-in-region method as previously described [137] applied to the chromosome mass. The data was reported as the background correct ABK intensity ratioed to the background corrected DAPI intensity.

2.4.11 Quantification of Bub3 levels during congression and drug wash-in experiments

Measurements of the Bub3 levels at misaligned and bioriented KTs was done in living cells seeded onto Concanavalin A coated coverslips and imaged on the microscope system described previously using either the spinning disk or widefield modalities. Prometaphase cells with 1-2 polar chromosomes were identified by eye and initially subjected to time-lapse imaging by acquiring images every 1-2 minutes until the misaligned chromosome began congressing at which point images were acquired every 10 seconds to follow alignment. The fluorescence intensity of the Bub3-TagRFP-T signal was then measured in Metamorph by drawing a region around each KT and subtracting the local background signal from an identical region positioned nearby in the cytosol. The background corrected signals for each misaligned KT (defined as the frame prior to the onset of congression) were summed for the total Bub3 at a sister KT pair except in cases where the sisters were too close together to be resolved in which case a single region was drawn encompassing both sisters. The fluorescence quantification was repeated once the KT pair was bioriented as evidenced by its position in the metaphase plate and an observed increase in centromere stretch. The relative difference between misaligned and bioriented Bub3 levels was calculated

by dividing the background corrected integrated intensity values at the misaligned KTs by that measured at the same pair of KTs upon biorientation. The fold-change value between the misaligned and aligned KTs was expressed as % Bub3 retained at bioriented KTs by dividing 100 by the fold-change value. The control measurements were done on the parental cell line expressing Bub3-TagRFP-T alone while the experimental measurements were done on the same cell line transiently transfected with Spc105ΔN-EGFP.

Quantification of Bub3 levels at kinetochores in the drug wash-in experiments was done in cells co-expressing Bub3-TagRFP-T and Spc105-EGFP. Cells were seeded on Concanavalin A-coated coverslips for ∼15 minutes, brought up to a final volume of 2 mls with media, and then treated for at least 1 hour with colchicine (25 μM) and MG132 (10 μM). Cells were then subjected to spinning disk confocal Z-sectioning before and after replacing the media with fresh media containing colchicine (25 μM) and MG132 (10 μM) supplemented with either BI2536 (1 μM) or binucleine 2 (40 μM). In Metamorph, the background-corrected fluorescence intensities were measured using the region-in-region method as previously described [137] on concentric regions encompassing all the KTs drawn in the maximum-intensity projection of an Spc105-EFGP Z-series and transferred to the corresponding maximum-intensity projection of the Bub3-TagRFP-T channel. The data was reported as the background corrected Bub3 intensity ratioed to the background corrected Spc105 intensity.

CHAPTER 3

SINGLE MOLECULE 'TUG-OF-WAR' USING MOTOR PROTEINS AND DNA ORIGAMI TO PULL ON SPC105(10XMEED)

3.1 Background

In previous chapters, we demonstrated that KNL1 binds to MTs at its N terminus and it has been shown that its C terminus binds to the outer KT. Additionally, KNL1 is the location of MCC checkpoint protein binding which is controlled through phosphoregulation between Aurora B kinase and PP1 phosaphatase. In Figure 2.2 E we showed that Aurora B kinase phosphorylation of KNL1(10xMEED) increased Bub3 binding by thirty times background. However, there was a significant amount of Bub3 that was pulled out by non-phosphorylated KNL1(10xMEED). Therefore, we hypothesized that Bub3 also interacts with non-phosphorylated MEED motifs as part of KNL1's function as a tension sensor. The following chapter includes a description of experiments used to determine if KNL1 is under tension in metaphase cells, as well as an ongoing project aimed at testing our tension sensor hypothesis *in vitro*.

3.1.1 Tension as a signal

A biological signal represents a space and time record of a biological event. These signals coordinate cellular machinery to independently or cooperatively perform a specific task that contributes to cell survival and function. Sensory machinery interprets signals from external and internal stimuli that then propagates and passes on information to subsequent steps in a signaling cascade. So often in biology signals

are thought to be in chemical form, such as in the case of post-translational modifications (PTMs) like phosphorylation. Molecular signals are commonly a change in the structure of a protein or its physical location, which are frequently regulated by PTMs. These chemical changes often increase or reduce affinities between molecules or protein complexes that, in turn, indirectly promotes or inhibits a specific cellular mechanism from occurring. PTMs can directly regulate the activation state of an enzyme, but sometimes indirectly regulate activation by preventing binding of a co-activator molecule. A classic example of chemical signaling occurs during the Spindle Assembly Checkpoint (SAC), described in the introduction as the wait anaphase signal generated by the Mitotic Checkpoint Complex (MCC) to prevent anaphase onset until all of the chromosomes have properly bioriented. When the MCC interacts with Cdc20 after it has been phosphorylated it inhibits the interaction with and activation of APC/C (see Figure 1.5 A in Chapter 1), which is therefore prevented from tagging its substrates for degradation [53, 55]. These series of chemical modifications function together to inhibit or activate APC/C which controls the timing of anaphase onset. Chemical signals, like the phosphoregulation of the MCC, are essential to many molecular processes throughout biology.

Several other types of signals exist in biology that also play a vital role in the survival and essential function of the cell. Mechanosensory proteins undergo a conformational change due to the transduction of forces caused by physical stimuli in their polypeptide chain. For example, there is a system of transmembrane channels found in *Mycobacterium tuberculosis* that open when the bacteria are under hypoosmotic stretch. The forces that stretch the bacterial membrane change the angle of one of the alpha helices that make up the channel which, in turn, increase the diameter of the pore and allow the non-selective release of material to prevent membrane damage [70]. In this example, changes in the cellular environment induced a conformational change in the channel which caused a downstream effect to save the cell. Similar to

chemical signals, mechanical stimuli can also impact how proteins interact however, mechanosensory proteins tend to undergo larger structural changes in response to a signal. Intrinsically disordered proteins (IDPs), also described in the introduction, can adjust their shape depending on their environment. The disordered nature of IDPs allows them to be flexible when they need to be flexible and become structured in certain conditions such as pH changes or interactions with a binding partner. In this way, disordered proteins may be ideal candidates as mechanosensors in that their flexible nature can withstand the conformational stresses that often accompany mechanical stimuli.

The signaling that occurs during the SAC is so important, that if any errors occur during the checkpoint, the resulting daughter cells will be aneuploidy. It is widely accepted in the field of mitosis that checkpoint signaling depends on KT-MT attachments [39]. However, it has been proposed that tension also contributes to satisfying the checkpoint. The hypothesis that tension plays a role in SAC signaling is controversial and is experimentally difficult to tease apart from the contributions of attachment since the forces that create tension require KT-MT attachment. In favor of tension contributing the SAC signaling, our lab and others have observed and measured tension at bioriented KTs [81, 120, 136, 129]. For example, one group observed via EM imaging that bioriented KTs become distorted in such a way that suggests the existence of pulling forces across its structure [120]. Our lab found that an important KT protein CENP-C was under hundreds of piconewtons of force at bioriented KTs [136], which implies that other KT proteins may be under tension as well. While the presence of tension has been shown in many publications to date, the contribution of tension to satisfaction of the SAC has never been definitively observed. The argument against the contribution of tension is that it is only present as a result of attachment and therefore does not directly contribute to the downstream signals that turn off the SAC. Indeed, while this has been a topic of much debate

and research, the question as to whether tension contributes to SAC signaling has not yet been answered. Studying this process will not only lead to a more complete global comprehension of how cells manage to divide correctly millions of times a day; it would also shine light on understanding the physical signals that are so important in biology.

3.1.2 Measuring Molecular Tension

A large portion of the proteins that comprise the kinetochore are predicted to be disordered; a property conserved throughout evolutionary history. IDPs are more flexible than their folded counterparts, which makes them ideal for functions that require changes in structural conformation. For example, kinases possess flexible linker regions between its two lobes which allow it to switch between an inactive or active state. IDPs challenge the archetypal notion of structure-function relationships in that their lack of structure is may be essential to their function. In fact, as mentioned in earlier chapters, our central hypothesis is that the disordered nature of KNL1 allows for it to be stretched to accommodate the different kinetochore architectures in attached versus unattached states. We hypothesize that the flexible nature of KNL1 and its role as a signaling hub make it an ideal candidate for the KT tension sensor. IDPs are a relatively new type of protein and therefore many traditional biochemical techniques used to characterize protein structure do not generally work. For example, NMR is a powerful technique used to get detailed information on protein structure and dynamics, but it relies on an averaged image of the structure. Since IDPs probably have anywhere from tens to hundreds of stable conformations, techniques like NMR would only be able to provide information on small regions of IDPs, if at all [60]. Additionally, there are disorder prediction tools that use statistical analysis of protein sequences in order to provide a rough estimate of partly structured regions, but they are not yet able to provide exact secondary structure classes [29]. However, due to the

prevalence of IDPs and availability of increasingly fast computational power, there is a push in the field to be able to model the possible structures of IDPs.

While the body of evidence for the contribution of tension to SAC satisfaction is growing, there is an important piece missing that would settle the argument once and for all. In order for tension to play a role in SAC signaling, there must be a tension sensor: a molecule or complex whose function it is to detect biorientation through tension sensing and transmit this information to turn off the SAC. The sensor should theoretically be a stably bound KT protein, so that it detects the lack and presence of tension and uses this information to inhibit or trigger anaphase onset. As previously discussed, this protein would also likely be flexible in order to withstand the deformations the KT undergoes upon biorientation. Many potential SAC tension sensors have been proposed, and the search for its identity is an area of active research, but the mystery remains unsolved. We propose the SAC tension sensor is the disordered KT protein KNL1 (Spc105). As laid out in Chapters 1 and 2, KNL1 is a large and disordered subunit of the KMN network that binds to the inner KT at its C terminus and to MTs and PP1 phosphatase at its N terminus. Its disordered nature gives it flexibility to withstand any conformational changes that may occur during biorientation. Another important reason KNL1 is an excellent candidate for a tension sensor is that it is the binding hub for checkpoint proteins at non-bioriented KTs. Therefore, the signaling complex that can inhibit or initiate anaphase onset assembles on the disordered region of KNL1 and would rely on the structure of KNL1 in order to correctly bind to or not bind to it. In other words, the ability for the checkpoint proteins to bind to KNL1 directly influences SAC signaling and therefore is the control mechanism for which it can turn the tension sensing function into another signal that has downstream effects.

If our hypothesis is correct, then the tension sensing ability of KNL1 would directly influence SAC signaling. More specifically, our model for how KNL1 is a tension sensor

is that checkpoint proteins bind to KNL1 when it is not under tension, which occurs at non-bioriented KTs where KNL1 is not attached to the MTs. Upon biorientation, the N terminus of KNL1 attaches to MTs which pull on KNL1 and extend the protein, which reduces its affinity for checkpoint proteins that then disassociate from the KT and initiate anaphase onset. Since the MELT motifs are directly next to each other in the amino acid sequence, we propose that perhaps they stochastically move closer to each other in space when KNL1 is not under tension. Having a cluster of two or three MELT motifs increases the affinity for MCC proteins (ref), that are now more likely to bind to KNL1. Upon biorientation and application of tension, the KNL1 protein is stretched in such a way that separates the MELT motifs from each other, which then reduces its affinity for checkpoint proteins.

In order to test our hypothesis of KNL1 as a tension sensor, we first needed to determine if it is under tension in cells. We did this by using a novel force sensor called the tension sensor-module (TS-Mod) that consists of two fluorophores on either side of an elastic linker that extends when it is under tension (Figure 3.1 A) [135]. Tension is measured using FRET, a commonly used technique to investigate molecular interactions. It relies on the transfer of energy from a donor molecule to an acceptor molecule which only occurs if they are in close proximity to one another. In the TSMod system, there is high FRET when the protein is not under tension, and low FRET when it is under high tension. We inserted the TS-Mod tension sensor into the middle of the disordered region of KNL1 and transfected it into S2 cells (Figure 3.1 B). We treated cells overnight with vinblastine to depolymerize MTs, which makes unattached KTs that are not under tension. We compared the vinblastine treated cells with untreated cells that have bioriented KTs and found that there was no significant difference in their FRET ratios (data not shown) (Figure 3.1 C). We hypothesized that the location of the tension sensor was perhaps too far away from where KNL1 attaches to the KT to have a measurable amount of tension. Therefore, we moved

the sensor closer to the KT binding region of KNL1 and found that this also resulted in no significant difference in FRET (data not shown). While both attempts at measuring tension using the TSMod tension sensor did not show significant evidence of force transduction, there are several explanations as to why the negative result may have occurred that do not necessitate this conclusion. For example, the FRET measurements were done at the moment in time when every chromosome was observed to have bioriented, which may have been too early to take the measurements. It is conceivable that KNL1 is not under tension until later in metaphase which may function to ensure proper and stable attachments have occurred before anaphase onset. Finally, a limitation of using a FRET-based sensor is that it may not be sensitive enough to detect the differences in tension, as quantification of FRET data often has a high signal-to-noise ratio. Therefore, the negative result from our TS-Mod experiments do not necessarily indicate that KNL1 is not under tension in cells. In fact, recent work measuring the distance between the N- and C- termini in human cells suggests KNL1 is stretched at bioriented KTs [123], which helps support our hypothesis and motivates our future work.

3.2 Pulling on proteins via "tug-of-war" of MT motor proteins

3.2.1 Experimental Set Up

As previously stated, it is experimentally difficult to determine if tension contributes to SAC signaling independent of attachment since attachment is required *in vivo* for tension to occur. Therefore, we have developed an *in vitro* approach to more directly test our model of KNL1 as a tension sensor to complement our data in cells. The inspiration for our experiment comes from our collaborator Dr. Nathan Derr at Smith College who published work in Science describing a "tug-of-war" using DNA origami and motor proteins in which he determined the relative strengths of opposing

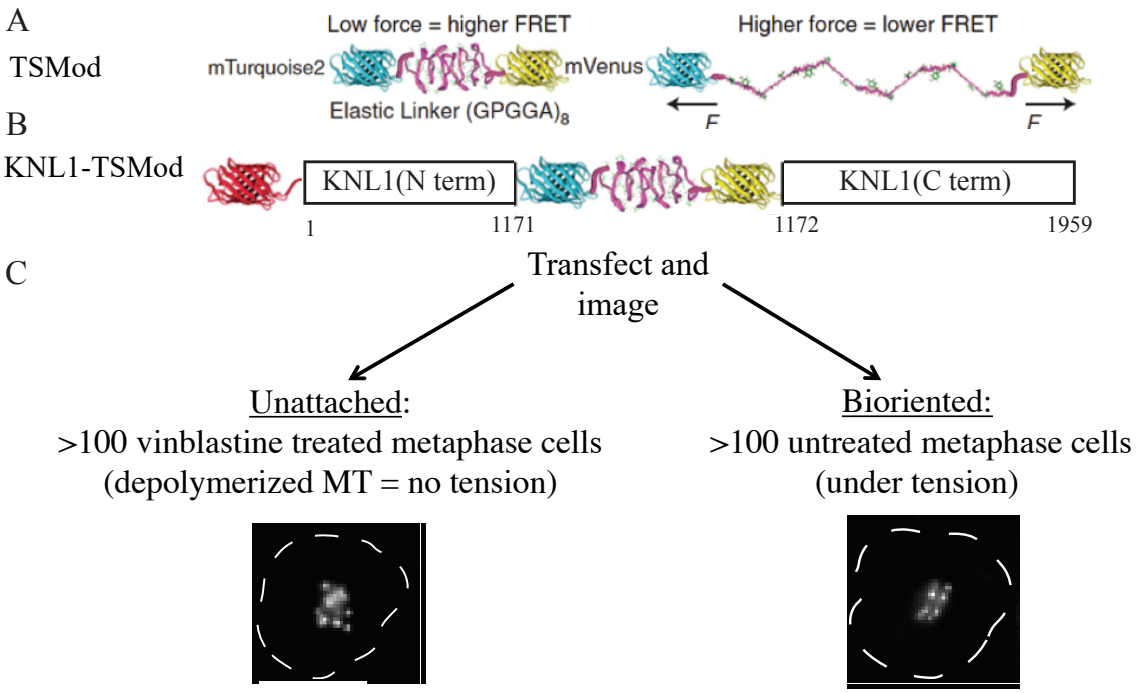

Figure 3.1. Measuring tension of *Drosophila* Spc105-B in metaphase cells using TSMod. (A) Schematic of TSMod tension sensor. When the protein is not under tension, there is low force and therefore high FRET. When the protein is under tension at higher force, the elastic linker gets stretched and there is lower FRET. (B) The TSMod tension sensor was inserted into the disordered region of KNL1, and transfected into S2 cells. (C) We treated overnight with vinblastine which depolymerized the MT and made unattached KTs as our control, low force measurements. Cells were imaged in metaphase when the KT should be under tension and the FRET measurements were taken. There was not a significant difference between the FRET ratios of the treated and untreated cells (data not shown), however we believe this is due to experimental design and does not definitively indicate that KNL1 is not under tension in metaphase cells.

motors kinesin and dynein [30]. Our experiment is designed to mimic the stretching of KNL1 at bioriented KTs using motors attached to either end of the protein. DNA origami is used to make the "chassis" upon which the motors are attached via oligo tags (Figure 3.2). The opposing motor proteins will bind to the different ends of KNL1 using oligo labels attached to DNA chassis. This works by first purifying the 10xMEED portion of Spc105 with an N terminal SNAP tag and C terminal CLIP tag and labeling each tag with a different oligo that bind to the DNA chassis. The motors

are then attached to the chassis, and upon addition of ATP, will move in opposite directions which will pull on KNL1 which we will observe using TIRF microscopy (Figure 3.3). Importantly, the amount of tension applied to KNL1 will be highly tuneable simply by adjusting the number of each motor protein. Our hypothesis is that when KNL1 is not under tension, it has a higher affinity for MCC components such as Bub3. Upon application of force, we propose that Bub3 has reduced affinity for KNL1, which would occur at bioriented KTs, turning off the SAC and allowing anaphase onset.

Ultimately, the goal for the tug-of-war experiment is to determine if stretching KNL1 changes its affinity for the checkpoint protein Bub3. In the results section of Chapter 2, we demonstrated that the 10xMEED region of Spc105 binds to Bub3 independent of phosphorylation, however it binds 30 times better upon phosphorylation by Aurora B (Figure 2.2 E). Additionally, PP1 binding to the KT decreases the affinity of checkpoint proteins for KNL1, the mechanism of how this occurs is not understood. It could be that PP1 directly dephosphorylates KNL1, or that it indirectly promotes the dephosphorylation of KNL1 through other means ([24]. While phosphoregulation of KNL1 plays a major role in its affinity for checkpoint proteins, we propose that there is a non-chemical regulatory feature of this interaction. As described in detail in previous chapters, we propose that KNL1 acts as a tension sensor for the SAC. The mechanism we propose is that Bub3 has higher affinity for KNL1 when it is not under tension, and upon MT binding, KNL1 gets pulled on which reduces its affinity for Bub3. The purpose of the tug-of-war experiment is to directly test this hypothesis in a simplified and controlled *in vitro* set-up, in a way that is independent of KT-MT attachment. First, we will bind labeled 10xMEED to the DNA chassis that are attached to their respective opposite direction motors. Then we will add Bub3 in the absence of ATP at which time we should observe Bub3 colocalizing to 10xMEED. We will visualize their co-localization by overlapping

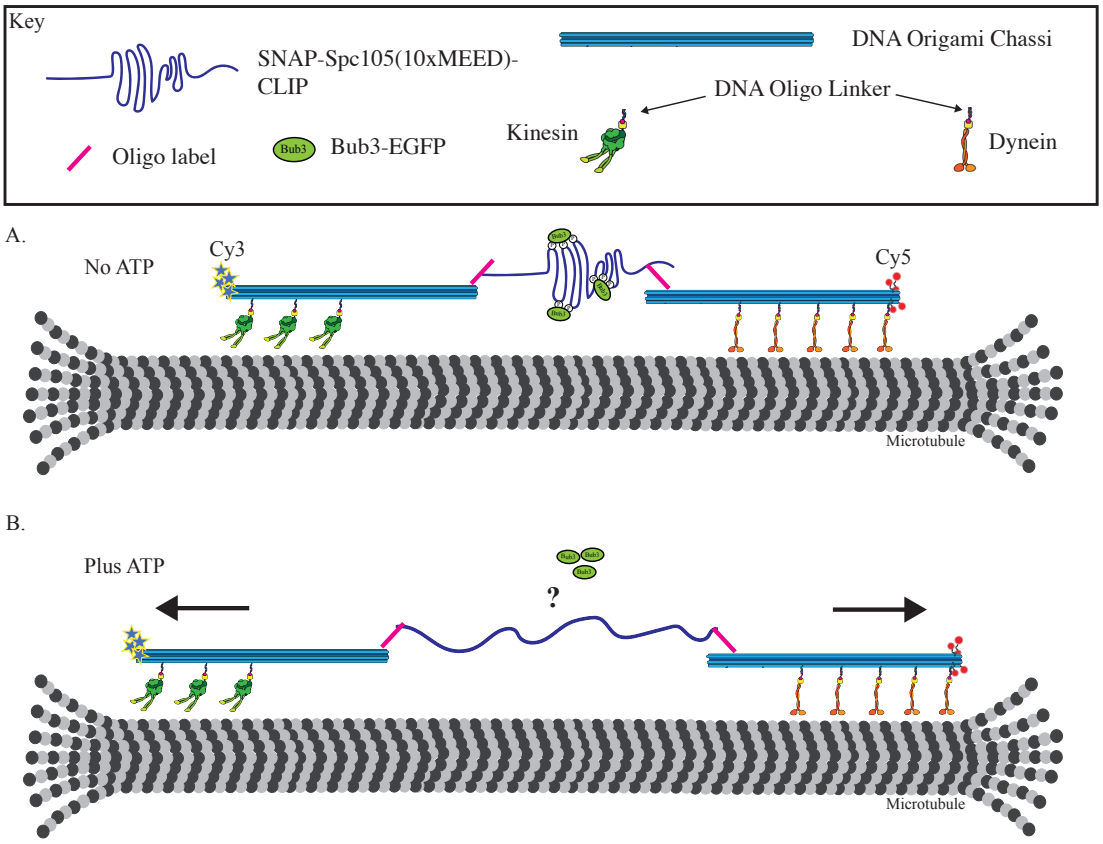

Figure 3.2. Experimental design of the tug-of-war experiment to test if tension changes the affinity of checkpoint proteins for Spc105(10xMEED) This experiment is designed to determine if stretching the disordered region of Spc105 reduces its affinity for checkpoint protein Bub3 to test our hypothesis of Spc105 as a tension sensor. (A) The experimental design of our tug-of-war experiment includes opposing MT motor proteins dynein and kinesin that link to a DNA origami chassis via oligos. The chassis bind to the N- and C-termini of oligo labeled SNAP-10xMEED-CLIP, which links the protein to the motor protiens on either end. In the absence of ATP, Bub3 binds to the 10xMEED region of Spc105 (see Figure 2.2 E), therefore we should see colocalization of Cy3-labeled dynein chassis and Cy5-labeled kinesin chassis as well as EGFP labeled Bub3. When ATP is added in (B), the motors move apart along the microtubules and 10xMEED gets stretched. If our hypothesis is correct we predict that Bub3 will no longer co-localize with the Cy3-labeled dynein chassis and Cy5-labeled kinesin chassis due to its reduced affinity for stretched Spc105(10xMEED).

puncta with Bub3-EGFP and the Cy3 and Cy5 chassis. Upon addition of ATP, the motors will move along MT in opposite directions, therefore we should see the Cy3 and Cy5 puncta moving away from each other. If our hypothesis is correct, we pre-

dict the Bub3 signal no longer co-localizes with the chassis (see figure). Importantly, the amount of tension on the molecule will be carefully monitored to ensure that the amount of force put on 10xMEED will be close to physiological levels. To do this, we could use a version of 10xMEED with a TS-Mod tension sensor to measure the amount of tension in our assay.

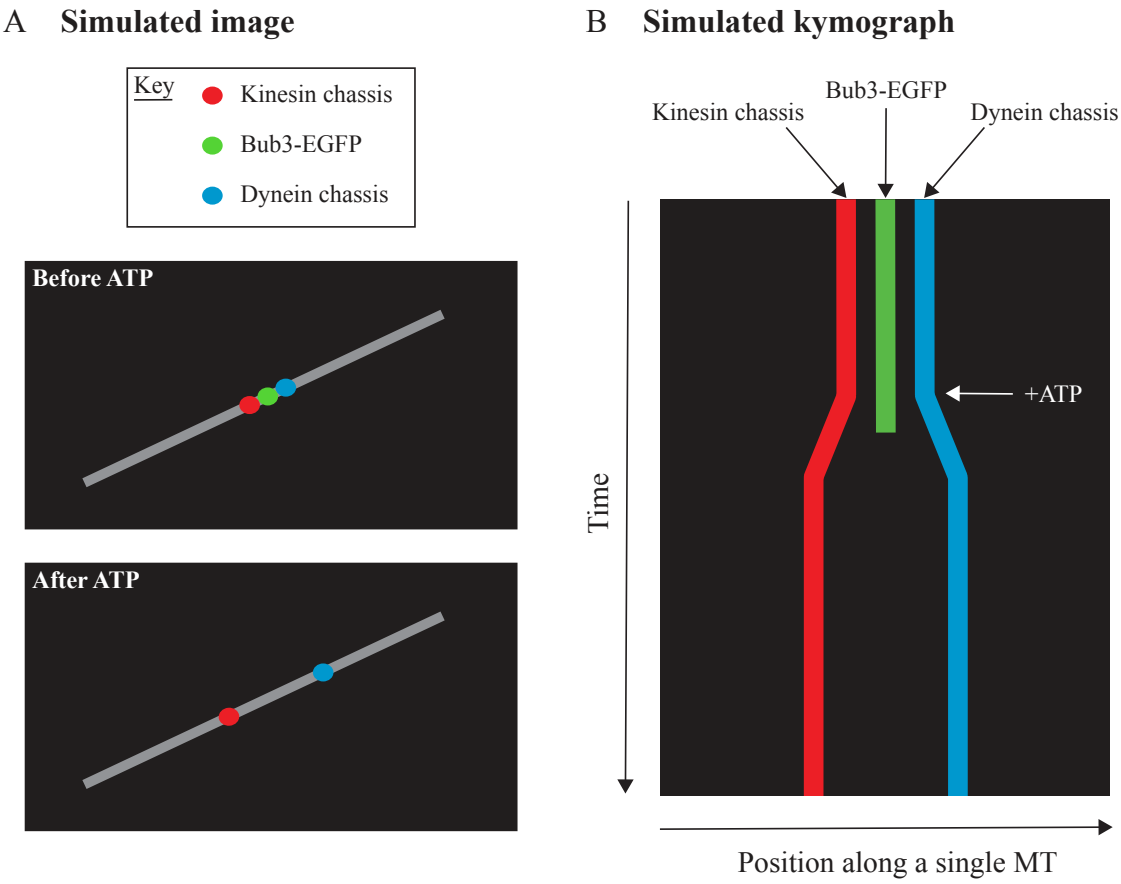

Figure 3.3. Tug-of-war expected results An example of expected results before and after ATP is added to the tug-of-war experiment chambers. (A) Before ATP is added, the Cy3-labeled dynein chassis, Cy5-labeled kinesin chassis, and Bub3-EGFP should colocalize on a microtubule. When ATP is added we predict the Bub3-EGFP spot will disappear as it has reduced affinity for Spc105, and the two Cy3-labeled dynein chassis and Cy5-labeled kinesin chassis spots will move away from each other. (B) Simulated kymograph of the expected results in (A).

3.2.2 Results

So far, we have sucdessfully purified the SNAP-10xMEED-CLIP protein and labeled it with the SNAP- and CLIP-oligo labels. This was done by incubating the protein with both oligos, and then incubating this mixture with fluroescently tagged complementary oligos. The protein-oligo complex was run on a high percentage SDS-PAGE gel at a low voltage to prevent disassociation of the oligo label from the protein. The gel was imaged on a Typhoon imaging system that detects each complementary oligo individually using the fluorescently labelled complementary oligos. We had three conditions using the SNAP-10xMEED-CLIP that had been labeled with both the SNAP and the CLIP oligos for this experiment: the first was with only the SNAP-Cy3 complementary oligo, the second was with the CLIP-Cy5 complementary oligo only, and the last was with both the SNAP-Cy3 and CLIP-Cy5 complementary oligos. The Typhoon imaging revealed that we had successfully labeled both tags with the oligos (Figure 3.4). Next, we wanted to demonstrate that the each of piece of this complex experiment fit together and could move along MTs. To start, we used a reduced number of parts of the experiment to ensure that our motor and chassis set-up will bind to the oligo-labeled SNAP-10xMEED-CLIP. We started by using kinesin attached to its chassis labeled with Cy3, and the dynein chassis, but not the dynein motor, labeled with Cy5. In a control experiment without labeled SNAP-10xMEED-CLIP, we observed the Cy3-chasis-kinesin motor moving along MTs, but the dynein chassis was not. This demonstrates the kinesin chassis successfully attached to the kinesin motor, and that the dynein chassis does not bind to the kinesin motor. Excitingly, we observed movement of both the kinesin and dynein chassis upon addition of the labelled SNAP-10xMEED-CLIP, indicating that the 10xMEED links the two chassis together in a proof-of-concept of our experimental set-up (Figure 3.5 A-C). More experiments are ongoing to determine if we can successfully bind both motors to the 10xMEED. However, we are considering using only one motor which is sim-

pler and will still generate the necessary tension across the 10xMEED to perform the experiment.

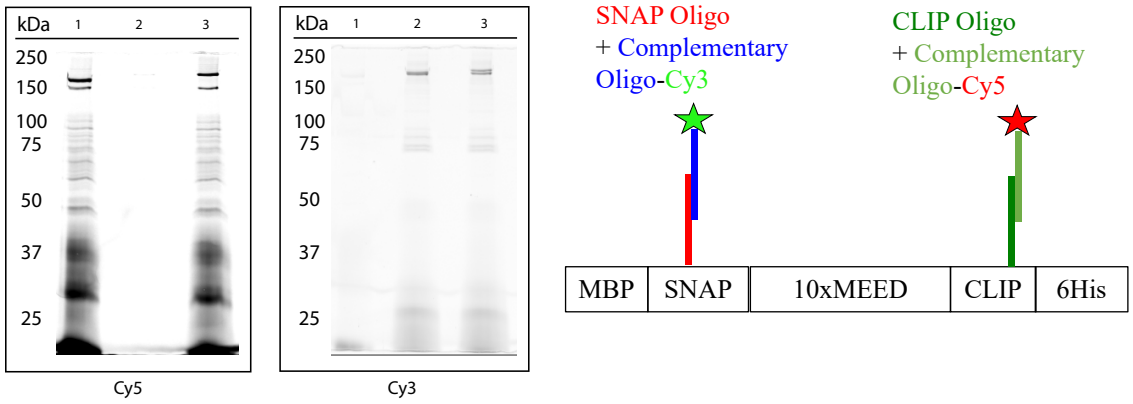

Lane 1: MBP-SNAP-10xMEED-CLIP-6His Labeled +Complementary oligo-Cy5
Lane 2: MBP-SNAP-10xMEED-CLIP-6His Labeled +Complementary oligo-Cy3
Lane 3: MBP-SNAP-10xMEED-CLIP-6His Labeled +Complementary oligo-Cy3 + Complementary oligo-Cy5

Figure 3.4. Oligo labeling of *Drosophila* SNAP-Spc105(10xMEED)-CLIP First, SNAP-10xMEED-CLIP was labeled with the SNAP- and the CLIP-oligos and the excess oligos were removed by sequencial dialysis. The labeled SNAP-10xMEED-CLIP was incubated with complementary oligos that are fluorescently labeled to determine if the labeling was successful. To do so, the mixture was run on an SDS-PAGE gel in a cool water bath in order to prevent disruption of the hybridization of the oligo and protein. Lane 1 contained labeled 10xMEED with only the Cy5 oligo complementary to the CLIP oligo, Lane 2 contained the Cy3 oligo complementary to the SNAP oligo, and Lane 3 had both fluorescently labeled complementary oligos. Using the Typhoon imaging system, the gel was imaged in both Cy5 and Cy3 and we were able to confirm that SNAP-10xMEED-CLIP was successfully labeled with both oligos.

While this experimental set-up is useful to testing our hypothesis of KNL1 as a tension sensor, it can be used to answer a myriad of questions as to how tension effects the structure and function of proteins. There are several other techniques that have been used to pull on proteins currently in use such as an optical trap or magnetic beads. While these techniques are also tuneable and may work very for certain conditions, they require specialized equipment that may not be readily available. Additionally, these techniques generally work by pulling in one direction, whereas our

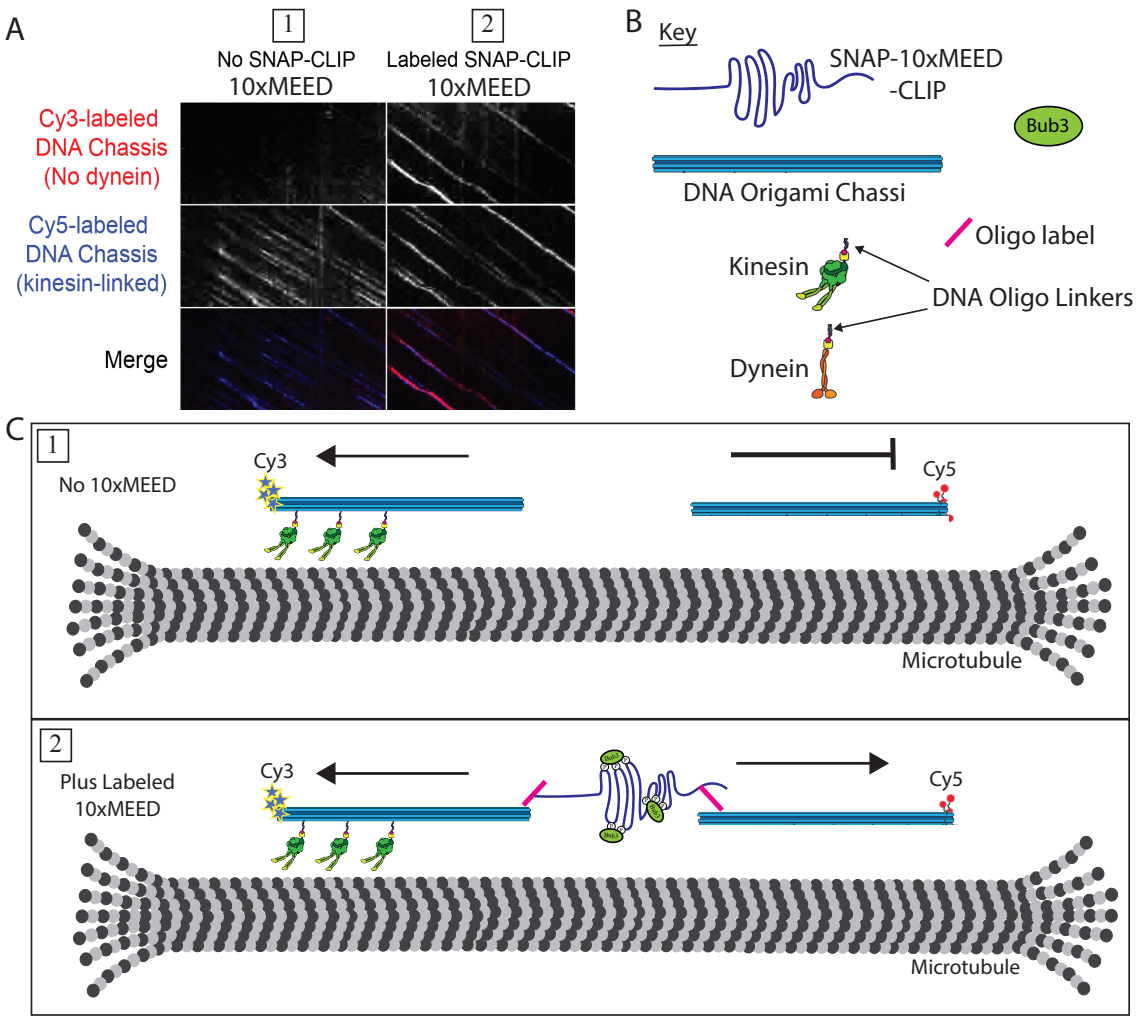

Figure 3.5. Results of tug-of-war proof of concept experiment (A) TIRF images demonstrating colocalization of several of the components of the experiment drawn in "C" (B) Key of the components in the schematic (C) Schematic of experiments shown in A. In "1" the chambers contain the Cy3-dynein chassis bound to the dynein motor, and the Cy5-kinesin chassis with no kinesin motors. The kymograph in "A" demonstrates that without the 10xMEED, the Cy3-labeled DNA chassis do not move, and the Cy5-labeled DNA chassis move along the MTs. This indicates that the dynein motors only link to the dynein chassis, and that without 10xMEED the two chassis are not linked. When the labeled SNAP-10xMEED-CLIP is added to the chamber in "2", it links the two chassis, and the merged kymographs demonstrate that the 10xMEED links the two chassis together.

system allows for more flexibility as it pulls in both directions which may be more physiologically relevant. Our tug-of-war experiment uses easily accessible reagents and TIRF microscopy, which are relatively accessible in comparison to other tech-

niques that may require special equipment. Importantly, the tug-of-war experiment does not address the phosphoregulatory portion of the interaction between checkpoint proteins and KNL1. We are in no way suggesting that the phosphoregulation of KNL1 is not an essential, if not dominate regulatory mechanism of its interactions with checkpoint proteins. We are hypothesizing that perhaps they work in a symbiotic way to generate a robust and highly accurate method of reading tension at KTs. The detailed explanation of how we propose phosphoregulation and tension sensing function together during the SAC can be found in the next chapter.

3.3 Materials and Methods

3.3.1 Labeling and verifying 10xMEED with oligos for tug-of-war experiment

First, SNAP-10xMEED-CLIP was diluted to 1 μM (final volume 100 μl) in labeling buffer (10 mM Tris HCl ph 8.0, 150 mM KCl, 10% glycerol, 10 mM BME, and 0.1% Triton X). The protein was mixed with 50 μl of each oligo (30 μM) and incubated for an hour at room temperature with occasional mixing. The mixture was dialyzed using 10 kDa cutoff dialysis cups for two times 2 hours in 1 L of labeling buffer.

In order to verify the protein was labeled with each oligo, the oligo labeled protein was incubated with fluorescently labeled complementary oligos and visualized using the Typhoon imaging system of an SDS-PAGE gel. 10 μL of the oligo labeled SNAP-10xMEED-CLIP was mixed with 1 μl of 100 μM fluorescent complement(s). The mixture was incubated on ice for 30 minutes with occasional stirring. SDS-PAGE loading dye was added to the mixture and loaded onto a 20% SDS-PAGE gel without boiling. It is important to note that the samples were not boiled and the electrophoresis chamber was kept cool in a water bath during electrophoresis because high temperatures can disrupt hybridization. The gel was transferred to ddH_2O and

imaged on the Typhoon for TMR and/or Cy3. Following imaging, the gel was also stained with Coomassie.

CHAPTER 4

FUTURE DIRECTIONS

Firstly, some aspects of our past and on-going experiments can be improved to enable us to make more concrete conclusions from our observations. For example, in the previous section the work with the TS-Mod tension sensor was discussed, and while the negative did not support our hypothesis, we do not believe this is enough evidence to conclude that KNL1 is not under tension in cells. In fact, recently published work from Uchida et al. 2021 demonstrated human KNL1 is stretched at bioriented KTs *in vivo*. This finding suggests that indeed KNL1 is under tension and supports our model. In order to prove or disprove our hypothesis that KNL1 is a tension sensor, we need to determine if it is structurally able to withstand the forces of KT deformation that occur during biorientation. We propose using an *in silico* modeling program like the worm like chain (WLC) model which is used to predict the behavior of a protein it is stretched. Unfortunately, the technique requires the PDB structural information on the protein in order to model the energy required for it to be stretched. Additionally, work in on going to create prediction algorithms that model the many possibly transient structures any given disordered protein may adopt in specific conditions. While modeling impact of tension on the protein sequence is not a direct measurement in cells, it could be a valuable starting point to determine if it can withstand the physiological levels of force required for KNL1 to perform the tension sensing function we have proposed. Additionally, it could give us valuable information about where to insert the TS-Mod tension sensor within the sequence

of KNL1 for future experiments. Perhaps a collaboration with a computer scientist would be a helpful partnership in beginning to answer this important question.

The data in the results section of Chapter 2 (Figure 2.2 E) indicates 10xMEED binds to Bub3 *in vitro* and was increased when 10xMEED was phosphorylated by Aurora B. While the experiment was repeated several times and always indicated that Bub3 binds to 10xMEED better than the control MBP-TST, the results varied by a considerable margin when we quantified the Western blots. Additionally, we have had not yet been able to visualize Bub3 co-localizing with the SNAP-10xMEED-CLIP in the tug-of-war experiments. A plausible explanation for both of these observations is that Bub3 was not purified correctly. Many beta-propeller proteins, like Bub3, require chaperone proteins found in insect cells but are not found in bacteria to fold properly. We made a fusion protein with N- and C-terminal solubility tags, which probably helped maintain its solubility, but may not mean that it is folded correctly. Additionally, when the N terminal solubility tag was moved to the C terminus, or cleaved off the N terminus, Bub3 became insoluble and crashed out of solution. We hypothesize the Bub3 that we purified and used in experiments contained several populations of partially or improperly folded Bub3. This would explain why the results of the pulldowns were variable, and perhaps why we have not seen it colocalize with the 10xMEED in the tug-of-war experiments. Currently, a new graduate student is working on purifying *Drosophila* Bub3 from insect cell purification system. The new well-folded Bub3 should help future with iterations of the tug-of-war experiments as well as any future work with purified Bub3.

4.1 Translating to Human KNL1

When working in a model system, one of the most important aspects to consider is how translatable are the findings to other organisms especially humans. We know that the fundamental protein constituents of the kinetochore are present in

Drosophila melanogaster model system, and as such it acts as an "essentials only" tool kit for studying kinetochore function. This makes it an advantageous system to work in because not only is it relatively easier to work with in the lab, but it also makes it simpler to reach conclusions in this reduced environment. Cell division is a particularly "well-oiled machine" in that since it is the basis of life itself, much of the machinery and mechanisms that drive this process are conserved. However, due to the complexity of cell division and the controversial nature of the model we are proposing, we have begun to design experiments with human proteins. First, we cloned and purified a portion of human KNL1 with three MELT motifs, and the same N terminal SNAP and C terminal CLIP motifs that are used in the tag-of-war experiments with 10xMEED. We have already determined via an *in vitro* kinase assay that this region of human KNL1 is phosphorylated by Mps1. Next, we are going to oligo label the human KNL1 and use it in the same tug-of-war experiments described in the previous chapter. Using the human version of KNL1 will help us determine if the phenotypes we observed with *Drosophila* Spc105 were model specific or are evolutionarily conserved.

4.2 Sensing biorientation through tension and spatial positioning

Previous work found that although Aurora B activity is reduced at bioriented in comparison to non-bioriented KTs, it is still present and active at attached KTs [74]. If Aurora B is present and active, why does phosphorylation of its outer KT substrates decrease at attached KTs? The spatial positioning model posits that phosphorylation of substrates in the outer kinetochore depends on their distance from kinases such as Aurora B docked in the inner centromere. At non-bioriented, unattached KTs, which are presumably not under tension and therefore still in close proximity to the kinases at the inner centromere, phosphorylation readily occurs.

Once KTs bind to MTs and become bioriented, substrates in the outer KT get pulled away from kinases, which results in reduced phosphorylation of their substrates. As previously mentioned, Aurora B phosphorylation of the PP1 binding site at the N terminus of KNL1 reduces the affinity of PP1 for the KT. Therefore, the spatial positioning model also explains how the enzyme dominance shifts from kinases to phosphatases even though the kinases are still present and active at bioriented KTs. The data presented in Chapter 2 extends the spatial positioning model to include the mechanism by which KNL1 acts as a tension sensor in a way that synergizes both the phosphoregulation of checkpoint protein localization and a mechanical signal that contributes to SAC satisfaction. The model we propose is that at kinetochores under low tension, phosphorylation of Spc105 by Aurora B reduces its affinity for MTs and increases its affinity for checkpoint proteins while inhibiting PP1 from binding to its N terminus. The checkpoint proteins maintain the wait signal of the SAC and prevent anaphase onset. Once stable KT-MT attachments have been established through the Ndc80 complex, the outer KT moves away from the centromere and Aurora B. Once Aurora B can no longer phosphorylate the N terminus of KNL1, it can now bind to MTs and PP1. PP1 promotes dephosphorylation of MELT motifs, which reduces the affinity of the MCC to the kinetochore and turns off the checkpoint.

Many years of research and debate have been devoted to understanding the contribution of tension to checkpoint signaling. We would be remiss if we did not address the likelihood that our hypothesis is wrong, and KNL1 is not the tension sensor of the SAC. Indeed, the evidence presented in Chapter 2 would still provide an answer to the very important question as to the function of MT binding of KNL1. Perhaps the answer to this question is much simpler than we originally hypothesized. It could be, and would still concur with our data, that the reason KNL1 binds to MTs, is so that it gets pulled on and away from Aurora B in order to allow for PP1 to bind to KTs. Indeed, Uchida et al. 2021 found that when they reduced KT stretch that

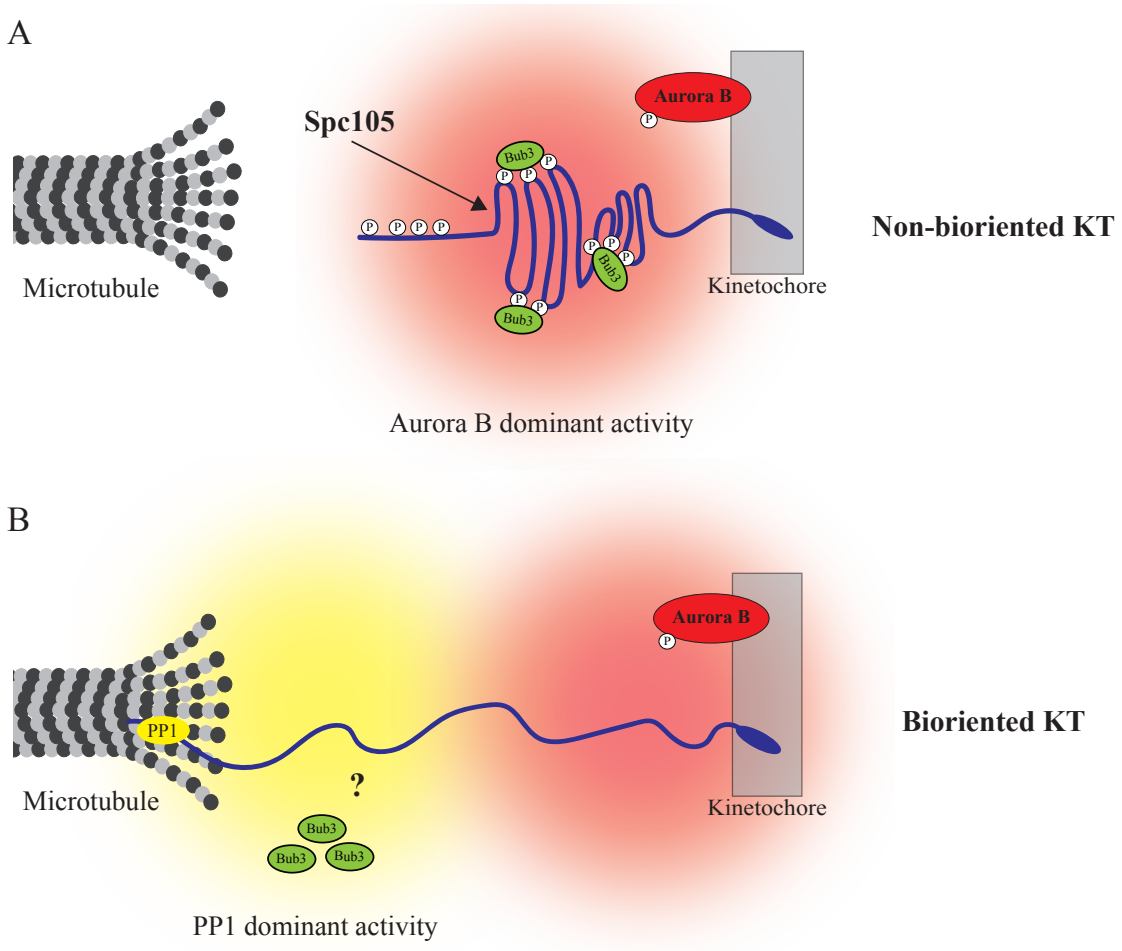

Figure 4.1. Proposed model of *Drosophila* Spc105 as a tension sensor (A) At a non-bioriented KT, Spc105 is not under tension and therefore highly phosphorylated by Aurora B kinase. When Aurora B phosphorylates the MEED motifs in Spc105, it increases its affinity for checkpoint protein Bub3. Aurora B phosphorylation of the N terminus inhibits PP1 phosphatase from binding and localizing to the KT. (B) When KNL1 binds to MT at bioriented KTs, its N terminus stretches Spc105 away from the Aurora B dominant zone which allows for PP1 to bind to the N terminus, which promotes dephosphorylation of the middle region, and reduces its affinity for Bub2. Simultaneouly, this moves the MEED motifs away from each other in space, which also decreases the affinity of Bub3 for Spc105. This model proposes a synergistic mechanism of tension sensing and spatial positioning for Spc105 at the kinetochore.

PP1 localization to KTs was also reduced and they also observed a metaphase delay. Similarly, in Figure 2.13 D we also observed a metaphase delay and reduction in PP1 when we interrupted MT binding (specifically with the PP1-Spc105(ΔN)-EGFP rescue experiment).

4.3 Final Comments

In summary, Spc105 is involved in regulation of the spindle assembly checkpoint through modulation of checkpoint protein localization and microtubule binding. The different affinity of checkpoint proteins for Spc105 during metaphase is highly phosphoregulated, however the precise mechanism and timing of this regulation is still unknown. We showed that the disordered middle region of *Dm*Spc105 is phosphorylated by Aurora B and inhibiting the kinase activity of Aurora B reduces the affinity of checkpoint protein Bub3 for the KT. In other species, the interaction between Spc105 and Bub3 is regulated by different kinases: specifically Mps1 in humans and Plk1 in *C. elegans*. Regulation of Bub3 localization by Aurora B phosphorylation of *Dm*Spc105 is novel and may be unique to *Drosophila*, however it could be a fruitful avenue of research to increase our understanding of the intricate balance between phosphatases and kinases during the SAC. This complexity is due to, at least in part, the fact that Aurora B has many other functions in mitosis. For example, Aurora B negatively regulates the localization of PP1 phosphatase, which is thought to dephosphorylate the Bub3-binding domains in Spc105 to decrease their affinity for the KT. There is a balance between kinases and phosphatases during the SAC that shifts from kinase dominant to phosphatase dominant to turn off SAC signaling. However, we do not understand the catalyst of the shift. In previous sections, the possibility of the spatial positioning model as the answer to this puzzle was discussed, which fits with our observations and also would explain the purpose of the MT binding function of Spc105. However, more work needs to be done in order to determine the validity of the model.

The MT binding function of Spc105 is conserved in other model species, however the purpose of this function is unknown. In addition, there is little sequence specificity across species, therefore it is difficult to determine MT binding domains among the different models. We identified the first four hundred amino acids as an important

MT binding domain in *Drosophila*, however we acknowledge that there may be other MT binding domains beyond the first four hundred amino acids. Additionally, there are two isoforms of *Dm*Spc105 that only differ in the first nine amino acids. Isoform B contains an N terminal MT binding domain that is not present in Isoform A. We also propose the presence of another MT binding domain in amino acids 300-400, however this region may also contribute to oligomerization that promotes MT binding. This hypothesis comes from the observation of decreased MT binding upon addition of 1,6-HD which disrupts weak hydrophobic interactions such as those that occur when disordered proteins self-associate. We observed the same decrease in MT binding upon deletion of the 300-400 amino acid region and addition of 1,6-HD to Spc105-B(1-400) suggesting that both of these conditions reduce binding for the same reason, which we propose is oligomerization. Interestingly, this region is also phosphorylated by Aurora B which decreases its affinity for MTs. This observation is one that promotes the validity of the spatial positioning model in that perhaps the shift from kinase dominant activity to phosphatase dominant activity occurs when the N terminus binds to MT, upon establishment of the interaction the N terminus gets pulled away from the Aurora B active area, which allows for PP1 to bind to the KT via the N terminal region of Spc105. More experiments are needed to provide supporting evidence for this theory, but it is one that should be considered for future directions as it is vital to our understanding of the checkpoint.

Upon establishing that the N terminus of Spc105 binds to MTs in *Drosophila*, we then deleted this region to observe the S2 cells progression through the cell cycle. Deletion of the first four hundred amino acids (Spc105ΔN) resulted in a significant delay in metaphase. Weakened KT-MT attachments are often the cause of a metaphase delay, however these cells had hyper-stretched KTs indicative of more stable KT-MT attachments. Another major cause of metaphase delay is retention of checkpoint proteins and in fact, we observed Spc105ΔN expressing cells retained significantly

higher levels of checkpoint protein Bub3 than wild type cells. These results indicate that checkpoint proteins are being retained at Spc105ΔN KTs causing the metaphase delay independent of KT-MT attachment. The fact that the KT-MT attachment was not disrupted is interesting because we already established that the region we deleted in the Spc105ΔN binds to MTs which suggests the MT binding function of Spc105 is not directly contributing to the overall KT-MT attachments. However, in order to confirm this observation and more readily quantify the KT-MT attachment status in Spc105ΔN expressing cells we designed an experiment using a photo-activatable (PA) version of GFP fused to tubulin. Using this approach, we photo-activated the region of the spindle closest to the chromosomes and measured the rate at which the signal dissipated out of the spindle. These measurements gave us the half-life of the KT and non-KT populations of the spindle, which were in congruence with our earlier K-K measurements confirming that the Spc105ΔN expressing cells had hyper-stable attachments despite deleting the MT-binding region of Spc105.

Aurora B can decrease the stability of KT-MT attachments by phosphorylating the subunits of the MT binding protein complex Ndc80. It has been observed localizing at the KT, however the binding partner for Aurora B at the KT is unknown. Therefore, a reasonable explanation for the hyper-stable attachments in our Spc105ΔN expressing cells could be that Aurora B binds to the N terminus of Spc105 and by deleting its binding site we are reducing its KT localization and possibly phosphorylation of Ndc80. Therefore, we performed IF on the Spc105ΔN expressing cells, and used non-expressing cells as our WT control and blotted for active Aurora B at the centromere and the KT. We observed no difference in active Aurora B localization at the KT during metaphase in our Spc105ΔN versus full length Spc105 expressing cells.

The N terminus of Spc105 has two main functions: (1) binding to MTs and (2) acting as the main docking site for PP1 phosphatase. In order to better understand the contributions of each of these functions, we made rescue chimera proteins by

adding back each function separately and together to the Spc105ΔN mutants. We rescued the MT binding function by adding a well-established MT binding protein Tau to the N terminus of Spc105ΔN. This chimera partially rescued the metaphase delay but not entirely. Next, we added back the PP1 binding domain RRISF flanked by disordered regions to the N terminus of Spc105ΔN and found that this also partially rescued but not completely. Finally, when we added back both the MT binding domain of Tau and the PP1 binding domain, this completely rescued the metaphase delay that we observed in the Spc105ΔN expressing cells. This suggests that both MT- and PP1-binding play an important role to the function of the N terminus of Spc105 in the SAC. In addition to assaying for the metaphase delay, we also quantified PP1 levels localized to each chimera and compared it to the amount localized in WT Spc105 expressing cells. Not surprisingly the Spc105ΔN and the Tau-Spc105ΔN did not have any PP1 localized at their KTs. However, the Tau-PP1-Spc105ΔN had higher PP1 localization than the PP1-Spc105ΔN, even though there is no evidence that PP1 binds to the Tau. We propose that perhaps the disordered Tau protein provided flexibility and perhaps distance from the KT that enhanced PP1 binding in the Tau-PP1-Spc105ΔN versus the PP1-Spc105ΔN.

Our original hypothesis for this thesis was that Spc105 act as a tension sensor for the SAC through binding its N terminus to MTs, which stretches the middle of the protein, pulling apart the MEED motifs which reduces its affinity for Bub3 and leads to anaphase onset. This hypothesis disregards the essential phosphoregulatory piece of the system that has already been established in other model organisms. As previously mentioned, the spatial positioning model may be an elegant way to link the proposed tension sensing function of Spc105 with the phosphoregulation of Aurora B and PP1. Perhaps the tension applied to the disordered Spc105 proteins causes stretch that changes its affinity for Bub3 by pulling apart the MEEDs and pulls it away from Aurora B activity simultaneously. This could provide a robust two-

pronged approach to reducing MCC production at the KT, and thereby reducing the SAC signal. However, the system may be straightforward than our original hypothesis and may be that the pulling of Spc105 could simply be to reduce ABK proximity to Spc105 and therefore phosphorylation of its Bub3 binding domains. The tug-of-war experiment described in the beginning of this chapter is aimed at determining if pulling on Spc105 changes its affinity for Bub3, and will help ascertain the validity of our model in a controlled environment.

Whether Spc105 acts directly as a tension sensor, or simply is the flexible hub for checkpoint protein binding is an important distinction to make in order to better understand why such a large, energetically expensive protein has such high value for a seemingly simple task. It is vital to our global view of cell division to study Spc105 and better grasp its role in the SAC in order to progress in the field of mitotic research. Tension sensing exists throughout biology, through adhesion molecules in cancer cells to ion channels in plants, it is an important way cells regulate certain essential functions. There is increasing amounts of evidence that indicate that tension directly regulates the cell cycle however, the identity of a definitive tension sensor currently eludes research. The disordered protein Spc105 is a likely candidate due to its flexible nature and its function as a binding hub for checkpoint proteins, however more work needs to be done to directly establish its tension sensing abilities.

... ...

BIBLIOGRAPHY

[1] Alfieri, Claudio, Chang, Leifu, and Barford, David. Mechanism for remodelling of the cell cycle checkpoint protein mad2 by the atpase trip13. *Nature 559*, 7713 (2018), 274–278.

[2] Alfieri, Claudio, Chang, Leifu, Zhang, Ziguo, Yang, Jing, Maslen, Sarah, Skehel, Mark, and Barford, David. Molecular basis of APC/c regulation by the spindle assembly checkpoint. 431–436. Number: 7617.

[3] Alushin, Gregory M., Ramey, Vincent H., Pasqualato, Sebastiano, Ball, David A., Grigorieff, Nikolaus, Musacchio, Andrea, and Nogales, Eva. The Ndc80 kinetochore complex forms oligomeric arrays along microtubules. *Nature 467* (Oct. 2010), 805–812.

[4] Amano, Miho, Suzuki, Aussie, Hori, Tetsuya, Backer, Chelsea, Okawa, Katsuya, Cheeseman, Iain M, and Fukagawa, Tatsuo. The cenp-s complex is essential for the stable assembly of outer kinetochore structure. *The Journal of cell biology 186*, 2 (2009), 173–182.

[5] Amin, Mohammed A, Agarwal, Shivangi, and Varma, Dileep. Mapping the kinetochore map functions required for stabilizing microtubule attachments to chromosomes during metaphase. *Cytoskeleton 76*, 6 (2019), 398–412.

[6] Audett, Margaux R, and Maresca, Thomas J. The whole is greater than the sum of its parts: at the intersection of order, disorder, and kinetochore function. *Essays in Biochemistry 64*, 2 (2020), 349–358.

[7] Bajaj, Rakhi, Bollen, Mathieu, Peti, Wolfgang, and Page, Rebecca. KNL1 Binding to PP1 and Microtubules Is Mutually Exclusive. *Structure 26* (Oct. 2018), 1327–1336.

[8] Barisic, Marin, and Maiato, Helder. The tubulin code: a navigation system for chromosomes during mitosis. *Trends in cell biology 26*, 10 (2016), 766–775.

[9] Boke, Elvan, Ruer, Martine, Wühr, Martin, Drechsel, David, Hyman, Anthony A., and Mitchison, Timothy J. Amyloid-like self-assembly of a cellular compartment. *Cell 166* (July 2016), 637–650.

[10] Broad, Amanda J., DeLuca, Keith F., and DeLuca, Jennifer G. Aurora b kinase is recruited to multiple discrete kinetochore and centromere regions in human cells. Number: e201905144.

[11] Caldas, Gina V., DeLuca, Keith F., and DeLuca, Jennifer G. KNL1 facilitates phosphorylation of outer kinetochore proteins by promoting aurora b kinase activity. 957–969. Number: 6.

[12] Carmena, Mar, and Earnshaw, William C. The cellular geography of aurora kinases. 842–854. Number: 11 Publisher: Nature Publishing Group.

[13] Carmena, Mar, Wheelock, Michael, Funabiki, Hironori, and Earnshaw, William C. The chromosomal passenger complex (cpc): from easy rider to the godfather of mitosis. *Nature reviews Molecular cell biology 13*, 12 (2012), 789–803.

[14] Cheeseman, Iain M. The kinetochore. a015826. Number: 7 Company: Cold Spring Harbor Laboratory Press Distributor: Cold Spring Harbor Laboratory Press Institution: Cold Spring Harbor Laboratory Press Label: Cold Spring Harbor Laboratory Press Publisher: Cold Spring Harbor Lab.

[15] Cheeseman, Iain M., Anderson, Scott, Jwa, Miri, Green, Erin M., Kang, Jungseog, Yates, John R., Chan, Clarence S. M., Drubin, David G., and Barnes, Georjana. Phospho-regulation of kinetochore-microtubule attachments by the aurora kinase ipl1p. 163–172. Number: 2.

[16] Cheeseman, Iain M., Chappie, Joshua S., Wilson-Kubalek, Elizabeth M., and Desai, Arshad. The conserved KMN network constitutes the core microtubule-binding site of the kinetochore. *Cell 127* (Dec. 2006), 983–997.

[17] Cheeseman, Iain M., and Desai, Archad. Molecular architecture of the kinetochore-microtubule interface. *Molecular Cell Biology 9* (Jan. 2008).

[18] Cheeseman, Iain M., Niessen, Sherry, Anderson, Scott, Hyndman, Francie, Yates, John R. III, Oegema, Karen, and Desai, Archad. A conserved protein network controls assembly of the outer kinetochore and its ability to sustain tension. *Genes & Development 18* (2004), 2255–2268.

[19] Chmátal, Lukáš, Yang, Karren, Schultz, Richard M, and Lampson, Michael A. Spatial regulation of kinetochore microtubule attachments by destabilization at spindle poles in meiosis i. *Current Biology 25*, 14 (2015), 1835–1841.

[20] Cimini, Daniela, Wan, Xiaohu, Hirel, Christophe B., and Salmon, E. D. Aurora kinase promotes turnover of kinetochore microtubules to reduce chromosome segregation errors. 1711–1718. Number: 17.

[21] Clute, Paul, and Pines, Jonathon. Temporal and spatial control of cyclin b1 destruction in metaphase. *Nature cell biology 1*, 2 (1999), 82–87.

[22] Collin, Philippe, Nashchekina, Oxana, Walker, Rachael, and Pines, Jonathon. The spindle assembly checkpoint works like a rheostat rather than a toggle switch. *Nature cell biology 15*, 11 (2013), 1378–1385.

[23] Conde, Carlos, Osswald, Mariana, Barbosa, João, Moutinho-Santos, Tatiana, Pinheiro, Irina, Maiato, Helder, and Sunkel, Claudio E. Drosophila Polo regulates the spindle assembly checkpoint thorugh Mps1-dependent BubRI phosphorylation. *The EMBO Journal 32*, 12 (2013), 1761–1777. Number: 12.

[24] Cordeiro, Marilia H., Smith, Richard J., and Saurin, Adrian T. Kinetochore phosphatases suppress autonomous polo-like kinase 1 activity to control the mitotic checkpoint. e202002020. Number: 12.

[25] De Antoni, Anna, Pearson, Chad G, Cimini, Daniela, Canman, Julie C, Sala, Valeria, Nezi, Luigi, Mapelli, Marina, Sironi, Lucia, Faretta, Mario, Salmon, Edward D, et al. The mad1/mad2 complex as a template for mad2 activation in the spindle assembly checkpoint. *Current Biology 15*, 3 (2005), 214–225.

[26] DeLuca, J.G., Gall, Walter E., Ciferri, Claudio, Cimini, Daniela, Musacchio, Andrea, and Salmon, E.D. Kinetochore microtubule dynamics and attachment stability are regulated by Hec1. *Cell 127*, 6 (2006), 1105–1108. Number: 6.

[27] DeLuca, Keith F, Lens, Susanne M A, and DeLuca, Jennifer G. Temporal changes in hec1 phosphorylation control kinetochore–microtubule attachment stability during mitosis. 13.

[28] DeLuca, Keith F, Meppelink, Amanda, Broad, Amanda J, Mick, Jeanne E, Peersen, Olve B, Pektas, Sibel, Lens, Susanne MA, and DeLuca, Jennifer G. Aurora a kinase phosphorylates hec1 to regulate metaphase kinetochore–microtubule dynamics. *Journal of Cell Biology 217*, 1 (2018), 163–177.

[29] Deng, Xin, Gumm, Jordan, Karki, Suman, Eickholt, Jesse, and Cheng, Jianlin. An overview of practical applications of protein disorder prediction and drive for faster, more accurate predictions. *International journal of molecular sciences 16*, 7 (2015), 15384–15404.

[30] Derr, N.D., Goodman, B.S., Jungmann, R., Leschziner, A.E., Shih, W.M., and Reck-Peterson, S.L. Tug-of-war in motor protein ensembles revealed with a programmable DNA origami scaffold. *Science 338* (Nov. 2012), 662–665.

[31] Desai, Archad, Rybina, Sonja, Muller-Reichert, Thomas, Shevchenko, Andrej, Shevchenko, Anna, Hyman, Anthony, and Oegema, Karen. KNL-1 directs assembly of the microtubule binding interface of the kinetochore in c. elegans. 2421–2435.

[32] Dick, Amalie E, and Gerlich, Daniel W. Kinetic framework of spindle assembly checkpoint signalling. *Nature cell biology 15*, 11 (2013), 1370–1377.

[33] Dou, Zhen, Liu, Xing, Wang, Wenwen, Zhu, Tongge, Wang, Xinghui, Xu, Leilei, Abrieu, Ariane, Fu, Chuanhai, Hill, Donald L, and Yao, Xuebiao. Dynamic localization of mps1 kinase to kinetochores is essential for accurate spindle microtubule attachment. *Proceedings of the National Academy of Sciences 112*, 33 (2015), E4546–E4555.

[34] Eggert, Ulrike S, Kiger, Amy A, Richter, Constance, Perlman, Zachary E, Perrimon, Norbert, Mitchison, Timothy J, and Field, Christine M. Parallel chemical genetic and genome-wide RNAi screens identify cytokinesis inhibitors and targets. e379. Number: 12.

[35] Eliezer, David. Biophysical characterization of intrinsically disordered proteins. *Current opinion in structural biology 19*, 1 (2009), 23–30.

[36] Emanuele, Michael J., McCleland, Mark L., Satinover, David L., and Stukenberg, P. Todd. Measuring the stoichiometry and physical interactions between components elucidates the architecture of the vertebrate kinetochore. 4882–4892. Number: 10.

[37] Espeut, Julien, Cheerambathur, Dhanya K, Krenning, Lenno, Oegema, Karen, and Desai, Arshad. Microtubule binding by knl-1 contributes to spindle checkpoint silencing at the kinetochore. *Journal of Cell Biology 196*, 4 (2012), 469–482.

[38] Espeut, Julien, Lara-Gonzalez, Pablo, Sassine, Mélanie, Shiau, Andrew K., Desai, Arshad, and Abrieu, Ariane. Natural loss of mps1 kinase in nematodes uncovers a role for polo-like kinase 1 in spindle checkpoint initiation. 58–65. Number: 1.

[39] Foley, Emily A., and Kapoor, Tarun M. Microtubule attachment and spindle assembly checkpoint signalling at the kinetochore. *Nature Reviews 14* (2013), 25–37.

[40] Gambogi, Craig W, and Black, Ben E. The nucleosomes that mark centromere location on chromosomes old and new. *Essays in biochemistry 63*, 1 (2019), 15–27.

[41] Gascoigne, Karen E, Takeuchi, Kozo, Suzuki, Aussie, Hori, Tetsuya, Fukagawa, Tatsuo, and Cheeseman, Iain M. Induced ectopic kinetochore assembly bypasses the requirement for cenp-a nucleosomes. *Cell 145*, 3 (2011), 410–422.

[42] Genin, Anne, Desir, Julie, Lambert, Nelle, Biervliet, Martine, Van Der Aa, Nathalie, Pierquin, Genevieve, Killian, Audrey, Tosi, Mario, Urbina, Montse, Lefort, Anne, Libert, Frederick, Pirson, Isabelle, and Abramowicz, Marc. Kinetochore KMN network gene CASC5 mutated in primary microcephaly. 5306–5317. Number: 24.

[43] Gibson, Daniel G, Young, Lei, Chuang, Ray-Yuan, Venter, J Craig, Hutchison, Clyde A, and Smith, Hamilton O. Enzymatic assembly of DNA molecules up to several hundred kilobases. 343–345. Number: 5.

[44] Godek, Kristina M, Kabeche, Lilian, and Compton, Duane A. Regulation of kinetochore–microtubule attachments through homeostatic control during mitosis. *Nature Reviews Molecular Cell Biology 16*, 1 (2015), 57–64.

[45] Gordon, D.J., Resio, B., and Pellman, D. Causes and consequences of aneuploidy in cancer. *Nature Reviews 13* (2012), 189–203.

[46] Gudimchuk, Nikita, Vitre, Benjamin, Kim, Yumi, Kiyatkin, Anatoly, Cleveland, Don W, Ataullakhanov, Fazly I, and Grishchuk, Ekaterina L. Kinetochore kinesin cenp-e is a processive bi-directional tracker of dynamic microtubule tips. *Nature cell biology 15*, 9 (2013), 1079–1088.

[47] Hara, Masatoshi, and Fukagawa, Tatsuo. Kinetochore assembly and disassembly during mitotic entry and exit. *Current opinion in cell biology 52* (2018), 73–81.

[48] Hayette, S, Tigaud, I, Martel, S, Corbo, L, Charrin, C, Beillard, E, Deleage, G, Magaud, J P, and Rimokh, R. AF15q14, a novel partner gene fused to the MLL gene in an acute myeloid leukaemia with a t(11;15)(q23:a14). 4446–4450.

[49] Heinrich, Stephanie, Geissen, Eva-Maria, Kamenz, Julia, Trautmann, Susanne, Widmer, Christian, Drewe, Philipp, Knop, Michael, Radde, Nicole, Hasenauer, Jan, and Hauf, Silke. Determinants of robustness in spindle assembly checkpoint signalling. *Nature cell biology 15*, 11 (2013), 1328–1339.

[50] Hendrickx, Annick, Beullens, Monique, Ceulemans, Hugo, Den Abt, Tom, Van Eynde, Aleyde, Nicolaescu, Emila, Lesage, Bart, and Bollen, Mathieu. Docking Motif-Guided Mapping of the Interactome of Protein Phosphatase-1. *Chemistry & Biology 16* (Apr. 2009), 365–371.

[51] Hinshaw, Stephen M, and Harrison, Stephen C. The structure of the ctf19c/ccan from budding yeast. *Elife 8* (2019), e44239.

[52] Hiruma, Yoshitaka, Sacristan, Carlos, Pachis, Spyridon T., Adamopoulos, Athanassios, Kuijt, Timo, Ubbink, Marcellus, von Castelmur, Eleonore, Perrakis, Anastassis, and Kops, Geert J.P.L. Competition between MPS1 and microtubules and kinetochores regulates spindle checkpoint signaling. *Science 348* (June 2015), 1264–1267.

[53] Hoffman, David B., Pearson, Chad G., Yen, Tim J., Howell, Bonnie J., and Salmon, E.d. Microtubule-dependent changes in assembly of microtubule motor proteins and mitotic spindle checkpoint proteins at PtK1 kinetochores. 1995–2009. Number: 7 Publisher: American Society for Cell Biology (mboc).

[54] Hori, Tetsuya, Amano, Miho, Suzuki, Aussie, Backer, Chelsea B, Welburn, Julie P, Dong, Yimin, McEwen, Bruce F, Shang, Wei-Hao, Suzuki, Emiko, Okawa, Katsuya, et al. Ccan makes multiple contacts with centromeric dna to provide distinct pathways to the outer kinetochore. *Cell 135*, 6 (2008), 1039–1052.

[55] Howell, Bonnie J, Moree, Ben, Farrar, Emily M, Stewart, Scott, Fang, Guowei, and Salmon, E. D. Spindle checkpoint protein dynamics at kinetochores in living cells. 953–964. Number: 11.

[56] Hyman, Anthony A, Weber, Christoph A, and Jülicher, Frank. Liquid-liquid phase separation in biology. *Annual review of cell and developmental biology 30* (2014), 39–58.

[57] Ikeda, Masanori, and Tanaka, Kozo. Plk1 bound to bub1 contributes to spindle assembly checkpoint activity during mitosis. *Scientific reports 7*, 1 (2017), 1–15.

[58] Ji, Zhejian, Gao, Haishan, and Yu, Hongtao. Kinetochore attachment sensed by competitive mps1 and microtubule binding to ndc80c. *Science 348*, 6240 (2015), 1260–1264.

[59] Jo, Yongsang, and Jung, Yongwon. Interplay between intrinsically disordered proteins inside membraneless protein liquid droplets. *Chemical Science 11*, 5 (2020), 1269–1275.

[60] Kay, Lewis E. The importance of dynamics in structural biology. *Nature Structural and Molecular Biology 18*, 12 (2011), 1308–1309.

[61] Kern, David M., Kim, Taekyung, Rigney, Mike, Hattersley, Neil, Desai, Arshad, and Cheeseman, Iain M. The outer kinetochore protein KNL-1 contains a defined oligomerization domain in nematodes. 229–237. Number: 2 Publisher: American Society for Cell Biology (mboc).

[62] Kerres, Anne, Jakopec, Visnja, and Fleig, Ursula. The conserved spc7 protein is required for spindle integrity and links kinetochore complexes in fission yeast. 2441–2454. Number: 7 Publisher: American Society for Cell Biology (mboc).

[63] Kiyomitsu T, Murakami H, Yanagida M. Protein interaction domain mapping of human kinetochore protein blinkin reveals a consensus motif for binding of spindle assembly checkpoint proteins bub1 and bubr1. *Molecular Cellular Biology 31*, 5 (Nov. 2011), 998–1011.

[64] Kiyomitsu T, Obuse C, Yanagida M. Blinkin/af15q14 is required for chromosome alignment and the mitotic checkpoint through direct interaction with bub1 and bubr1. *Developmental Cell 13*, 5 (Nov. 2007), 663–676.

[65] Klare, Kerstin, Weir, John R, Basilico, Federica, Zimniak, Tomasz, Massimiliano, Lucia, Ludwigs, Nina, Herzog, Franz, and Musacchio, Andrea. Cenp-c is a blueprint for constitutive centromere–associated network assembly within human kinetochores. *Journal of Cell Biology 210*, 1 (2015), 11–22.

[66] Kops, Geert J.P.L., and Gassmann, Reto. Crowning the kinetochore: The fibrous corona in chromosome segregation. 653–667. Number: 8.

[67] Krenn, Veronica, Overlack, Katharina, Primorac, Ivana, van Gerwen, Suzan, and Musacchio, Andrea. KI motifs of human knl1 enhance assembly of comprehensive spindle checkpoint complexes around MELT repeats. 29–39. Number: 1.

[68] Krenn, Veronica, Wehenkel, Annemarie, Li, Xiaozheng, Santaguida, Stefano, and Musacchio, Andrea. Structural analysis reveals features of the spindle checkpoint kinase bub1–kinetochore subunit knl1 interaction. *Journal of Cell Biology 196*, 4 (2012), 451–467.

[69] Kuhn, Jonathan, and Dumont, Sophie. Spindle assembly checkpoint satisfaction occurs via end-on but not lateral attachments under tension. 1533–1542.

[70] Kung, Ching, Martinac, Boris, and Sukharev, Sergei. Mechanosensitive channels in microbes. *Annual review of microbiology 64* (2010), 313–329.

[71] Lampson, Michael A, and Cheeseman, Iain M. Sensing centromere tension: Aurora b and the regulation of kinetochore function. *Trends in cell biology 21*, 3 (2011), 133–140.

[72] Lawrimore, Josh, Bloom, Kerry S, and Salmon, ED. Point centromeres contain more than a single centromere-specific cse4 (cenp-a) nucleosome. *Journal of Cell Biology 195*, 4 (2011), 573–582.

[73] Lince-Faria, Mariana, Maffini, Stefano, Orr, Bernard, Ding, Yun, Florindo, Cláudia, Sunkel, Claudio E, Tavares, Álvaro, Johansen, Jørgen, Johansen, Kristen M, and Maiato, Helder. Spatiotemporal control of mitosis by the conserved spindle matrix protein megator. *Journal of Cell Biology 184*, 5 (2009), 647–657.

[74] Liu, Dan, Vader, Gerben, Vromans, Martijn J. M., Lampson, Michael, and Lens, Susanne M. A. Sensing Chromosome Bi-Orientation by Spatial Separation of Aurora B Kinase from Kinetochore Substrates. *Science 323* (Oct. 2008), 1350–1353.

[75] Liu, Dan, Vleugal, Mathijs, Backer, Chelsea B., Hori, Tetsuya, Fukagawa, Tasuo, Cheeseman, Iain M., and Lampson, Michael A. Regulated targeting of protein phosphatase 1 to the outer kinetochore by KNL1 opposes Aurora B kinase. *Journal of Cell Biology 10*, 1083 (Mar. 2010). Number: 1083.

[76] Liu, Song-Tao, Rattner, Jerome B, Jablonski, Sandra A, and Yen, Tim J. Mapping the assembly pathways that specify formation of the trilaminar kinetochore plates in human cells. *The Journal of cell biology 175*, 1 (2006), 41–53.

[77] London, Nitobe, and Biggins, Sue. Signalling dynamics in the spindle checkpoint response. *Nature reviews Molecular cell biology 15*, 11 (2014), 736–748.

[78] London, Nitobe, Ceto, Steven, Ranish, Jeffrey A., and Biggins, Sue. Phosphoregulation of Spc105 by Mps1 and PP1 Regulates Bub1 Localization to Kinetochores. *Current Biology 22* (May 2012), 900–906.

[79] Maiato, H., DeLuca, Jennifer, Salmon, E. D, and Earnshaw, William C. The dynamic kinetochore-microtubule interface. 5461–5477. Number: 23.

[80] Maiato, Helder, Gomes, Ana Margarida, Sousa, Filipe, and Barisic, Marin. Mechanisms of chromosome congression during mitosis. *Biology 6*, 1 (2017), 13.

[81] Maresca, Thomas J., and Salmon, E.D. Welcome to a new kind of tension: translating kinetochore mechanics into a wait-anaphase signal. *Journal of Cell Biology 123*, 825–835.

[82] McEwen, Bruce F, Dong, Yimin, and VandenBeldt, Kristin J. Using electron microscopy to understand functional mechanisms of chromosome alignment on the mitotic spindle. *Methods in cell biology 79* (2007), 259–293.

[83] Meadows, John C., Shepperd, Lindsey A., Vanoosthuyse, Vincent, Lancaster, Theresa C., Sochaj, Alicja M., Buttrick, Graham J., Hardwick, Kevin G., and Millar, Jonathan B. A. Spindle checkpoint silencing requires association of PP1 to both spc7 and kinesin-8 motors. 739–750. Number: 6 Publisher: Elsevier.

[84] Monda, Julie K, and Cheeseman, Iain M. The kinetochore–microtubule interface at a glance. *Journal of cell science 131*, 16 (2018).

[85] Moura, Margarida, Osswald, Mariana, Leça, Nelson, Barbosa, Joao, Pereira, António J, Maiato, Helder, Sunkel, Claudio E, and Conde, Carlos. Protein phosphatase 1 inactivates mps1 to ensure efficient spindle assembly checkpoint silencing. *Elife 6* (2017), e25366.

[86] Musacchio, Andrea. The molecular biology of spindle assembly checkpoint signaling dynamics. R1002–R1018. Number: 20.

[87] Musacchio, Andrea, and Desai, Arshad. A molecular view of kinetochore assembly and function. 5. Number: 1 Publisher: Multidisciplinary Digital Publishing Institute.

[88] Musacchio, Andrea, and Salmon, Edward D. The spindle-assembly checkpoint in space and time. *Molecular Cell Biology 8* (May 2007).

[89] Nakajima, Hiroyuki, Toyoshima-Morimoto, Fumiko, Taniguchi, Eri, and Nishida, Eisuke. Identification of a consensus motif for plk (polo-like kinase) phosphorylation reveals myt1 as a plk1 substrate*. 25277–25280. Number: 28 Publisher: Elsevier.

[90] Nasa, Isha, Rusin, Scott F., Kettenbach, Arminja N., and Moorhead, Greg B. Aurora b opposes PP1 function in mitosis by phosphorylating the conserved PP1-binding RVxF motif in PP1 regulatory proteins. Number: 530 Publisher: American Association for the Advancement of Science Section: Research Article.

[91] Nekrasov, Vladimir S., Smith, Melanie A., Peak-Chew, Sew, and Kilmartin, John V. Interactions between centromere complexes in saccharomyces cerevisiae. 4931–4946.

[92] Nijenhuis, Wilco, Vallardi, Giulia, Teixeira, Antoinette, Kops, Geert J. P. L., and Saurin, Adrian T. Negative feedback at kinetochores underlies a responsive spindle checkpoint signal. *Nature Cell Biology 16*, 12 (Dec. 2014), 1257–1266. Number: 12.

[93] Nishino, Tatsuya, Rago, Florencia, Hori, Tetsuya, Tomii, Kentaro, Cheeseman, Iain M, and Fukagawa, Tatsuo. Cenp-t provides a structural platform for outer kinetochore assembly. *The EMBO journal 32*, 3 (2013), 424–436.

[94] Pachis, Spyridon T, and Kops, Geert JPL. Leader of the sac: molecular mechanisms of mps1/ttk regulation in mitosis. *Open biology 8*, 8 (2018), 180109.

[95] Pagliuca, Cinzia, Draviam, Viji M., Marco, Eugenio, Sorger, Peter K., and Wulf, Peter De. Roles for the conserved spc105p/kre28p complex in kinetochore-microtubule binding and the spindle assembly checkpoint. e7640. Number: 10 Publisher: Public Library of Science.

[96] Palmer, Douglas K, O'Day, Kathleen, Wener, Mark H, Andrews, Brian S, and Margolis, Robert L. A 17-kd centromere protein (cenp-a) copurifies with nucleosome core particles and with histones. *The Journal of cell biology 104*, 4 (1987), 805–815.

[97] Petrovic, Arsen, Mosalaganti, Shyamal, Keller, Jenny, Mattiuzzo, Marta, Overlack, Katharina, Krenn, Veronica, De Antoni, Anna, Wohlgemuth, Sabine, Cecatiello, Valentina, Pasqualato, Sebastiano, Raunser, Stefan, and Musacchio, Andrea. Modular assembly of RWD domains on the mis12 complex underlies outer kinetochore organization. 591–605. Number: 4.

[98] Petrovic, Arsen, Pasqualato, Sebastiano, Dube, Prakash, Krenn, Veronica, Santaguida, Stefano, Cittaro, Davide, Monzani, Silvia, Massimiliano, Lucia, Keller, Jenny, Tarricone, Aldo, Maiolica, Alessio, Stark, Holger, and Musacchio, Andrea. The MIS12 complex is a protein interaction hub for outer kinetochore assembly. *Journal of Cell Biology 190*, 5 (Sept. 2010), 835–852.

[99] Pot, Isabelle, Measday, Vivien, Snydsman, Brian, Cagney, Gerard, Fields, Stanley, Davis, Trisha N, Muller, Eric GD, and Hieter, Philip. Chl4p and iml3p are two new members of the budding yeast outer kinetochore. *Molecular biology of the cell 14*, 2 (2003), 460–476.

[100] Primorac, Ivana, Weir, John R., Chiroli, Elena, Gross, Fridolin, Hoffman, Ingrid, van Gerwen, Suzan, Ciliberto, Andrea, and Musacchio, Andrea. Bub3 reads phosphorylated MELT repeats to promote spindle assembly checkpoint signaling. *eLife 2* (Sept. 2013), e01030.

[101] Przewloka, Marcin R., Zhang, Wei, Costa, Patricia, Archambault, Vincent, Paolo D'Avino, Pier, Lilly, Kathryn S., Laue, Ernest D., McAinsh, Andrew D., and Glover, David M. Molecular analysis of core kinetochore composition and assembly in Drosophila melanogaster. *PLoS ONE 2*, 5 (May 2007), e478. Number: 5.

[102] Qi, Hongying, Rath, Uttama, Ding, Yun, Ji, Yun, Blacketer, Melissa J, Girton, Jack, Johansen, Jørgen, and Johansen, Kristen M. East interacts with megator and localizes to the putative spindle matrix during mitosis in drosophila. *Journal of cellular biochemistry 95*, 6 (2005), 1284–1291.

[103] Qi, Hongying, Rath, Uttama, Wang, Dong, Xu, Ying-Zhi, Ding, Yun, Zhang, Weiguo, Blacketer, Melissa J, Paddy, Michael R, Girton, Jack, Johansen, Jørgen, et al. Megator, an essential coiled-coil protein that localizes to the putative spindle matrix during mitosis in drosophila. *Molecular biology of the cell 15*, 11 (2004), 4854–4865.

[104] Rath, Uttama, Wang, Dong, Ding, Yun, Xu, Ying-Zhi, Qi, Hongying, Blacketer, Melissa J, Girton, Jack, Johansen, Jørgen, and Johansen, Kristen M. Chromator, a novel and essential chromodomain protein interacts directly with the putative spindle matrix protein skeletor. *Journal of cellular biochemistry 93*, 5 (2004), 1033–1047.

[105] Régnier, Vinciane, Vagnarelli, Paola, Fukagawa, Tatsuo, Zerjal, Tatiana, Burns, Elizabeth, Trouche, Didier, Earnshaw, William, and Brown, William. Cenp-a is required for accurate chromosome segregation and sustained kinetochore association of bubr1. *Molecular and cellular biology 25*, 10 (2005), 3967–3981.

[106] Rieder, C L, Cole, R W, Khodjakov, A, and Sluder, G. The checkpoint delaying anaphase in response to chromosome monoorientation is mediated by an inhibitory signal produced by unattached kinetochores. 941–948. Number: 4.

[107] Rieder, Conly L, Cole, Richard W, Khodjakov, Alexey, and Sluder, Greenfield. The checkpoint delaying anaphase in response to chromosome monoorientation is mediated by an inhibitory signal produced by unattached kinetochores. *The Journal of cell biology 130*, 4 (1995), 941–948.

[108] Roscioli, Emanuele, Germanova, Tsvetelina E., Smith, Christopher A., Embacher, Peter A., Erent, Muriel, Thompson, Amelia I., Burroughs, Nigel J., and McAinsh, Andrew D. Ensemble-level organization of human kinetochores and evidence for distinct tension and attachment sensors. 107535. Number: 4.

[109] Rosenberg, Jessica S., Cross, Frederick R., and Funabiki, Hironori. KNL1/Spc105 Recruits PP1 to Silence the Spindle Assembly Checkpoint. *Current Biology 21*, 11 (June 2011), 942–947. Number: 11.

[110] Roy, Babhrubahan, Verma, Vikash, Sim, Janice, Fontan, Adrienne, and Joglekar, Ajit P. Delineating the contribution of spc105-bound PP1 to spindle checkpoint silencing and kinetochore microtubule attachment regulation. 3926–3942. Number: 12.

[111] Salimian, Kevan J, Ballister, Edward R, Smoak, Evan M, Wood, Stacey, Panchenko, Tanya, Lampson, Michael A, and Black, Ben E. Feedback control in sensing chromosome biorientation by the aurora b kinase. *Current Biology 21*, 13 (2011), 1158–1165.

[112] Schittenhelm, Ralf B, Chaleckis, Romanas, and Lehner, Christian F. Intrakinetochore localization and essential functional domains of drosophila spc105. 2374–2386. Number: 16 Publisher: John Wiley & Sons, Ltd.

[113] Shepperd, Lindsey A., Meadows, John C., Sochaj, Alicja M., Lancaster, Theresa C., Zou, Juan, Buttrick, Graham J., Rappsilber, Juri, Hardwick, Kevin G., and MIlar, Jonathan B.A. Phosphodependent recruitment of Bub1 and Bub3 to Spc7/KNL1 by Mph1 kinase maintains the spindle checkpoint. *Current Biology 22*, 10 (May 2012), 891–899. Number: 10.

[114] Sikirzhytski, Vitali, Renda, Fioranna, Tikhonenko, Irina, Magidson, Valentin, McEwen, Bruce F, and Khodjakov, Alexey. Microtubules assemble near most kinetochores during early prometaphase in human cells. *Journal of Cell Biology 217*, 8 (2018), 2647–2659.

[115] Sironi, Lucia, Mapelli, Marina, Knapp, Stefan, De Antoni, Anna, Jeang, Kuan-Teh, and Musacchio, Andrea. Crystal structure of the tetrameric mad1–mad2 core complex: implications of a 'safety belt'binding mechanism for the spindle checkpoint. *The EMBO journal 21*, 10 (2002), 2496–2506.

[116] Smurnyy, Yegor, Toms, Angela V., Hickson, Gilles R., Eck, Michael J., and Eggert, Ulrike S. Binucleine 2, an isoform-specific inhibitor of *Drosophila* aurora b kinase, provides insights into the mechanism of cytokinesis. 1015–1020. Number: 11.

[117] Steegmaier, Martin, Hoffmann, Matthias, Baum, Anke, Lénárt, Péter, Petronczki, Mark, Krššák, Martin, Gürtler, Ulrich, Garin-Chesa, Pilar, Lieb, Simone, Quant, Jens, Grauert, Matthias, Adolf, Günther R., Kraut, Norbert, Peters, Jan-Michael, and Rettig, Wolfgang J. BI 2536, a potent and selective inhibitor of polo-like kinase 1, inhibits tumor growth in vivo. 316–322. Number: 4.

[118] Sudakin, Valery, Chan, Gordon K.T., and Yen, Tim J. Checkpoint inhibition of the APC/c in HeLa cells is mediated by a complex of BUBR1, BUB3, CDC20, and MAD2. 925–936. Number: 5.

[119] Suzuki, Aussie, Badger, Benjamin L, and Salmon, Edward D. A quantitative description of ndc80 complex linkage to human kinetochores. *Nature communications 6*, 1 (2015), 1–14.

[120] Suzuki, Aussie, Hori, Tetsuya, Nishino, Tatsuya, Usukura, Jiro, Miyagi, Atsushi, Morikawa, Kosuke, and Fukagawa, Tatsuo. Spindle microtubules generate tension-dependent changes in the distribution of inner kinetochore proteins. *Journal of Cell Biology 193*, 1 (2011), 125–140.

[121] Tanaka, Tomoyuki U, Rachidi, Najma, Janke, Carsten, Pereira, Gislene, Galova, Marta, Schiebel, Elmar, Stark, Michael JR, and Nasmyth, Kim. Evidence that the ipl1-sli15 (aurora kinase-incenp) complex promotes chromosome bi-orientation by altering kinetochore-spindle pole connections. *Cell 108*, 3 (2002), 317–329.

[122] Tromer, Eelco, Snel, Berend, and Kops, Geert J.P.L. Widespread recurrent patterns of rapid repeat evolution in the kinetochore scaffold KNL1. 2383–2393. Number: 8.

[123] Uchida, Kazuhiko S.K., Jo, Minji, Nagasaka, Kota, Takahashi, Motoko, Shindo, Norihisa, Shibata, Katsushi, Tanaka, Kozo, Masumoto, Hiroshi, Fukagawa, Tatsuo, and Hirota, Toru. Kinetochore stretching-mediated rapid silencing of the spindle-assembly checkpoint required for failsafe chromosome segregation. S0960982221001275.

[124] Uversky, Vladimir N, Oldfield, Christopher J, and Dunker, A Keith. Intrinsically disordered proteins in human diseases: introducing the d2 concept. *Annu. Rev. Biophys. 37* (2008), 215–246.

[125] Venkei, Zsolt, Przewloka, Marcin R., Ladak, Yaseen, Albadri, Shahad, Sossick, Alex, Juhasz, Gabor, Novák, Béla, and Glover, David M. Spatiotemporal dynamics of spc105 regulates the assembly of the drosophila kinetochore. 110032. Number: 2 Publisher: Royal Society.

[126] Vleugel, Mathijs, Tromer, Eelco, Omerzu, Manja, Groenewold, Vincent, Nijenhuis, Wilco, Snel, Berend, and Kops, Geert JPL. Arrayed bub recruitment modules in the kinetochore scaffold knl1 promote accurate chromosome segregation. *Journal of Cell Biology 203*, 6 (2013), 943–955.

[127] Volkov, Vladimir A, Dogterom, Marileen, Musacchio, Andrea, et al. Multivalency of ndc80 in the outer kinetochore is essential to track shortening microtubules and generate forces. *Elife 7* (2018), e36764.

[128] Walker, Diana L, Wang, Dong, Jin, Ye, Rath, Uttama, Wang, Yanming, Johansen, Jørgen, and Johansen, Kristen M. Skeletor, a novel chromosomal protein that redistributes during mitosis provides evidence for the formation of a spindle matrix. *The Journal of cell biology 151*, 7 (2000), 1401–1412.

[129] Wan, Xiaohu, O'Quinn, Ryan P., Pierce, Heather L., Joglekar, Ajit P., Gall, Walt E., DeLuca, Jennifer G., Carroll, Christopher W., Liu, Song-Tau, Yen, Tim J., McEwen, Bruce F., Stukenberg, P. Todd, Desai, Archad, and Salmon, E.D. Protein architecture of the human kinetochore microtubule attachment site. *Cell 137*, 4 (2009), 672–684. Number: 4.

[130] Wei, Gang, Takimoto, Masato, Yoshida, Ikuya, Mao, Pei-zhong, Koya, Richard Chikara, Miura, Tetsuya, and Kuzumaki, Noboru. Chromosomal assignment of a novel human gene d40. 71–72.

[131] Welburn, JP, Vleugal, Mathijs, Liu, Dan, Yates, JR3rd, Lampson, Michael A., Fukagawa, Tastuo, and Cheeseman, Iain M. Aurora B phosphorylates spatially distinct targets to differentially regulate the kinetochore-microtubule interface. *Molecular Cell 38*, 383–392.

[132] Yamagishi, Yuya, Yang, Ching-Hui, Tanno, Yuji, and Watanabe, Yoshinori. MPS1/mph1 phosphorylates the kinetochore protein KNL1/spc7 to recruit SAC components. 746–752. Number: 7 Publisher: Nature Publishing Group.

[133] Yamaguchi, Masaya, VanderLinden, Ryan, Weissmann, Florian, Qiao, Renping, Dube, Prakash, Brown, Nicholas G., Haselbach, David, Zhang, Wei, Sidhu, Sachdev S., Peters, Jan-Michael, Stark, Holger, and Schulman, Brenda A. Cryo-EM of mitotic checkpoint complex-bound APC/c reveals reciprocal and conformational regulation of ubiquitin ligation. 593–607. Number: 4.

[134] Yan, Kaige, Yang, Jing, Zhang, Ziguo, McLaughlin, Stephen H, Chang, Leifu, Fasci, Domenico, Ehrenhofer-Murray, Ann E, Heck, Albert JR, and Barford, David. Structure of the inner kinetochore ccan complex assembled onto a centromeric nucleosome. *Nature 574*, 7777 (2019), 278–282.

[135] Ye, Anna A., Cane, Stuart, and Maresca, Thomas J. Chromosome biorientation produces hundreds of piconewtons at a metazoan kinetochore.

[136] Ye, Anna A., Cane, Stuart, and Maresca, Thomas J. Chromosome biorientation produces hundreds of piconewtons at a metazoan kinetochore. *Nature communications 7*, 1 (2016), 1–9.

[137] Ye, Anna A., and Maresca, Thomas J. Measuring mitotic forces. In *Methods in Cell Biology*, vol. 144. Elsevier, pp. 165–184.

[138] Ye, Anna A., Deretic, Jovana, Hoel, Christopher M., Hinman, Albert W., Cimini, Daniela, Welburn, Julie P., and Maresca, Thomas J. Aurora a kinase contributes to a pole-based error correction pathway. 1842–1851. Number: 14.

[139] Zhang, Gang, Kruse, Thomas, López-Méndez, Blanca, Sylvestersen, Kathrine Beck, Garvanska, Dimitriya H, Schopper, Simone, Nielsen, Michael Lund, and Nilsson, Jakob. Bub1 positions mad1 close to knl1 melt repeats to promote checkpoint signalling. *Nature communications 8*, 1 (2017), 1–12.

[140] Zhang, Gang, Lischetti, Tiziana, and Nilsson, Jakob. A minimal number of MELT repeats supports all the functions of KNL1 in chromosome segregation. *Journal of Cell Science 127* (2014), 871–884.